Summer 2017

Electrochemical behavior of dense electrodes for impedancemetric NOx sensors

Nabamita Pal
Louisiana Tech University

ELECTROCHEMICAL BEHAVIOR OF DENSE ELECTRODES

FOR IMPEDANCEMETRIC NOx SENSORS

by

Nabamita Pal, MS, M.Tech, B.Tech

A Dissertation Presented in Partial Fulfillment
of the Requirements for the Degree of
Doctor of Philosophy

COLLEGE OF ENGINEERING AND SCIENCE
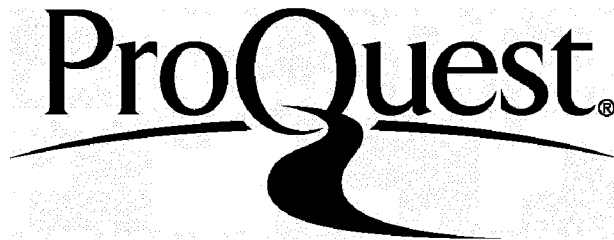LOUISIANA TECH UNIVERSITY

August 2017

ProQuest Number: 10753660

ProQuest 10753660

LOUISIANA TECH UNIVERSITY

THE GRADUATE SCHOOL

06/15/2017
Date

We hereby recommend that the dissertation prepared under our supervision by

Nabamita Pal, MS

entitled **Electrochemical Behavior of Dense Electrodes for Impedancemetric NO$_x$**

Sensors

be accepted in partial fulfillment of the requirements for the Degree of

Doctor of Philosophy in Engineering (Micro and Nanoscale Systems)

Supervisor of Dissertation Research

Head of Department

Engineering

Department

Recommendation concurred in:

Advisory Committee

Approved:

Director of Graduate Studies

Approved:

Dean of the Graduate School

Dean of the College

ABSTRACT

NO_x (NO and NO_2) exhaust gas sensors for diesel powered vehicles have traditionally consisted of porous platinum (Pt) electrodes along with a dense ZrO_2 based electrolyte. Advancement in diesel engine technology results in lower NO_x emissions. Although Pt is chemically and mechanically tolerant to the extreme exhaust gas environment, it is also a strong catalyst for oxygen reduction, which can interfere with the detection of NO_x at concentrations below 100 ppm. Countering this behavior can add to the complexity and cost of the conventional NO_x sensor design. Recent studies have shown that dense electrodes are less prone to heterogeneous catalytic oxygen reactions, thereby enabling greater NO_x sensitivity. Sensors composed of this novel architecture (i.e., dense electrode and porous electrolyte) are still in an inchoate stage of research. There is particular interest in acquiring greater knowledge of the sensing behavior of non-catalytic dense electrodes as they may offer a lower cost alternative to using Pt electrodes.

This work focuses on the potential of the perovskite, strontium-doped lanthanum manganite (LSM), and LSM based composite materials as NO_x sensor electrodes. Perovskite based electrodes are attractive because of their chemical, electrical, and thermal properties. To make LSM based composites three materials of different conductivities were chosen, namely, Au, yttria-stabilized zirconia (YSZ) and

strontium-doped lanthanum cobalt ferrite (LSCF). Au was selected for its electronic conductivity, YSZ was chosen because of its ionic conductivity and LSCF was selected as a mixed conductor. LSM-Au, LSM-YSZ and LSM-LSCF composite based NO_x sensors were fabricated and analyzed using the impedancemetric method for NO_x sensing. The goal was to investigate the electrochemical response, gas cross sensitivity, response rate, and rate-limiting mechanisms due to electrode reactions involving NO, NO_2, O_2, H_2O, and CH_4 that impact the NO_x sensing response.

From the impedancemetric analysis, it was found that LSM-Au based NO_x sensors showed much improved NO_x sensitivity along with lower water and CH_4 cross-sensitivity. Mixing YSZ and LSCF with LSM did not demonstrate any significant improvement in sensing performance.

Dense gold (Au) is also a promising alternative electrode to Pt, since it does not readily promote O_2 reduction and is highly stable under exhaust gas conditions. Yet, the low melting temperature of Au (i.e, 1060 °C) limits the manufacturing feasibility as a NO_x sensor electrode. Since Pt electrodes are compatible with high temperature sensor manufacturing processes and Au offers desirable electrochemical sensing behavior Au/Pt twine electrodes were studied as a part of this thesis. The preliminary results showed the Pt component of the Au/Pt twine electrodes did not compromise the NO_x sensing capability of Au electrode.

APPROVAL FOR SCHOLARLY DISSEMINATION

The author grants to the Prescott Memorial Library of Louisiana Tech University the right to reproduce, by appropriate methods, upon request, any or all portions of this Dissertation. It is understood that "proper request" consists of the agreement, on the part of the requesting party, that said reproduction is for his personal use and that subsequent reproduction will not occur without written approval of the author of this Dissertation. Further, any portions of the Dissertation used in books, papers, and other works must be appropriately referenced to this Dissertation.

Finally, the author of this Dissertation reserves the right to publish freely, in the literature, at any time, any or all portions of this Dissertation.

Author ___Nabamita Pal___

Date ___07 / 17 / 17___

DEDICATION

To my dear parents, Dr. Ujjal K. Pal, and Mrs. Ratna Pal, and my husband, Gaurab Dutta.

TABLE OF CONTENTS

ix

LIST OF TABLES

LIST OF FIGURES

ACKNOWLEDGMENTS

CHAPTER 1

INTRODUCTION

1.1 Research Motivation

Nitrogen oxide (NO) and nitrogen dioxide (NO_2) are two very harmful and toxic

gases, which together are called NO_x gases. There are many sources of NO_x in the

environment like factories, different utility equipment, and motor vehicles. Among all the

sources, diesel motor vehicles act as a major contributor of NO_x in the environment. NO_x

can cause harmful phenomena like acid rain and photochemical smog. It can impair a

person's visual capability of a human being and affect the lungs as well. So, it is a

necessity to limit the amount of NO_x in the environment. This is the reason behind

stringent NO_x emission standards made by the Environmental Protection Agency (EPA)

for diesel vehicles in the US and other countries. These emission standards are becoming

more stringent day by day. In addition, advancements in diesel engine technology are

resulting in substantially lower NO_x emissions. It is expected that future NO_x sensors will

need to detect emissions below 10 parts per million (ppm). Current NO_x sensors are able

to detect NO_x down to about 100 ppm. Hence, more sensitive and selective NO_x sensors

are needed to sense single digit ppm levels of NO_x in the exhaust gas mixture.

NO$_x$ sensors available in the market place today are made of mainly a zirconia

thick film electrolyte and platinum electrodes (Pt). These sensors are located in the

vehicle's exhaust pipes and allow precise measurements of the NO_x concentration in

the exhaust gas. These NO_x sensors are also known as smart NO_x sensors (SNSs) integrated with sensor control units capable of operating independently of the engine control units (ECUs). NGK Insulators LTD (**Figure 1-1**) and Continental Corporation are among the few companies who manufacture NO_x sensors for vehicle exhaust systems.
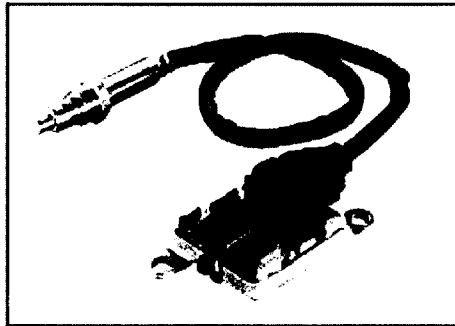
Figure 1-1: NGK NO_x sensor for diesel engine exhaust systems.

These sensors are robust and efficient, but until now the accuracy level achieved by this type of sensor is ±10 ppm [1]. As diesel engine technology improves, so too must NO_x sensor technology by providing sensors with even greater sensitivity, selectivity and accuracy. This necessity has made the diesel exhaust system NO_x sensor study a budding field for research.

1.2   Dissertation Overview

The goal of this research was to study the electrochemical behavior of dense electrodes for the purpose of selectively sensing lower concentrations of NO_x emissions from diesel engines. In this thesis study, perovskite based single-phase and composite electrodes, as well as Au/Pt twine electrodes were studied.

This dissertation consists of seven chapters. The first chapter discusses the research motivation and dissertation outline.

Chapter 2 covers the basic theories and background of NO_x sensing. This chapter starts with a basic discussion about the diesel engine exhaust system followed by NO_x emission standards, different types of NO_x sensing strategies, reviews of relevant electrode and electrolyte materials, and NO_x sensor operation.

Chapter 3 is comprised of the sensor fabrication methods, a brief discussion about the instruments used and sensor characterization techniques.

Chapter 4 consists of the detailed study about single-phase dense electrodes. LSM electrodes have been discussed in this chapter with vivid outcomes in terms of the sensing performance, selectivity, water and oxygen cross-sensitivity, probable rate limiting mechanisms and sensor accuracy.

Chapter 5 covers the study of dense composite electrodes. LSM-Au and LSM-YSZ and LSM-LSCF based composite electrode based NO_x sensors have been discussed in detail followed by a discussion about a novel composite NO_x sensor, which was composed of a dense composite electrode and a porous composite electrolyte.

Chapter 6 is composed of the detailed discussion about Au/Pt twinned electrodes for NO_x sensing.

Chapter 7 summarizes the findings and draws conclusions followed by a brief discussion on the scope of future work.

CHAPTER 2

BACKGROUND AND THEORY

The first part of this chapter, Section 2.1 discusses the exhaust system of a diesel

engine followed by a discussion of NO_x emission standards in United States and Europe

in Section 2.2. Section 2.3 presents a brief discussion about the different types of NO_x

sensors depending on their NO_x sensing technique. Thereafter, Section 2.4 discusses the

basic theory of impedance spectroscopy followed by the descriptions of different dense

electrode and porous electrolyte materials used for NO_x sensors fabrication in Section 2.5

and 2.6. The last section of this chapter is 2.7, which presents a description of the NO_x

sensor operation.

2.1   Diesel Engines

Diesel engines have a very high efficiency and compression ratio, which have

made it most widely used for internal combustion engines. Diesel engines are also called

'lean engines' as the fuel combustion takes place in an excess amount of oxygen. Diesel

engines operate via direct injection of fuel into a high-pressure combustion chamber

where the fuel goes through the following steps: atomization, evaporation, and diffusion.

Due to an excess of air, the flame speed becomes lower compared to gasoline engines,

though, lean burn engines are more proficient due to its higher compression ratio and

lower throttling losses. However, diesel engines have some undesirable chemical

component formation due to its lean burning technology. Particulate matter, hydrocarbons and NO_x are a few among them. This dissertation concentrates on NO_x sensors used in automotive diesel exhaust systems.

Diesel engines produce a lesser amount of NOx compared to gasoline engines due to lower flame temperatures caused by dilution in excess air inside the combustion chamber. Yet, the after-treatment system comprised of a three-way catalytic converter is not as effective at converting NOx in diesel engines because of the presence of large amount of air [2], [3]. The reducing gases that could have a reaction with the NOx tend to get oxidized by the overpowering quantity of additional oxygen.

To reduce the NO_x formation in a diesel engine reduction in flame temperature will be fruitful according to Zeldovich mechanism [4]. Delaying fuel injection timing can be a process to reduce flame temperature, but that can cause an increase in particulate formation according to particulate-NO_x trade-off curve [5], [6]. Exhaust gas recirculation (EGR) can be another way to lower the flame temperature, but this will reduce the amount of oxygen in the combustion chamber, which in turn will sacrifice the engine efficiency. Injection of a mixture of diesel and water can decrease NO_x formation, but this kind of mixture would be incompatible with modern diesel engine technology.

To treat NO_x after its generation is not as simple as in gasoline engines because of the excess air present. In the presence of a large amount of oxygen, it is difficult to reduce NO_x components at ppm levels. Selective catalytic reduction (SCR) is the most used method to reduce NO_x in diesel vehicles. In this process, a reducing agent, most commonly urea, is injected upstream of the exhaust gas in a catalytic converter mainly made of ziolytes. Urea forms ammonia, which reacts with NO_x and reduces it to nitrogen

and water. An alternative to SCR is the lean NO_x trap (LNT). In the NO_x trap, a catalytic

oxidation component converts NO to NO_2, and then NO_2 is absorbed by an alkaline earth

metal oxide BaO and forms a nitrite [7]. Regeneration of the nitride needs fuel, which

reduces the fuel efficiency of the engine. In spite of incorporating these NO_x abetment

methods, some amount (ppms) of NO_x reaches the tail pipe of the vehicle and get emitted

in the environment. To measure the NO_x concentration, it is necessary to mount a NO_x

sensor at the end portion of the tail pipe of the exhaust system in diesel vehicles.

Figure 2-1 shows the schematic of a diesel engine exhaust system.
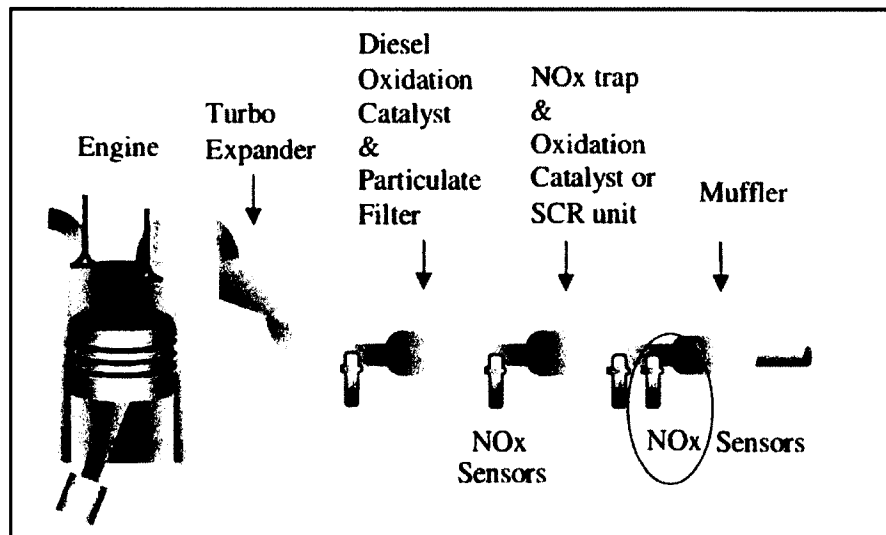
Figure 2-1: Simplified schematic of a diesel engine exhaust system.

NO_x sensors are a particular type of electrochemical cell that is derived from

oxygen sensor technology. It consists of electrodes and an electrolyte.

2.2   NOₓ Emission Standards

This section discusses NOx emissions standards for the US and Europe. These

standards are getting more stringent over time [8], [9]. In the US, the California Air

Resources Board and the Environmental Protection Agency have passed legislation for

on-board diagnostics (OBD) of heavy duty vehicles [10]. The NOx requirements

established for heavy duty vehicles in the US have consistently led Europe (**Figure 2-2**).
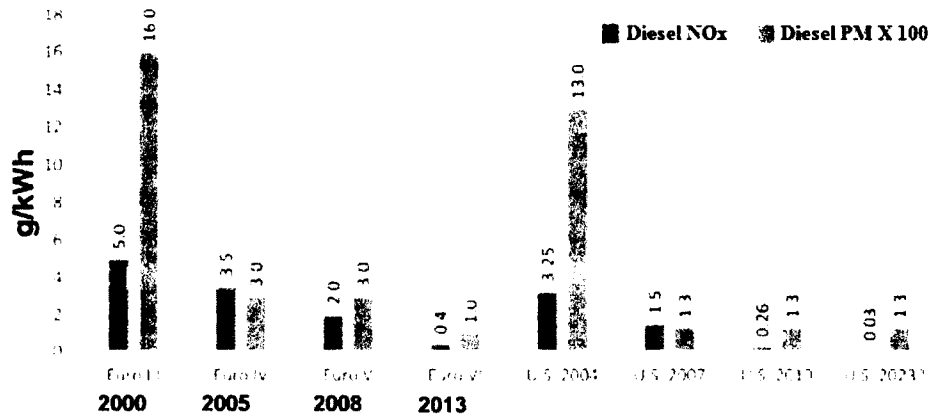
Figure 2-2: US and Europe Heavy Duty Engine emission standards [9].

From the above figure, it is apparent that to meet these standards, diesel vehicles

need to be monitored rigorously, and for that purpose, very sensitive and selective NO_x

sensors are needed. Environmental pollution control and fuel efficiency are major

motivations behind NO_x sensor related research work.

2.3   Different Types of NOₓ Sensors

There are three different kinds of sensitivity measurement techniques available for

NO_x sensors situated inside the diesel vehicle exhaust system. They are the (1)

amperometric, (2) potentiometric, and (3) impedancemetric approach. These distinctions

were made depending on the output electrical parameter (i.e., current, voltage, or impedance) of the sensor. Among these three types of sensors, the amperometric approach has been used in commercial NO_x sensing for over 40 years now. However, this method has some disadvantages like a very complicated circuit design and poor NO_x sensitivity below 10 ppm. Therefore, the potentiometric and impedancemetric methods are considered promising alternatives. Potentiometric sensors have a less complicated design, but they have displayed high cross-sensitivity towards hydrocarbons, CO and CO_2 [11]. Apart from possessing high cross-sensitivity to other gases, potentiometric sensors also display opposite electrical responses for NO and NO_2, which makes the data interpretation task challenging. The impedancemetric approach has been reported to show high sensitivity (down to 5 ppm) to NO_x [12–17], and it has a simple design.

Further details concerning each of these sensing methods are discussed in the following sections.

2.3.1   Amperometric NO_x Sensors

Commercial amperometric NOx sensors contain an array of two or three electrochemical cells in adjacent chambers [18], [19]. The first chamber eliminates excess O_2 from the exhaust gases while the second cell senses NOx gases. Diffusion through different chambers make the sensing response slower, and this type of sensor detects NO_x at concentration levels down to about 100 ppm.

As the exhaust gases flow inside the first chamber, the first cell electrochemically pumps O_2 out of the plenum so that it does not interfere with the NO_x measurement. This cell electrochemically reduces O_2 and pumps out O^{-2} ions. This is done by applying a bias of approximately -200 mV to -400 mV. A negative bias is essential to reducing O_2 to

8

oxygen ions. The current is proportional to O_2 concentration and is diffusion-limited.

Remaining gases diffuse into the next chamber, where a reduction catalyst reduces NO

into N_2 and O_2 (**Figure 2-3**). A bias of -400 mV is applied to the electrode of the sensing

cell to dissociate O_2, and then O_2 gets removed by electrochemical pumping [11]. This

diffusion limited current is proportional to the amount of oxygen that arrives at the

electrode from the dissociated NO_x [20].
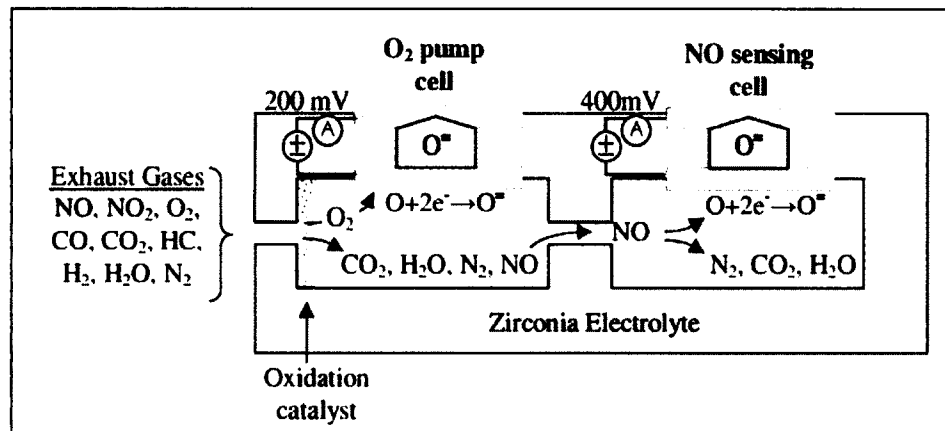
Figure 2-3: Amperometric NO_x sensor operation [10].

Shortcomings of Amperometric method

- The circuit design needed for this method is very complicated.

- The sensing is sluggish.

- Requires reference for ambient oxygen.

Potentiometric and impedancemetric sensing methods are able to overcome some of these

above mentioned disadvantages. These two methods are discussed in the following

sections.

2.3.2   Potentiometric NO_x Sensors

In this kind of sensor, the electrolyte is sandwiched between two electrodes. One of the electrodes is the sensing electrode, and the other one is the reference electrode. This is called 'Nernst Cell' structure. The electrodes are usually of different sizes. In these kind of sensors, the sensing electrode is exposed to exhaust gases, while the reference electrode may be exposed to the working gas or to atmospheric air. A potential difference exists due to the asymmetric electrodes and their different catalytic activities, disparate gas adsorption and different electrochemical reactions [21]. Typically, these types of sensors operate in the range of 500-600°C [11].

In **Figure 2-4** a potentiometric NO_2 sensor is shown, where the electrolyte is dense yttria-stabilized zirconia (YSZ) and electrodes are porous strontium-doped lanthanum manganite (LSM). This kind of potentiometric NO_x sensors are also called a 'mixed potential sensors'. Diesel vehicle exhaust gases contain both oxides and hydrocarbons species, so both reduction and oxidation reactions occur at the working electrode devoid of direct exchange of charge between the chemical species [22]. In this case, the open circuit potential results from both reduction and oxidation reactions. As these reactions tend to affect the potential in opposite directions, the result is a "mixed" potential. At the mixed potential, the current produced by multiple electrochemical reactions is equal to zero [23].
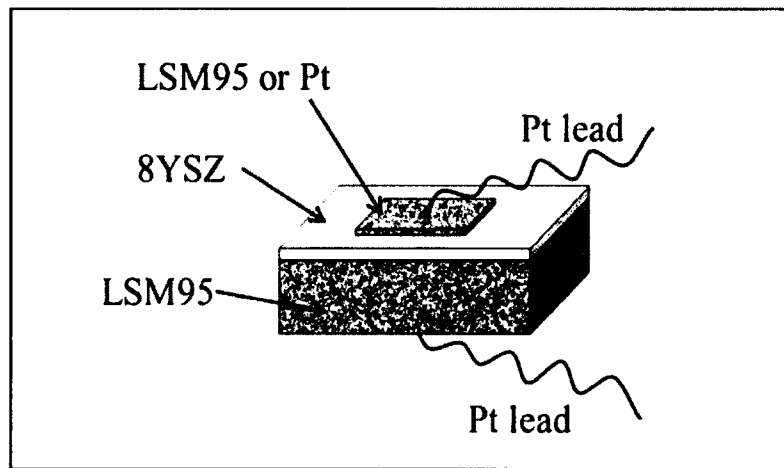
Figure 2-4: Schematic illustration of the NO_2 sensors [13].

Electrode materials for mixed potential sensors are selected to have absorption processes as the rate-limiting step. Electrodes typically comprise of semiconducting oxides or alloys of noble metals [11], [22].These sensors are strongly cross sensitive to several species (CO, O_2, hydrocarbons). Apart from this, NO and NO_2 generate electromagnetic forces (EMF) of opposite polarity, which incline to cancel each other out and decrease the signal's magnitude.

To address the problems related to cross-sensitivity and small potential difference, some sensing strategies have been developed for these sensors:

- Oxidizing all the hydrocarbons and CO by using noble metal catalyst.

- Achieving equilibrium of the NO_x mixture using noble metal catalyst.

- Conversion of NO to NO_2 by using a NO conversion electrode like Pt-Rh.

- NO_2 detection by using an oxide sensing electrode. The selectivity for a single NO_x species can be improved or inhibited by polarization of the sensing electrode. This gives control of selectivity to NO vs. NO_2 [22].

11

The operating temperature of the sensors can also be controlled to minimize cross sensitivity. If the temperature is below 600°C, then cross sensitivity to O_2 is reduced due to poor reaction kinetics [22]. In addition, with this technology it is challenging to detect total NO_x concentrations for lower ppm levels [24]. For these reasons, potentiometric NO_x sensors have not found widespread commercial use in automobile exhaust gas monitoring.

2.3.3   Impedancemetric NO_x Sensors

Impedancemetric NO_x sensing is a relatively new approach for automotive NO_x detection and monitoring. In comparison to amperometric and potentiometric NO_x sensing methods, the impedancemetric technique appears to offer greater sensitivity and accuracy. The impedancemetric response depends upon the operating frequency applied to the sensor, and the sensing response is generally based upon the modulus (i.e. $|Z|$, magnitude of the impedance) or the phase angle component of the impedance, θ. Mathematically, θ can be expressed as:

$$\theta = \arctan\frac{Z''}{Z'} \qquad \textbf{Eq. [1]}$$

The NO_x sensitivity can be determined from the expression $\Delta\theta/\Delta[NO]$ in units of degrees per ppm NO, where $\Delta\theta = \theta_{O2} - \theta_{NO}$. The term θ_{O2} is the angular phase response for baseline conditions where 10.5% O_2 and N_2 present; θ_{NO} corresponds to a specific amount of NO added to the gas stream.

The sensor geometry for impedancemetric NO_x sensors varies. Some studies have used sensors with configurations similar to those used in potentiometric studies. More elaborate configurations have involved sensing electrodes coiled around the electrolyte.

12

The sensor geometry can impact the sensing behavior as the distance between the

electrodes affects the oxygen ion transport path length. If this length is too large, then the

sensing response can diminish and become sluggish. The sensor geometry used in this

work is shown in Figure 2-5. The counter and working electrodes were separated by a

thick film porous electrolyte with a thickness of about 0.2 mm. This configuration

seemed to support sufficient NO_x sensing.

2.4   Electrochemical Impedance Spectroscopy Theory

Impedancemetric sensing is based on electrochemical impedance spectroscopy.

This section provides a discussion about the history and theory of electrochemical

impedance spectroscopy. **Figure 2-5** shows the diagram of an impedancemetric sensor.
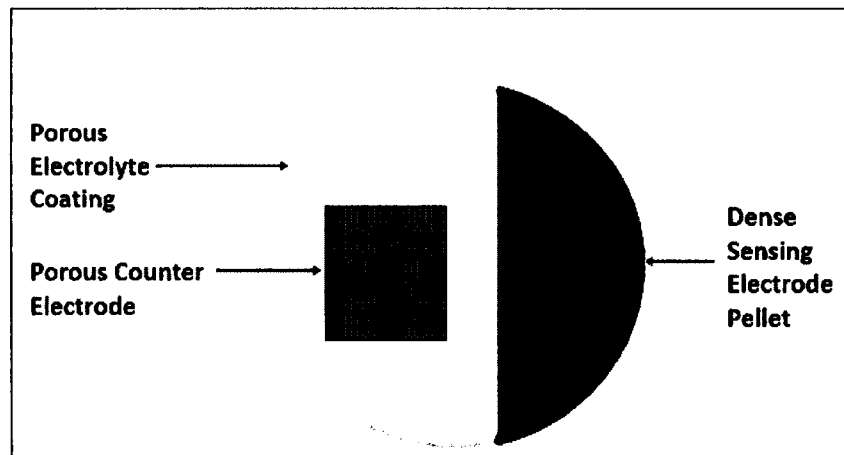
Figure 2-5: Impedancemetric NO_x sensor.

At the end of the 19th century, Oliver Heaviside defined the terms inductance,

capacitance, and impedance which established a mathematical foundation for electrical

circuit analysis. Walther Nernst is called the father of electrochemical impedance

spectroscopy (EIS) as he was given credit for measuring the dielectric constants of

aqueous electrolytes using the Wheatstone Bridge in 1894. James Bauerle was noted as the first to apply impedance spectroscopy methods to evaluating solid electrolytes in 1969 [25].

Electrochemical impedance spectroscopy has become a valuable and commonly used technique for examining the dynamics of mobile and bound charges within the bulk or at the interface of solid and liquid materials [26]. It is beneficial for studying the electrochemical behavior of NO_x sensors, and can provide knowledge about the NO_x reactions, and the composition, microstructure, and configuration of materials composing the sensor. Analysis of impedance data can also indicate potential reaction steps, such as adsorption, dissociation, diffusion, charge transfer and ionic transport that can promote or limit the electrochemical behavior of the sensor.

The impedance of a system can be measured by:

1) Applying a small signal alternating voltage, $v(t) = Vsin(\omega t)$

2) Measuring the current response $i(t) = Isin(\omega t + \theta)$

3) Calculating the impedance $Z(\omega) = v(t) / i(t)$.

The impedance is frequency-dependent. The phase angle, θ, quantifies lag or lead of i(t) with respect to v(t). **Figure 2-6** illustrates these essential concepts.

14
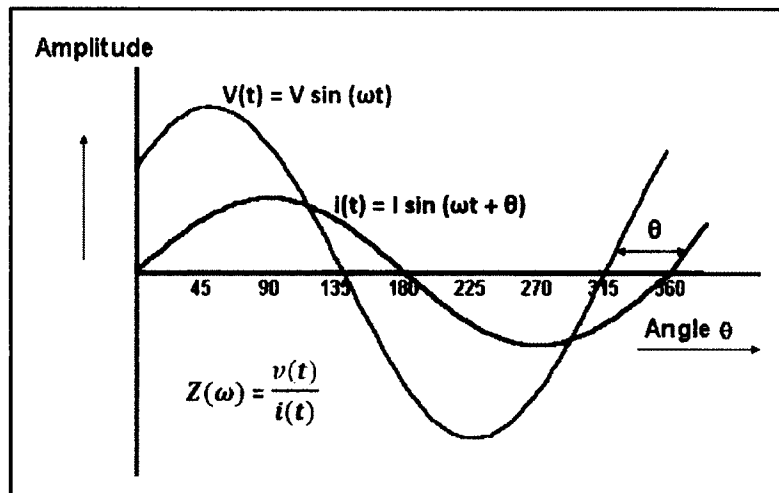
Figure 2-6: Basic concept of impedance spectroscopy.

The impedance is comprised of real and imaginary components represented by

Z_{real} (Z') and Z_{imag} (Z"), respectively. The expression for the impedance is as follows:

$Z(\omega) = Z' + jZ''$, where $j = \sqrt{-1}$. In the complex plane, the impedance can be

represented at each frequency by a vector whose magnitude, the modulus, is the length of

the vector as defined by the Pythagoras relationship:

$$|Z| = \sqrt{Z'^2 + Z''^2}$$ **Eq. [2]**

The angle that the vector makes with the abscissa is the phase angle θ

(**Figure 2-7**). This quantity also denotes the lag or lead of the response current at a

specific frequency. By trigonometry, the phase angle is defined on the complex plane as

$\tan^{-1}\left(\frac{Z''}{Z'}\right)$. The phase angle is usually the most sensitive parameter towards the

changes in the system. It is more sensitive than $|Z|$. Therefore, in impedancemetric

analysis, θ is often used as the measure of NO_x sensitivity.

15
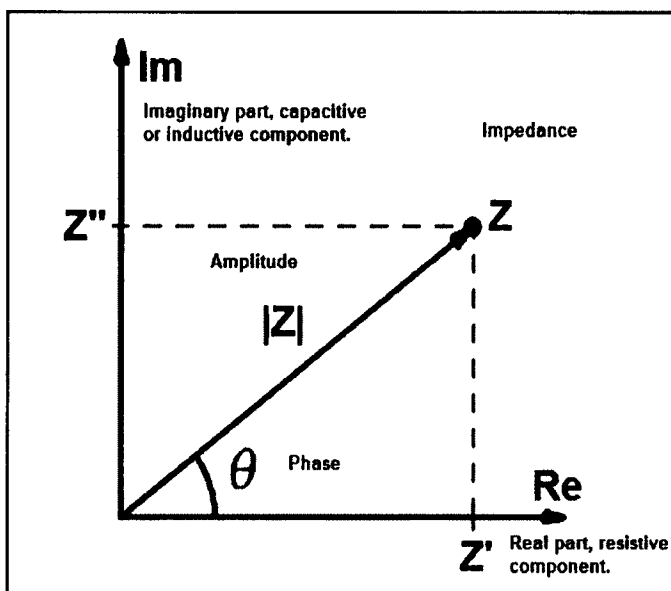
Figure 2-7: Relation between θ and |Z|.

2.4.1 Impedance Response

The Nyquist plot is a way to represent impedance data in the complex plane. For this reason, it is sometimes called a complex impedance plane plot [10]. Another name is a Cole-Cole plot. **Figure 2-8** is showing some basic information about the Nyquist plot. A Nyquist plot of impedance data recorded from a sensor with a yttria-stabilized zirconia electrolyte and strontium-doped lanthanum manganite working electrode exposed to 10.5% O_2 at 575°C, as shown in **Figure 2-8** below. The dominant features include two distinct arcs labeled "high frequency" (HFA) and "low frequency" (LFA).

The modulus and phase angle at 20 Hz are marked on the plot. The high frequency arc typically represents the reactions involving the bulk electrolyte, and these processes are kinetically controlled. So, for a specific temperature the behavior of HFA remains unchanged. The HFA is independent of the NO_x concentration of the system.

16

LFA represents the reactions at the triple phase boundary (TPB), and it is dependent on

the NO_x present in the environment. For this reason, the LFA plays an important role in

NO_x sensitivity measurements.
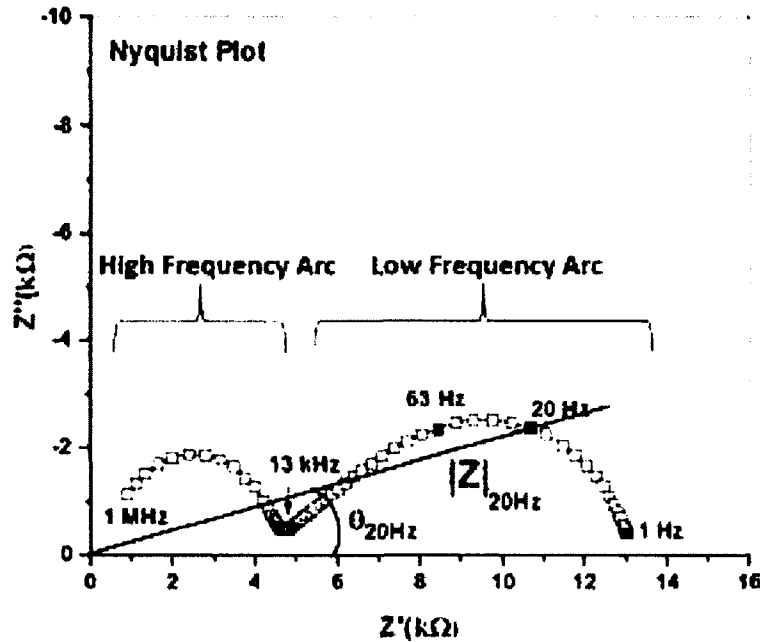
Figure 2-8: Familiarization with Nyquist plot.

From **Figure 2-9**, it is evident that the phase and $|Z|$ change with changes in NO_x

concentration. The LFA typically decreases with an increase in the NO_x concentration.

However, the HFA remains the same for both the 0 ppm and 100 ppm NO within the

Nyquist plot. This is the Nyquist plot of impedance data recorded from a sensor with a

YSZ electrolyte and LSM working electrode. Here, $|Z|_{20Hz}$ and θ_{20Hz} are the modulus of

the magnitude of impedance and phase angle at 20 Hz, respectively.

17
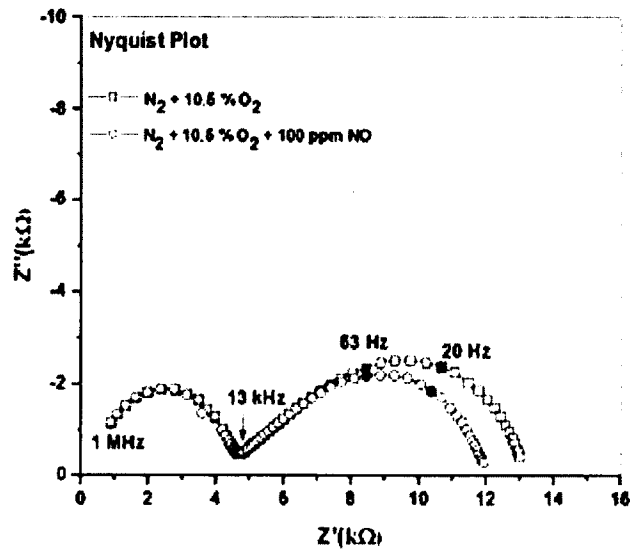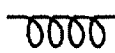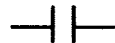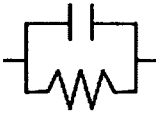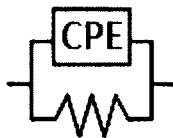
Figure 2-9: Change in LFA with change in NO$_x$ concentration.

2.4.2   Equivalent Circuit Analysis

The impedance response from electrochemical systems may be demonstrated by an equivalent circuit. The equivalent circuit can be helpful in explaining the physical processes going on at the electrode-electrolyte interface within a specific system. The output of the equivalent circuit must match the experimental data. There can be more than one circuit model for one system which fit the experimental results, but the appropriate model must explain the physical phenomenon associated with the electrochemical system appropriately.

Here, we will discuss different equivalent circuit elements that are commonly used to construct a circuit model (**Table 2-1**). If properly arranged, these elements can mimic the experimental result for the impedance plot. Resistors (R), capacitors (C) and inductors (L) are called ideal circuit elements, but there are also some other non-ideal elements like the constant phase element (CPE) and Warburg diffusion element (W).

18

Table 2-1: Details of different circuit elements

Element	Symbol	Circuit Symbol	Impedance (Z)	Physical Significance
Resistor	**R**	—/\/\/—	$R + j0$	Resistance of electrolyte or charge transfer
Inductor	**L**	ᴜᴜᴜᴜ	$0 + j\omega L$	Stray inductance from leads or human contact
Capacitor	**C**	—| |—	$0 + 1/j\omega C$	Capacitance from double layer charge
Constant Phase	**Q**	—|CPE|—	$1/[(j\omega)^n Q]$ $-1 < n < +1$	For C, n = +1 For R, n = 0 For L, n = -1
Warburg	**W**	—|W|—	$\sigma/\omega^{1/2} - j\sigma/\omega^{1/2}$ σ = Warburg parameter	Infinite or semi-infinite diffusion to electrode
Voigt	**(RC)**	(capacitor and resistor in parallel)	$(j\omega C + 1/R)^{-1}$	Interfacial charge transfer
Cole	**(RQ)**	(CPE and resistor in parallel)	$[(j\omega)^n Q + 1/R]^{-1}$ $0 < n < +1$	Electrode reactions along with grain boundary charge transfer

Sometimes two or more circuit elements are needed to make one element, like the Cole element. Similarly, a resister and a capacitor in parallel combination can be used to construct a Voigt element. A Nyquist plot with n number of arcs can be represented with

19

n number of Voigt circuits or a modified Voigt circuit (**Figure 2-10**), which is also called

Cole circuit in a series connection [27].
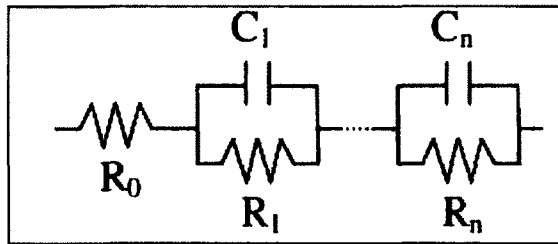
Figure 2-10: Voigt elements in series.

In **Figure 2-11**, a typical Nyquist plot of a NO_x sensor with dense LSM electrode

and porous YSZ electrolyte is shown along with its equivalent circuit.
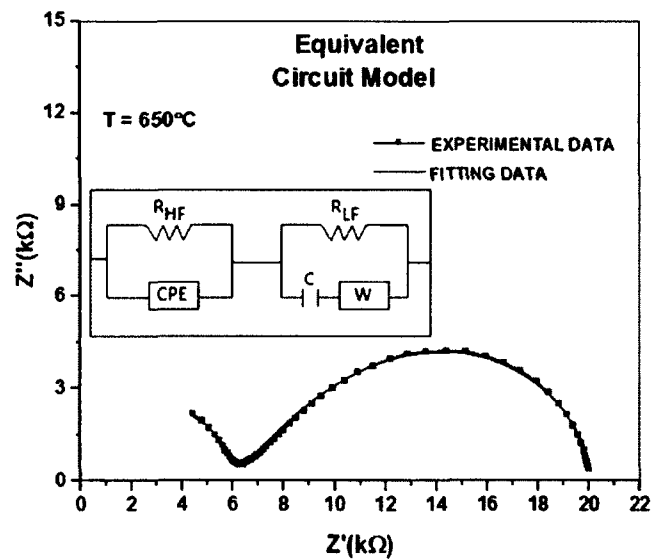
Figure 2-11: Nyquist plot with an equivalent circuit and the corresponding fitted data.

The fitting has been done using Marquardt-Levenberg or Simplex algorithm that

is part of the Gamry Echem Analyst software provided with the Gamry Reference 600

impedance analyzer.

It is possible to evaluate NO_x concentration from impedance data by calculating the phase angle difference at a specific frequency upon the introduction of NO_x. The change in phase is directly proportional to the change in the NO_x concentration, $\Delta\theta = \theta_1 - \theta_2$, where θ_1 and θ_2 are the phase angles for two different concentrations of NO_x in the system.

2.4.3   2-Point and 3-Point Impedancemetric Measurements

The impedance is typically collected using a 2-point or 3-point measurement technique. The 2-point method involves two electrodes where one is called the working electrode (WE) and the other the counter electrode (CE). The working electrode is the electrode in an electrochemical system in which the reaction of interest is occurring, and the counter electrode is the electrode that is used to close the circuit in the electrochemical cell. Using the 2-electrode method, the potential across the complete cell is measured [28].

The 3-point method involves another electrode called a reference electrode (RE) for the electrochemical measurement. The reference electrode is an electrode that has a stable and well-known electrode potential and it is used as a point of reference in the electrochemical cell for the potential control and measurement. In this case, the current flows between the CE and the WE [28]. The potential difference is controlled between the WE and the CE by positioning the RE. The 3-point setups have a distinct experimental advantage over 2-point setups as they can measure one half of the cell. That is, the potential changes of the working electrode are measured independent of the changes that may occur at the counter electrode. This is important and useful when the counter and working electrodes are different. For symmetric electrodes, the 2-point

21

impedance measuring technique is generally sufficient. Two-point and 3-point

measurement cell connection is shown in **Figure 2-12**.
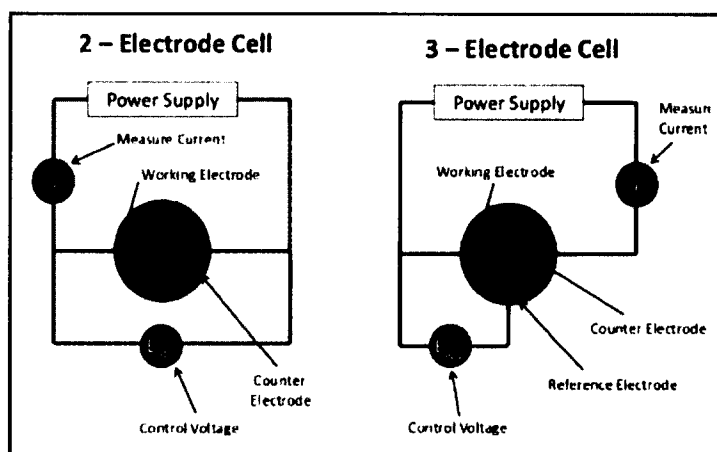
Figure 2-12: 2-point and 3-point measurements cell connection [28]

2.5   Dense NO$_x$ Sensing Electrodes

In electrochemical systems, the electrodes play a crucial role in the chemical

reactions taking place at the triple phase boundary (TPB). The TPB is the location where

the electrode, electrolyte and gas species come into contact [12]. To select the proper

sensing electrode, one has to depend on the empirical results as all the reaction

mechanisms are not clearly understood [22]. The NO$_x$ sensors that are available in the

market mainly use porous Pt based electrodes for NO$_x$ sensing purposes. Apart from

porous Pt other metals like Au and Ag have also been studied based on dense and porous

microstructures [16]. These studies have indicated that the microstructure of the

electrodes has a significant effect on the electrochemical behavior of the sensor. Different

electrode microstructures for different materials will be discussed in the subsequent

sections of this chapter.

2.5.1   Electrode Microstructure

Electrode microstructure is an important factor when it comes to NO_x sensing. The vast majority of the NO_x sensor electrode studies are based on porous electrode microstructures, as commercial NO_x sensors have porous electrodes to promote gas diffusion. Recent studies have found porous electrodes tend to enable heterogeneous catalysis, which can reduce the concentration of NO_x arriving at the triple-phase-boundary (TPB) [29]. This affects sensor accuracy, particularly for low NO_x concentrations, since electrochemical reactions affecting NO_x detection occur at the TPB. By adopting a dense microstructure for the electrodes and a porous microstructure for the electrolyte such reactions become limited; therefore, detecting NO_x can take place with greater accuracy [1], [16], [30]. For example, potentiometric studies comparing porous nano Au to dense Au electrodes for NO_x sensing verified sensors with the dense Au electrodes demonstrated greater sensitivity to NO_x [29]. Charge transfer was identified as the dominant rate limiting mechanism for the porous Au electrodes. Impedancemetric NO_x sensing studies on the NO_x sensing behavior of Au sensing electrodes have also found NO_x sensitivity to be greater for sensors composed of dense Au electrodes [16]. Related studies verified that dense Au sensing electrodes demonstrated rapid charge transfer kinetics, but were limited by dissociative adsorption of O_2 [26].

2.5.2   Single Phase Dense Electrodes

As stated in an earlier section, porous Pt electrodes are commonly used in NO_x sensors as the material tolerates the stringent exhaust gas environment [31]–[33]. However, Pt (atomic weight 78) whether porous or dense in the microstructure is a strong catalyst for O_2 reduction, which can interfere in accurately detecting NO_x at

23

concentrations below 10 ppm [16]. Au (atomic weight 79) is another well studied electrode material for NO_x sensors [34]–[37]. Au has good NO_x sensitivity and low water cross sensitivity, but it also has a thermal coefficient that is less compatible with the YSZ electrolyte [38]. This makes sensor durability challenging. Au also has a relatively low melting temperature that limits the fabrication temperature of the sensor [39]. To address these issues, metal oxides are under investigation. Some metal oxides (e.g., $LaSrMnO_3$) have a coefficient of thermal expansion coefficient that is close to that of the Y_2O_3-ZrO_2 electrolyte. For example, the thermal expansion coefficient of 8 mol% Y_2O_3-ZrO_2 and $La_{0.8}Sr_{0.2}MnO_3$ are $10.5 \times 10^{-6}/°C$ and $10.0 \times 10^{-6}/°C$, respectively. Several studies have found metal oxide electrodes, especially those with the perovskite (ABO_3) structure, demonstrate significant sensitivity to NO_x even with high concentrations of oxygen present [12], [40]–[45]. Perovskites are also attractive as a lower cost alternative to Pt electrodes.

Comparative studies on various perovskite electrodes have shown particularly high NO_x sensitivity in sensors with lanthanum-based perovskite electrodes [12], [40], [44], [45]. Ueda *et al.* reported strontium doped lanthanum manganite to show highest NO_2 sensitivity among all the La-based perovskite that were tested as sensing electrodes [45]. Woo *et al.* compared $LaSrMnO_3$ and Au sensing electrodes for NO_x sensing and found both of them to be almost equally sensitive, but in different operating temperatures [1]. In this study, $La_{0.8}Sr_{0.2}MnO_3$ (LSM) were evaluated as NO_x sensing electrodes. Au and Pt electrodes also have been studied in noble metallic electrodes.

The ceramic electrode material LSM is an electronic conductor. LSM is black in color and has a density of approximately 6.5 g/cm^3 [46]. The actual density will vary

24

depending on the processing method and actual stoichiometry. LSM has a rich electronic

phase diagram, including a doping-dependent metal-insulator transition, paramagnetism

and ferromagnetism [47]. LSM is a common cathodic material for solid oxide fuel cells

(SOFCs) because it has a thermal coefficient that is compatible with 8 mol% Y_2O_3-ZrO_2,

a widely studied electrolyte for SOFCs and solid state gas sensors.

2.5.3   Composite Dense Electrodes

An effective approach for enhancing gas sensor sensitivity and selectivity is

adding another component to the sensing electrode to form a composite, according to

numerous studies described in recent review articles by Miura *et al.* and Liu *et al.* [14],

[17]. Desired sensing properties can be tailored by varying the material composition and

microstructure of the electrode, which affect the electrochemical response of the sensor.

Numerous composite electrodes have been studied for enhanced sensitivity and

selectivity for CO, CO_2, NH_3 and hydrocarbon sensors [14], [48]–[60]. There have also

been some studies that have explored the potential of composite electrodes for NO_x

sensing [61]–[65]. For example, potentiometric NO_x sensors using Cr_2O_3-WO_3 sensing

electrodes demonstrated greater sensitivity to NO_2 along with a more rapid response time,

in comparison to WO_3 sensing electrodes [66]. Similar results were reported for Au-YSZ

composite sensing electrodes where impedance data indicated the addition of 10 wt%

YSZ to the Au electrode reduced the electrode resistance. The probable cause behind it is

the delocalization of electrode reaction through the entire electrode due to addition of

ionic conductor, thereby enhancing the electrochemical response of the sensor to NO_2

[67]. Perovskite composites have been used as catalysts for propane oxidation at solid

oxide fuel cells [68]; however, there appear to be limited studies concerning perovskite

composite electrodes with respect to NO_x sensing [69]. Impedance characterization studies on $La_{x-1}Sr_xMnO_3$ electrodes containing praseodymium- or gadolinium-doped ceria under NO_x gas environments suggest the ionic and electronic properties of the electrode can be modified to influence electrode reactions [70]. Thus, further study of perovskite composites for NO_x sensing can potentially provide insight for limiting undesirable reactions, such as water and oxygen cross-sensitivity, as well as offer additional knowledge regarding the role of electrode composition on reactions that influence NO_x gas sensing.

In addition to dense composite perovskite electrodes, Au-Pt composite electrodes were also considered. However, fabrication was not possible due to equipment limitations. As an alternative approach, Au/Pt twine electrodes were formed from Au and Pt wires. The idea was the Au would promote NO_x sensing while the Pt would support the electrode during high temperature firing steps. Initial experiments were carried out to verify the electrochemical behavior and NO_x sensing characteristics of the Au/Pt twined wires as the sensing electrode.

In this dissertation, LSM-Au, LSM-YSZ and LSM-LSCF composite electrodes, as well as Au/Pt twine electrodes, were studied in order to interpret their NO_x sensing properties.

2.6   Sensor Electrolyte

Yttria stabilized zirconia (YSZ) is an oxygen ion conductor. Structurally, YSZ comprises of large amount of zirconia (ZrO_2) with the balance containing yttria (Y_2O_3). Sometimes SiO_2 is added (1%) to reduce grain boundary development. These materials are the oxide form of the metals zirconium, yttrium, and silicon. Zirconium and yttrium are in neighboring columns on the periodic chart. Their valences differ by one. Yttrium (Y^{3+}) substitutes zirconium (Zr^{4+}) in the lattice. Since yttrium and zirconium are not isovalent, yttrium forms a different number of chemical bonds with neighboring oxygen atoms, and vacancies (lattice defects) are introduced to the lattice in order to maintain electro-neutrality. These vacancies are responsible for the oxygen ion (O_2^-) transport from one vacancy to another. Electrolytic ionic conductivity depends on temperature, composition (dopant concentration and distribution), microstructure (crystallographic phase), and density (porosity) [71]. Grain boundaries found at the interfaces of different phases exhibit vacancy depletion, retarding ion transfer. Micro cracks also increase resistance of the bulk material [71]. A high firing temperature during the sintering step raises both the density and the ionic conductivity. YSZ is not the best ionic conductor available. The bismuth oxide-based electrolytes have a much greater ionic conductivity than YSZ, but under low oxygen environment, these oxides degrades and become unstable. This property makes them unusable in exhaust gas sensors [72]. YSZ is stable, inexpensive and has very low electronic conductivity. Such properties make YSZ a favored electrolyte in SOFC and solid state gas sensor studies.

2.7   NO$_x$ Sensor Reaction Steps

NO$_x$ sensing reactions can involve several reaction steps. **Figure 2-13** illustrates

the diffusion of gases that may adsorb on the electrolyte surface and dissociate, as well as

undergo charge transfer at the triple-phase-boundary. The surface reaction steps can

occur in any order. Oxygen ion transport occurs through the electrolyte bulk. Although

the porosity of the electrolyte enables gas transport, it can also impede ionic transport. At

different sensor operating frequencies, some of the processes may contribute to the

impedance response, depending on the physical characteristics of the electrochemical

cell. The following reactions occur at the TPB during NO$_x$ sensing [73]:

$$\frac{1}{2}O^{2-} + 2e^- \leftrightarrow O^{2-} \qquad\qquad \text{Eq. [3]}$$

$$NO + O^{2-} \leftrightarrow NO_2 + 2e^- \qquad\qquad \text{Eq. [4]}$$

$$NO_2 \leftrightarrow NO + \frac{1}{2}O^2 \qquad\qquad \text{Eq. [5]}$$
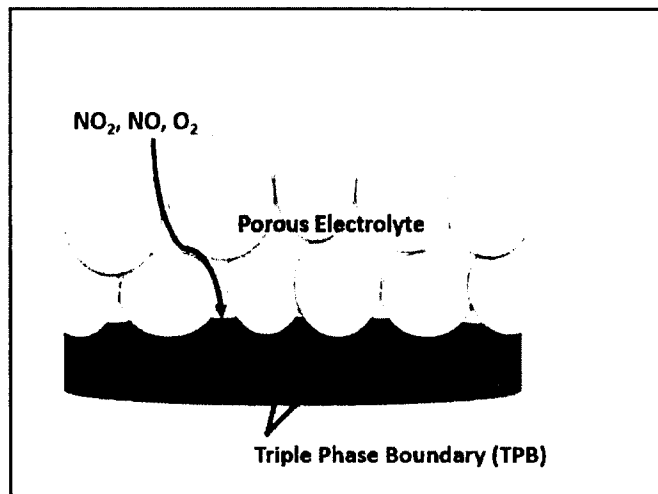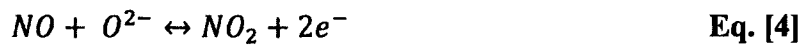
Figure 2-13: NO$_x$ sensing reaction steps.

28

CHAPTER 3

SENSOR FABRICATION, INSTRUMENTATION AND CHARACTERIZATION

In the first part of this chapter, Section 3.1 presents the NO_x sensor fabrication methods. This part for the NO_x sensor fabrication is divided into two sections: first one is for the dense perovskite electrode study and the other one is the Au/Pt twine electrode study. In Section 3.2, the instrumentation part or the experimental set-up in the laboratory is discussed. In Section 3.3 the characterization techniques used for the NO_x sensors are discussed. Scanning electron microscopy (SEM), energy dispersive x-ray spectroscopy (EDS), mercury intrusion porosimetry (MIP), x-ray powder diffraction (XRD), and Archimedes' method are discussed in the last section.

3.1   Sensor Fabrication

This section comprises of the details for the NO_x sensor electrodes and electrolytes fabrication. Two types of sensor fabrication process have been described in this section. The first one is dense perovskite based sensors and the other one is comprised of noble metal electrodes and porous electrolyte.

3.1.1   Perovskite Electrode Based NO_x Sensor Fabrication

LSM, LSM-Au, LSM-YSZ and LSM-LSCF electrodes were fabricated. The process mentioned here is common to all electrode fabrication. There were some small differences, which will be discussed in the section for that specific electrode.

LSM ($La_{0.8}Sr_{0.2}MnO_3$, Inframat Advanced Materials) powder was used to fabricate dense pellets for the single phase and composite electrodes. As received LSM powders were mixed with 3% B-76 Butvar (binder). The composites were made by adding the desired amount of Au, YSZ or LSCF powders. These powders were pressed into pellets under 200 MPa and sintered at temperatures ranging from 1350 -1400°C for 5-6 hours to achieve a reasonably dense microstructure. The diameter of the pellets was 11 mm with a thickness of about 1.1 mm following sintering. The electrode pellets were partially coated with an electrolyte slurry composed of YSZ (8 mol% Y_2O_3-doped ZrO_2, Tosoh Corp.) YSZ powder was mixed with ethanol, phosphate ester (dispersant) and B-76 Butvar (binder). The mixture was ball-milled for 16 hours using a 3D rotational mill to establish a homogeneous slurry. The electrolyte was coated on the electrode by using a paint brush. Several electrode pellets with a YSZ coating were fired at 1000°C for 1 hour where the furnace ramp rate was 2°C/min. Another slurry was made by ball-milling the electrode powder with methyl ethyl ketone (solvent), B-76 Butvar (binder) and corn oil (dispersant) for 22 hours. This electrode slurry was used to coat the counter electrode on the porous YSZ electrolyte and the pellets were then fired again at 1000°C (ramp rate was 2°C/min) for 1 hour resulting in **electrode$_{dense}$/YSZ$_{porous}$/electode$_{porous}$** cells to serve as NO_x sensors. The external leads were made for the sensors by attaching Au wires (0.2 mm dia., Alfa Aesar) with the electrodes using Au paste (Ted Pella Inc.).

Some LSM based NO_x sensors were fabricated with a Au counter electrode instead of a porous perovskite. In this case after partially coating the LSM pellet a Au wire (0.1mm dia. Alfa Aesar) was attached to the YSZ coated portion of the LSM pellet and the pellet along with the gold wire was fired in 1050°C for 1 hour to give the YSZ coating a porous microstructure. Then another gold wire was attached with the portion of the LSM pellet, which was not coated with YSZ slurry. This gold wire was attached on the LSM pellet by using a LSM paste. Here, the configuration of the sensor was LSM_{dense}/ YSZ_{Porous} /Au_{dense}. These gold wires were directly attached to Gamry impedance analyzer to collect electrical response.

3.1.2   Au/Pt Twine Electrodes Based NO_x Sensor Fabrication

Fabrication of Au/Pt sensing electrodes was carried out by wrapping Au and Pt wires together. Care was taken to ensure that the Au and Pt wires were evenly twisted together. The counter electrode was a Pt wire. The Pt and Au wires had a diameter of 0.25 mm.

The Au/Pt twine electrodes were attached to a YSZ electrolyte containing alumina. A low concentration of alumina was added to provide additional strength and to contribute to the conductivity of the electrolyte. The electrolyte was fabricated by mixing 8 mol% Y_2O_3-ZrO_2 (YSZ, Tosoh), 2 wt% Al_2O_3 (Alumina, Sigma Aldrich) and 3 wt% PVB 76 binder that was ball-milled with ethanol. Ethanol was evaporated from the slurry using a hot plate heated at 200-300°F. Due to ethanol absence, the slurry became dry. A mortar, pestle and sieve were used to make the dry slurry into a powder. Some of the resulting YSZ-2% Al_2O_3 powder was pressed into pellets. An Au/Pt twine electrode was placed over the electrolyte pellet along with a Pt counter electrode, and coated with the

YSZ-2%Al$_2$O$_3$ slurry. This slurry was made using the remaining YSZ-2%Al$_2$O$_3$ powder

and mixing it with ethanol. For performance comparison purposes, the sensors were also

fabricated with Au and Pt wires. The sensors were then fired at a temperature of 1050°C

for 1 hour. Both 2-point and 3-point measurements (discussed in Section 2.4.3) were

collected.

3.2   Instrumentation

The apparatus used to test the NO$_x$ sensors were contained within a fume hood.

The sensors were positioned in a quartz tube situated inside a tube furnace (Lindberg

Blue M, Thermo Scientific), which was programmable up to 1100°C. The furnace was

programmed with a heating/cooling rate of 2°C/min to avoid surface cracking on the

ceramic sensor. Two licensed NO$_x$ cylinders (500 ppm NO and 500 ppm NO$_2$) were used

as NO$_x$ sources. Air and N$_2$ were introduced to adjust the oxygen percentage and gas

mixture from the house lines. All of the gases were introduced to the system by four mass

flow controllers manufactured by MKS. Electrochemical impedance measurements were

collected using a Gamry Reference 600 (Gamry Instruments) for sensors operating at

temperatures ranging from 575 – 675°C. The electrodes of the sensors were connected to

the Gamry using ultra-thin gold wires (Alfa Aesar). Impedance spectroscopy data was

collected using a signal amplitude of 100 mV over a frequency range of 1 Hz - 1 MHz.

The sensors were exposed to NO and NO$_2$ at concentrations ranging from 0 - 100 ppm for

dry and humidified gas (3 – 10% water vapor) environments. The water vapor was

introduced to the system using a bubbler along with heated gas lines. The test exhaust gas

also contained O$_2$ at concentrations of 5% - 18% with N$_2$ as a balance. A standard gas

handling system with mass flow controllers was used to regulate and vary the gas

concentrations where the total flow rate was 500 sccm. Measurements were collected in triplicate to insure stable and reproducible data was collected. The experiment setup is shown in **Figure 3-1.**
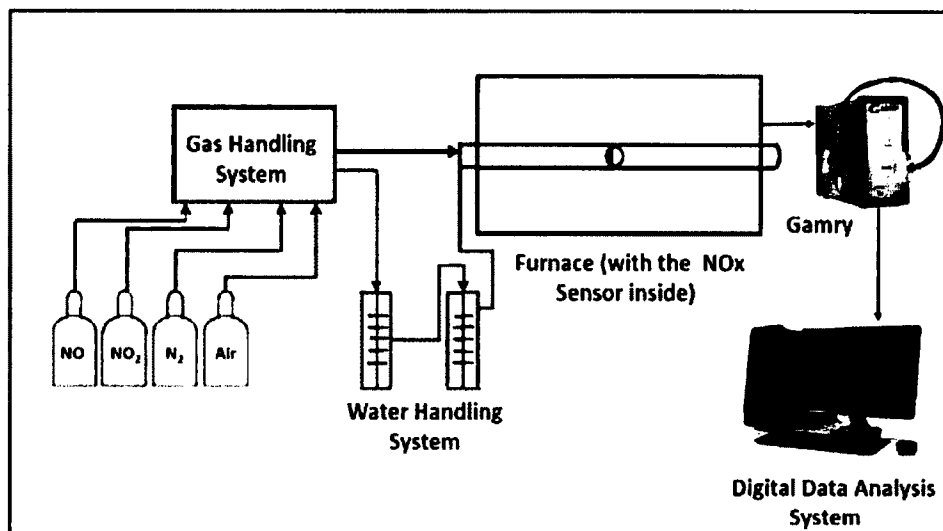
Figure 3-1: NO_x sensing set-up inside the laboratory.

3.3   Characterization

For microstructural characterization purposes, SEM, EDS, MIP, XRD and Archimedes' techniques were employed. The characterization results and images will be discussed in Chapters 4 and 5.

3.3.1   SEM and EDS

SEM imaging was used in this study for all the sensors to evaluate the microstructure of the electrodes and electrolytes. To study the composite electrode and electrolyte based NO_x sensors, EDS was primarily used for elemental mapping, which helped to interpret the distribution of the materials forming the composite. A mostly

33

homogeneous distribution of materials was observed for the LSM-YSZ electrodes and YSZ-Al$_2$O$_3$ electrolytes. For LSM-Au electrodes, this distribution was non-homogeneous. For specifically LSM-Au electrodes, backscattered SEM was used to get clear images of Au particles dispersed within LSM.

3.3.2 MIP

In this study, an AutoPore IV MIP machine manufactured by Micromeritics was used. The mercury porosimetry analysis technique is based on the intrusion of mercury into a porous structure under stringently controlled pressures from 0.2 to 50 psia (pound per square inch absolute). The increment can be as fine as 0.05 psia. This machine can determine a broader pore size distribution (0.003 to 1100 μm). Measuring the porosity was a very important task in this study. For solid state NO$_x$ sensors porosity is a key factor which can change the performance of the sensor substantially. So, MIP and the Archimedes' method (discussed later) were used to determine the porosity of the electrode and electrolyte pellets. For all the pellets, it was found that the porosity differed by ± 2% between the two porosity measurement techniques.

3.3.3 XRD

In this study, a Bruker D8 Discover XRD was used. XRD is a common technique used for determining information about the structures of crystals and atomic spacing inside them [1]. XRD was used mainly to determine the appropriate sintering temperature for the LSM-YSZ composite electrodes. For firing temperatures beyond 1300°C, there is a possibility of forming a resistive phase in LSM-YSZ electrodes due to chemical reactions between LSM and YSZ. If LSM and YSZ react, then a resistive phase can be

identified from XRD analysis. It was determined that the LSM-YSZ sensing electrodes could be fired as high as 1325 °C without resulting in unfavorable reactions.

3.3.4   Archimedes' Measurements

This is a manual process to calculate the density of a sample. It is based on Archimedes' buoyancy technique with dry weights, soaked weights and immersed weights in water (mercury, xylene or denatured alcohol if the refractory is water sensitive). In this method the apparent porosity, bulk density and apparent specific gravity are calculated from the dry, soaked and immersed weights. This technique was used to calculate the density of the electrodes and the porosity of the electrolyte pellets. The Archimedes' measurements were confirmed with MIP results.

CHAPTER 4

NO$_x$ SENSOR OPERATION WITH DENSE LSM SENSING ELECTRODES

In the first part of this chapter, Section 4.1 discusses NO$_x$ sensors with dense

La$_{0.8}$Sr$_{0.2}$MnO$_3$ (LSM) perovskite sensing electrodes and porous La$_{0.8}$Sr$_{0.2}$MnO$_3$ counter

electrodes. Section 4.2 presents the description of the NO$_x$ sensors consisting of dense

LSM sensing electrodes with Au wire counter electrodes.

4.1   Dense LSM Electrode Study with Porous LSM Counter Electrode

Dense LSM Electrode Study With Porous LSM Counter Electrode Using metal

oxide electrodes, particularly those with the perovskite (ABO$_3$) structure, instead of Pt

has been found to enable greater NO$_x$ sensitivity even with high concentrations of oxygen

present [12], [13], [20], [40]–[42], [45]. Among the most well studied perovskites is

strontium-doped lanthanum manganite (LSM), on account of its application in solid oxide

fuel cells. NO$_x$ sensor studies using LSM as the sensing electrode have found Sr

contributes to the NO$_x$ response as Sr promotes NO adsorption [45]. Although LSM is a

catalyst for oxygen reduction, sensors using LSM electrodes seem to exhibit lower cross-

sensitivity to oxygen in comparison to sensors composed of Pt electrodes.

There are few reports on the behavior of dense perovskites as NO$_x$ sensing

electrodes. Studies by Woo *et al.* found the sensing response to NO was comparable for

36

NO_x sensors utilizing $(La,Sr)MnO_3$ or Au sensing electrodes [12]. A key

difference was the sensors with $(La,Sr)MnO_3$ needed to be operated at 575 °C in order to

produce a similar sensing response to sensors using Au electrodes operated at 650°C

[12]. The difference in operating temperatures suggest that different kinetics were

involved. Greater understanding of the mechanisms and kinetic reactions governing

perovskite electrodes is needed to allow greater exploitation of the properties that

influence NO_x sensitivity.

4.1.1 Experimental

The fabrication process is discussed in detail in Sections 3.1.1 and 3.1.2. Here the

electrode powder consisted of LSM and 3 wt% binder. **Figure 4-1** shows the schematic

of the final sensor.

Porous
Electrolyte →
Coating

Porous Counter →
Electrode

Dense
Sensing
Electrode
Pellet
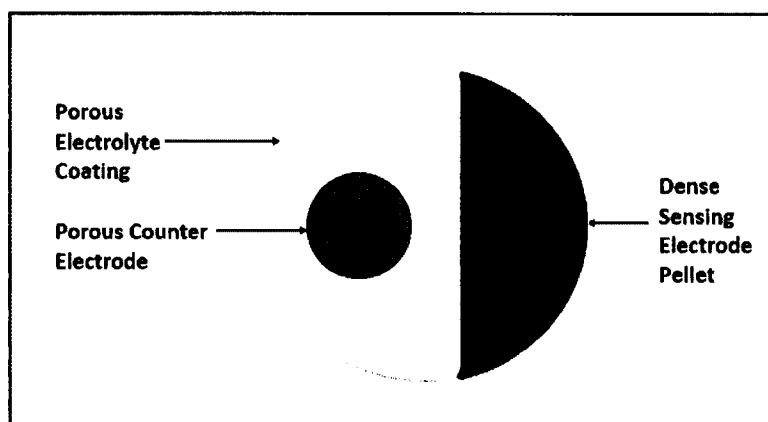
Figure 4-1: Schematic diagram of the NO_x gas sensor.

4.1.2 Characterization of the NO_x Sensor

Typical SEM images of the LSM electrode pellet and porous YSZ electrolyte

coating are shown in **Figure 4-2a** and **b**. Clear observable grains and grain boundaries

could be seen on the surface of the LSM pellet (**Figure 4-2a**). The LSM grain size was almost 20 μm × 20 μm.
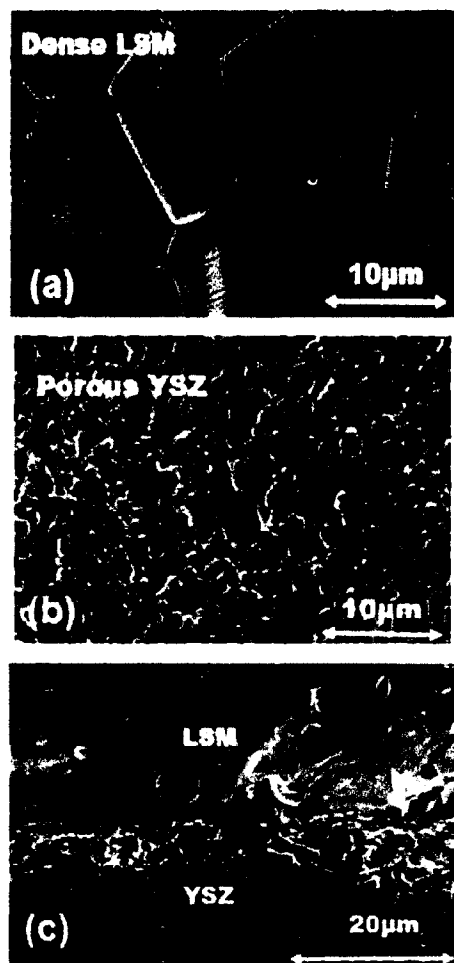
Figure 4-2: SEM images of the surface of (a) dense LSM pellet (b) porous YSZ coating and (c) cross-sectional view of the NO_x sensor.

Surface exchange reactions at LSM electrodes are reported to be more rapid along grain boundaries in comparison to the grain surface [74]. Thus, it is possible that the concentration of LSM grain boundaries along the TPB contributed to NO_x reaction rates. The density of LSM pellets without the YSZ coating was determined by the Archimedes' method to be about 92% ± 2%. Comparable results measured by MIP indicated the

pellets were 90% ± 3% dense. SEM surface images of the YSZ coating indicated a contiguous network of particles and dispersed pores as shown in **Figure 4-2b**. Prior studies of similarly prepared YSZ electrolyte coatings determined the electrolyte porosity to be approximately 46% based on computations analysis of SEM images [36]. The YSZ coating was determined to have a thickness of ~ 0.2 mm. Cross-sectional images indicated reasonable adhesion between the LSM electrode pellet and YSZ electrolyte coating (see **Figure 4-2c**). There were also some isolated closed pore within the dense LSM microstructure. The surface and cross-sections of the sensor components were free of cracks, and the low firing temperature of the YSZ electrolyte coating ensured the chemical integrity of the LSM/YSZ interface.

4.1.3 Result and Discussion

4.1.3.1 Impedance Behavior. Impedance measurements were collected for the LSM based NO_x sensors during operation with various concentrations of NO and NO_2 gases at temperatures ranging from 575 - 675°C. Thermodynamic conversion where much of the NO_2 is converted to NO at elevated temperatures [22]. Therefore, data presented in this work concentrates on sensor behavior with NO gas. **Figure 4-3a** shows the typical impedance response of LSM, sensing electrode based sensors with and without NO at an operating temperature of 575°C. **Figure 4-3b** shows the impedance response of the sensor with and without 10% water in the testing environment and **Figure 4-3c** displays the change in impedance response of the sensor with change in the operating temperature.

The impedance of the low frequency arc (LFA) of the Nyquist plots of the sensors decreased when sensors were exposed to 100 ppm NO or NO_2 in comparison to the baseline conditions with only 10.5% O_2 and N_2 present. The measured impedance was

lesser for humidified gas conditions compared to dry gas conditions for the sensors evaluated. This is illustrated in the data shown in **Figure 4-3b** where in each case the addition of 10% H_2O to the gas stream containing 10.5% O_2 and 100 ppm NO resulted in an impedance that was smaller than the dry gas measurements with oxygen and NO. Water vapor is understood to form hydroxyl groups at perovskite and YSZ surfaces [75], [76]. The addition of water vapor may facilitate the charge transfer process in the triple phase boundary which reduced the measured impedance [77]. From the impedance plot obtained in different temperatures (575°C - 675°C) it was found that the value of the impedance decreased with an increase in the temperature. Increase in temperature may help to proceed the NO_x reactions more readily causing a deduction in the measured impedance value. The impedance data for the sensors consistently presented a high frequency arc (HFA) followed by a substantially larger low frequency LFA.

The HFA described YSZ electrolyte reactions that is independent of gas concentration as it is kinetically controlled and remains same for all the NO_x concentrations at a particular temperature. The ionic conductivity of YSZ dependents on the yttria content and porous microstructure of the electrolyte coating, impacted reactions governing the electrolyte HFA response [36], [78]. The LFA described the impedance associated with reactions occurring at the sensing electrodes and electrode/electrolyte interface. The exhaust gases, O_2, NO, and NO_2, participate in interfacial reactions according to the equations described in Section 2.7.
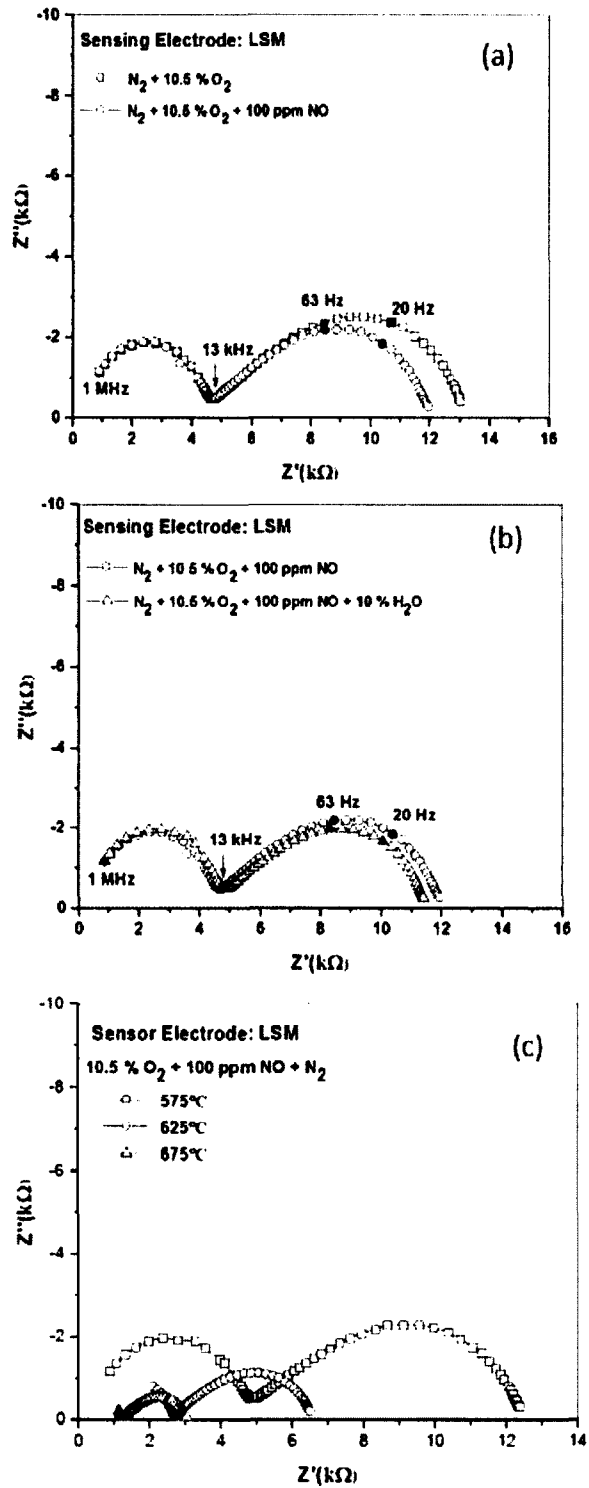
Figure 4-3: Change in impedance response of the NO$_x$ sensors with the change in (a) NO concentration, (b) dry and 10% water, and (c) operating temperature.

4.1.3.2   Equivalent Circuit Modeling. Equivalent circuit modeling was used to fit the measured impedance data in order to further study the electrical response of the LSM based NO_x sensors. As shown in **Figure 4-4**, two parallel circuits were found to model the impedance data where the high and low frequency arcs were described by $R_{HFA}CPE$ and $R_{LFA}(CW)$ circuits, respectively. This circuit model was used to fit all impedance data collected at the various operating temperatures and gas concentrations. The resistance, R_{HFA}, was associated with reactions taking place within the porous YSZ electrolyte, and the constant phase element, CPE, was related to the non-ideal capacitance behavior. The impedance, Z_{CPE}, due to the CPE is defined by:

$$Z_{CPE} = \frac{1}{Y_0(j\omega)^n}$$ **Eq. [6]**

where n is a constant such that $n = 1$ describes a capacitor with a value of Y_0. The angular frequency is $\omega = 2\pi f$, and f is the applied operating frequency. In the second parallel circuit, R_{LFA} was associated with the resistance of the LSM electrode and LSM/YSZ interfacial reactions. The model included a Warburg impedance, Z_W, and capacitor, C, which can be represented by the following relationships:

$$Z_W = [Y_0\sqrt{j\omega}]^{-1}$$ **Eq. [7]**

$$Z_C = [C\sqrt{j\omega}]^{-1}$$ **Eq. [8]**

The Warburg element described the impedance resulting from the diffusion of ionic species at the LSM/YSZ interface. The impedance due to capacitance effects has been associated with the oxygen coverage at the electrode/electrolyte interface within NO_x sensors [79], [80].

42
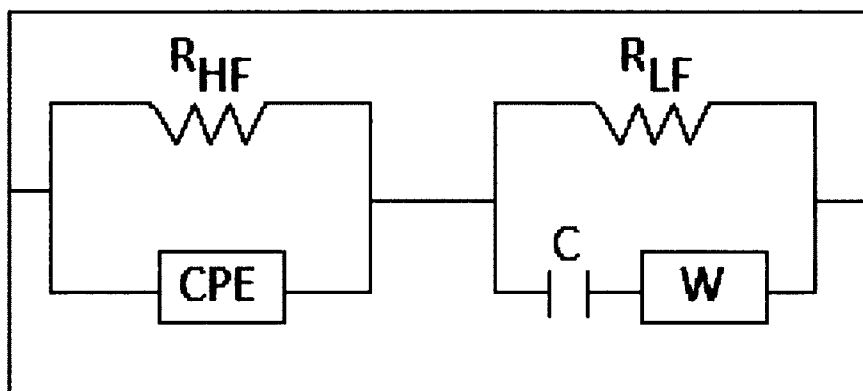
Figure 4-4: Equivalent electrical circuit for the LSM based NO$_x$ sensor.

For both the dry and humidified gas conditions, R_{LFA} decreased with an increasing

operating temperature most likely due to an increase in charge transfer reaction rates. The

magnitude of R_{LFA} determined by the model was slightly larger for humidified gas

conditions compared to dry conditions. The Warburg element took into account the slope

of the LFA that was approximately 45°. As the operating temperature increased, the

Warburg impedance also increased, and the humidified data was marginally higher in

magnitude in comparison to sensor data collected under dry conditions.

The model also indicated a decrease in capacitance as the sensor operating

temperature increased. However, the capacitance element tended to decrease for

humidified gas environments. If the capacitance described the oxygen coverage at the

LSM/YSZ interface, then the addition of water vapor may reduce the concentration of

oxygen at the interface. The water molecules or gas species resulting from water

reactions may block sites along the interface that oxygen molecules would have

occupied.

4.1.3.3   NO Sensitivity. The phase angle component of the impedance, θ, is highly

sensitive to changes in NO_x concentration. Hence, the change in the phase response, $\Delta\theta$,

was used to assess sensor sensitivity according to **Eq. [1]**:

$$\theta = tan^{-1}\frac{Z''(\omega)}{Z'(\omega)}$$

where $Z'(\omega)$ and $Z''(\omega)$ are the real and imaginary components of the impedance, and

$$\Delta\theta = \theta_{O_2} - \theta_{NO} \qquad \textbf{Eq. [9]}$$

where θ_{O2} corresponded to the baseline phase angle response with only 10.5% O_2 and N_2

present, and θ_{NO} corresponded to the phase angle response with the addition of NO in the

gas stream. The sensitivity of the LSM based sensors to various concentrations of NO is

shown in **Figures 4-5** at 575°C at an operating frequency of 20 Hz for dry and 10%

humidified conditions. The sensitivity of the LSM based sensors clearly had two different

regimes. The first one is from 0 – 50 ppm of NO and the second one is for 50 – 100 ppm

of NO.
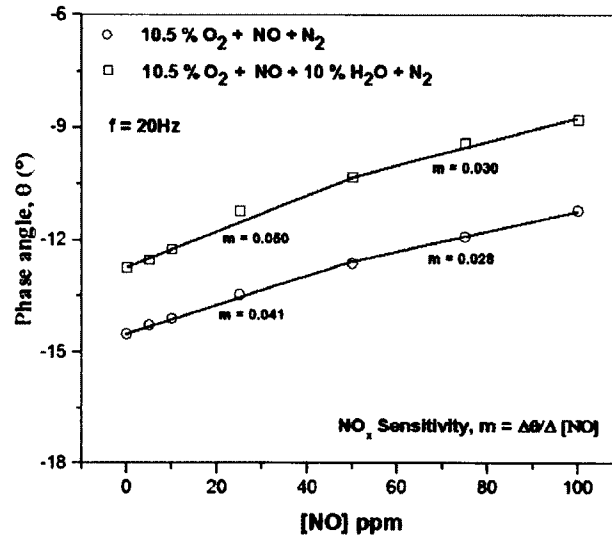
Figure 4-5: NO sensitivity plot for dry and 10% humidified condition at 575°C.

NO sensitivity was higher for humidified gas conditions shown in **Figure 4-6**. In this figure, the NO sensitivity for the LSM based sensors with different water concentrations (3% - 10%) has been shown for 20 Hz at 575°C. Some studies suggest heterogeneous catalytic oxygen reactions are inversely related to water reactions at perovskite electrodes[75]. For such a case, NO_x sensors should yield higher sensitivity responses in humidified versus dry gas conditions.
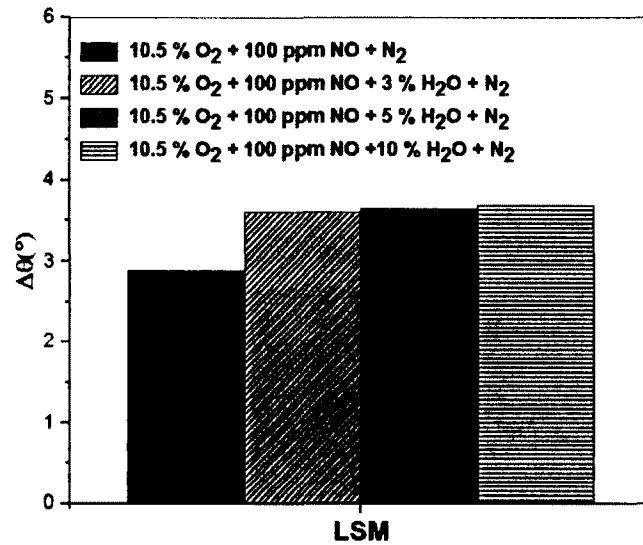
Figure 4-6: NO sensitivity comparison for dry and different humidified conditions at 575°C for 20 Hz.

Here, the LSM based NO_x sensors showed almost a 25% greater sensitivity to NO for humidified gas conditions. These results suggest the humidity of the gas stream may interfere with oxygen catalytic reactions, thereby allowing NO_x reactions to proceed more readily. From **Figure 4-6** it can be concluded that NO sensitivity of the NO_x sensor increased with the water participation, but it is almost independent of the concentration level of water.

4.1.3.4   Oxygen Dependence

In this study, the data was collected for different concentration of O_2 (5% - 18%).

Figure 4-7a shows the O_2 sensitivity of the LSM based NO_x sensor at 575°C for 20 Hz

and 1000 Hz without NO. **Figure 4-7b** shows the NO sensitivity of the LSM based NO_x

sensor with 10.5% O_2 at 575°C for 20 Hz and 1000 Hz.
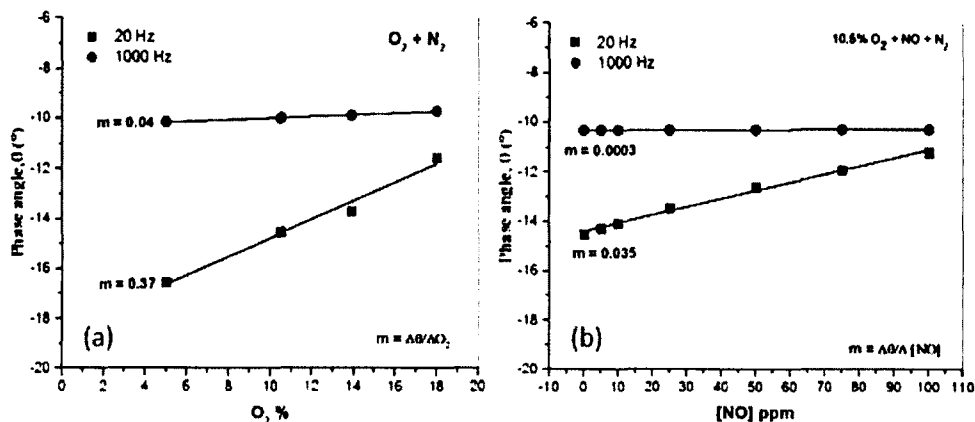
Figure 4-7: Comparison of (a) O_2 and (b) NO sensitivity of the LSM based NO_x
sensor at 575°C for 20 Hz and 1000 Hz.

Comparing both figures we can say the O_2 dependence of the sensor is dependent

on the operating frequency and at 1000 Hz the sensor has almost no sensitivity for NO,

but it is still sensitive to O_2. The same phenomena was observed in this ref article [73]. So

it can be concluded that at 1000 Hz and beyond, this sensor is working only as an O_2

sensor.

Oxygen reduction reactions at dense LSM electrodes have received attention for

SOFCs [74], [81], [82].Oxygen reduction reactions at the LSM electrode impact reactions

at the TPB where NO_x reactions occur. Numerous studies report oxygen reduction in

LSM taking place according to two separate reaction pathways. One reaction pathway

proceeds by oxygen diffusion to the TPB where the electrode, electrolyte and gas phase

come together, resulting in electrochemical oxygen reduction [81]. The other reaction pathway is based upon surface adsorption, resulting in oxygen ion transport through the electrode. This reaction pathway is typically limited to thin film LSM electrodes as oxygen ionic conductivity in LSM is low. In the present study, the porous YSZ electrolyte enabled oxygen gas diffusion to the TPB such that electrochemical reactions influenced by the LSM electrode were able to proceed. The oxygen concentration of the test gas was varied to determine the oxygen partial pressure dependence of the NO_x sensors and potential rate limiting reaction mechanisms. **Table 4-1** shows the NO_x sensor oxygen partial pressure dependence for operating temperature 575°C with and without NO and 10% water vapor where the oxygen concentration varied from 5 - 18% with N_2 as the background gas.

Table 4-1: PO_2 dependence of LSM based NO_x sensor at 575°C

Value of *m* in 575 °C			
$O_2 + N_2$	$O_2 + 75$ ppm NO + N_2	$O_2 + 10 \% H_2O + N_2$	$O_2 + 75$ ppm NO+ 10 % $H_2O + N_2$
- 0.17	- 0.13	- 0.27	- 0.24

The data can be described by the power law relationship, $R_{LF} \alpha (P_{O_2})^m$, where *m* is the slope and R_{LFA} was determined from equivalent circuit analysis. The slope associated with the oxygen partial pressure dependence is generally correlated with specific reaction mechanisms describing oxygen related processes at the electrode and electrode/electrolyte interface [83]. Here, *m* was found to range from approximately -0.17 to -0.27 as the operating condition changes. The data in **Table 4-1** corresponding to

47

sensor operation at 575°C suggested in humidified condition charge transfer was rate-limiting step m was close to -0.25. In dry conditions the LSM based sensor showed low PO_2 dependence.

4.1.3.5   Temperature Dependence. The temperature dependence of the sensors is described by the Arrhenius plot shown in **Figure 4-8** using R_{LF} values from the equivalent circuit modeling results. Analysis of this data was used to determine the activation energy of the sensors in the presence of 10.5% O_2 with 100 ppm NO under dry and 10% humidified gas conditions. The calculated activation energies were approximately 1.040 ± 0.034 eV and 1.034 ± 0.012 eV for dry without and with 100 ppm NO respectively. For 10% humidified condition, the activation energy for 100 ppm NO is reduced to 0.98 ± 0.020 eV. The slight decrease in the activation energy for humidified gas conditions is in agreement with the decrease in impedance observed in **Figure 4-3b** for the humidified data. This finding indicates the addition of water may interfere with sensor operation. The activation energies reported here are significantly lower than those typically reported for LSM based electrochemical devices. Most likely, this difference is related to the LSM electrode microstructure. More often, LSM electrodes are fabricated to have a porous microstructure, which is desirable for solid oxide fuel cells. However, dense electrodes have been found to limit heterogeneous catalysis in NO_x sensors, which promotes greater sensitivity to NO and NO_2 [1], [16]. In addition, the dense electrodes provide more efficient transport of electrons through electronic pathways within the LSM electrodes, thereby contributing to a lower activation energy. In other studies where dense Au electrodes have been incorporated in NO_x sensors, activation energies similar to those

determined in this study were reported [16], [26]. This indicates the impact of electrode microstructure on activation energy.
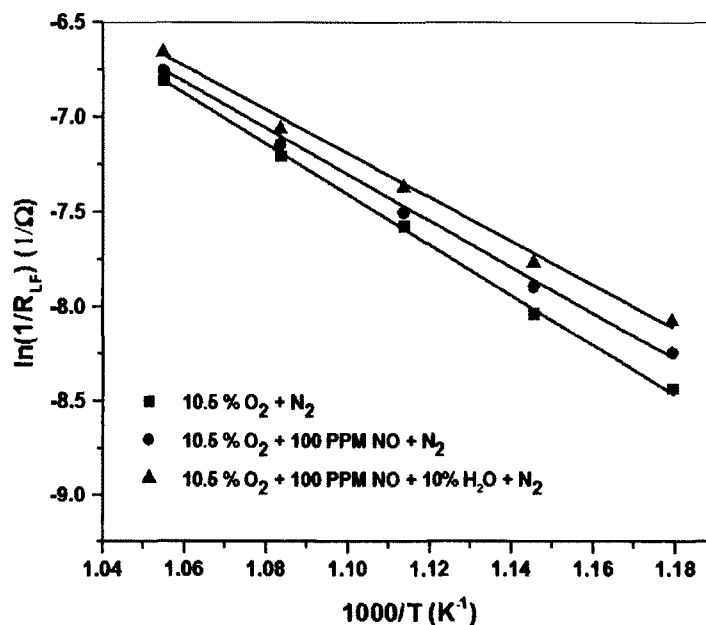
Figure 4-8: Plot to calculate activation energy for 0 and 100 ppm NO in dry and humidified condition for the LSM based NO_x sensor.

4.1.3.6 CH4 Cross-sensitivity

From Figure 4-9 it can be seen that at 575°C the LSM based sensor is more sensitive to NO than it is for CH_4, but as temperature increases the NO_x sensitivity is reduced substantially, but CH_4 sensitivity is not decreasing as rapidly as NO, as a result, in 625°C and 675°C the sensor becomes more sensitive to CH_4 than NO. As the operating temperature increased, NO sensitivity diminished. Woo *et al.* reported similar observations for LSM based NO_x sensors where NO sensitivity increased when the sensor operating temperature decreased from 650°C to 575°C. The decrease in sensitivity may be related to thermally activated oxygen kinetic reactions [84]. If oxygen reactions are

49

able to proceed more readily at the LSM/YSZ interface in comparison to NO reactions, then NO sensitivity may be compromised.
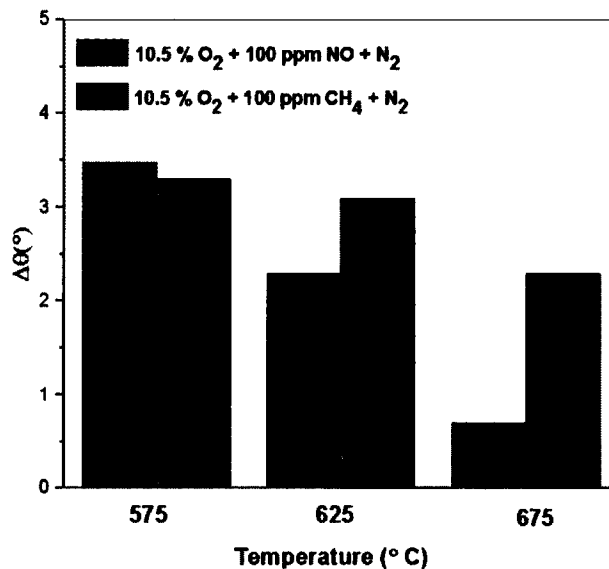
Figure 4-9: Cross-sensitivity study for CH_4 in dry condition at 575°C.

4.2 Dense LSM Electrode Study with Au Counter Electrode

4.2.1 Experimental

The fabrication process is discussed in detail in the Section 3.1.2.1. Here the electrode power consists of LSM and 3 wt% binder and the counter electrodes are Au wires. **Figure 4-10** shows the schematic of the final sensor.
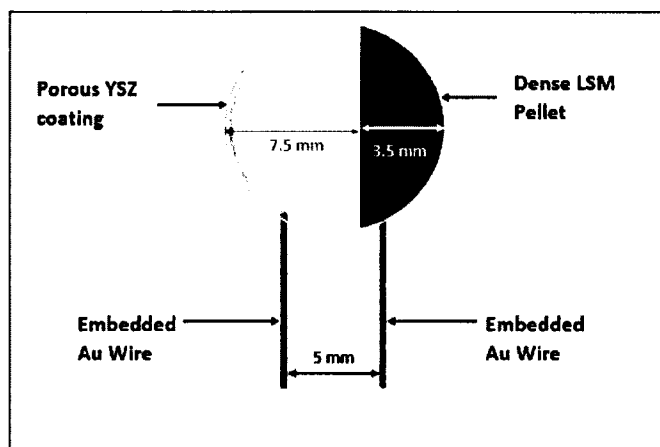
Figure 4-10: Schematic diagram of the NO_x gas sensor with Au counter electrode.

4.2.2 Result and Discussion

4.2.2.1 Impedance Behavior.

Impedance measurements were collected for the LSM based NOx sensors during operation with various concentrations of NO and NO_2 gases at temperatures ranging from 550 - 700°C. For each operating temperature, the impedance data for the sensors consistently presented a high frequency arc (HFA) followed by a substantially larger low frequency arc (LFA). The HFA described YSZ electrolyte reactions that were independent of gas concentration. The YSZ ionic conductivity, which depends on the yttria content and porous microstructure of the electrolyte coating, impacted reactions governing the electrolyte HFA response [36], [78]. The LFA described the impedance associated with reactions occurring at the LSM electrode and LSM/YSZ interface. The exhaust gases, O_2, NO, and NO_2, participate in interfacial reactions according to Equations 3, 4 and 5.

The LSM electrode provides electronic pathways for electrons to travel to the LSM/YSZ interface. Since the LFA dominated the overall impedance response of the sensors, the electrical properties of the LSM electrode, along with reactions occurring at

51

the LSM/YSZ interface influenced the behavior of the NO_x sensors. **Figure 4-11a** also shows the impedance of the LFA decreased as the sensor was exposed to greater concentrations of NO, thereby indicating the addition of NO at the LSM/YSZ interface promoted NO_x reactions described in Eq. 3, 4, 5. It is important to note that the embedded Au wire electrode within the sensors predominantly functioned to complete the electrical circuit of the sensor as the reaction area surrounding the Au wire was substantially smaller than that of the LSM pellet.
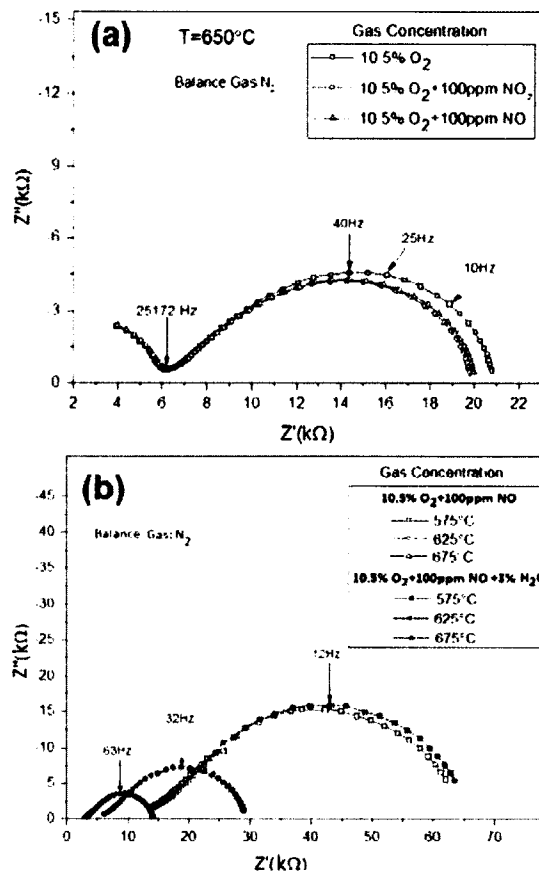
Figure 4-11: Electrical response of LSM based NOx sensor: (a) with and without NO and NO_2 gases at 650°C and for (b) dry and humidified gas conditions for various operating temperatures.

The impedance response for sensors exposed to NO_2 was very similar to that for NO, as shown in **Figure 4-11a**. This has been observed in other studies and attributed to thermodynamic conversion where much of the NO_2 is converted to NO at elevated temperatures [12]. Therefore, data presented in this work concentrates on sensor behavior with NO gas.

Figure 4-11b illustrates the impact of water vapor on the low frequency impedance response of the sensors as the operating temperature changed. (The high frequency data is not shown as it is independent of gas concentration.) The addition of about 3% water to the gas stream caused a slight increase in the LFA for the sensors. The impact of water on the sensor impedance became less significant as the operating temperature increased. For both the dry and humidified gas conditions, the magnitude of the impedance decreased with increasing sensor operating temperatures as reactions governing the electrode and electrode/electrolyte interface were able to proceed more readily.

There is some uncertainty regarding the mechanisms governing NO_x sensor behavior in humidified gas environments as the results from different studies tend to vary [75], [85]. The microstructure and materials composing sensor components, as well as the operating conditions can cause the results to differ. Some studies report humidified gas environments can increase OH-coverage on the surface of the LSM electrode, and limit molecular oxygen adsorption. Thus, oxygen kinetic reaction rates can be reduced in the presence of water. In such a case, NO_x reactions may proceed more readily, resulting in increased NO_x sensitivity [75].

4.2.2.2   Equivalent Circuit. Equivalent circuit for the LSM based NO_x sensor with Au counter electrode is exactly the same as discussed in Section 4.1.4.2.

4.2.2.3   NO Sensitivity. The sensitivity of the LSM based sensors to various concentrations of NO at different operating temperatures is shown in **Figures 4-12a** and **b** for measurements collected under dry and humidified gas conditions, respectively. The sensitivity of the LSM based sensors achieved a maximum in the temperature range 600°C - 625°C for both dry and humidified gas conditions. As the operating temperature increased, NO sensitivity diminished. Woo *et al.* reported similar observations for LSM based NO_x sensors where NO sensitivity increased when the sensor operating temperature decreased from 650°C to 575°C. The decrease in sensitivity may be related to thermally activated oxygen kinetic reactions [84]. If oxygen reactions are able to proceed more readily at the LSM/YSZ interface in comparison to NO reactions, then NO sensitivity may be compromised.

NO sensitivity was slightly higher for humidified gas conditions shown in **Figure 4-12b**. Some studies suggest heterogeneous catalytic oxygen reactions are inversely related to water reactions at perovskite electrodes [75]. For such a case, NO_x sensors should yield higher sensitivity responses in humidified versus dry gas conditions. Here, the LSM based NO_x sensors showed almost a 5% greater sensitivity to NO for humidified gas conditions. These results suggest the humidity of the gas stream may interfere with oxygen catalytic reactions, thereby allowing NO_x reactions to proceed more readily.

The NO sensitivity of the LSM based sensors with a Au counter electrode was significantly smaller than the LSM based sensors with a porous LSM counter electrode.

54

This was evident by comparing the sensing response at 575°C where $\Delta\theta/\Delta[NO]$ was

about 0.041 degrees/ppm NO for sensors with the porous LSM counter electrode, versus

about 0.015 degrees/ppm NO for sensors with the dense Au wire counter electrode. The

difference between the data could be due to adhesion problems between the Au and YSZ

electrolyte resulting in micro-cracks within the YSZ. The impedance at 650°C for the

sensors with the Au counter electrode was larger than the impedance for sensors with the

LSM counter electrode at 575°C. Generally, the impedance is larger at lower

temperatures due to kinetic limitations. This data indicated the LSM counter electrode

enabled the sensor to provide a more accurate response.
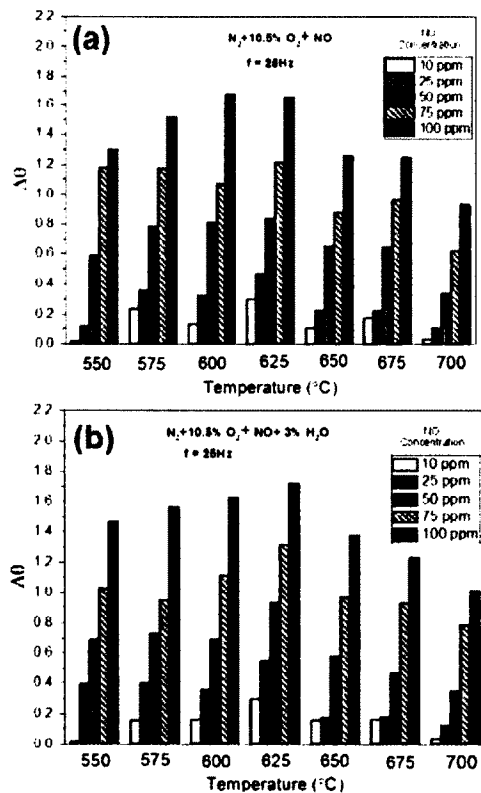
Figure 4-12: Sensitivity plot for (a) dry and (b) humidified condition for the NO$_x$ sensor in 20 Hz.

4.2.2.4   Oxygen Partial Pressure Dependence. **Figure 4-13** shows the NO_x sensor

oxygen partial pressure dependence for operating temperatures ranging from 550 – 700°C

where the oxygen concentration varied from 1 - 18% with N_2 as the balance gas. The data

can be described by the power law relationship, R_{LF} α $(P_{O_2})^m$, where m is the slope and

R_{LFA} was determined from the equivalent circuit analysis. The slope associated with the

oxygen partial pressure dependence is generally correlated with specific reaction

mechanisms describing oxygen related processes at the electrode and

electrode/electrolyte interface [74], [83], [86]. Here, m ranged from approximately -0.26

to -0.38 as the operating temperature increased. The data in **Figure 4-13** corresponding to

sensor operation at 550°C suggested the charge transfer was the rate-limiting step m was

close to -0.25. As the sensor operating temperature increased, electronic activity within

the LSM electrode increased such that the charge transfer was improved. As the slope of

the oxygen partial pressure data gradually became more negative with increasing

operating temperature, the dissociative adsorption of oxygen appeared to be a rate-

limiting mechanism [87].
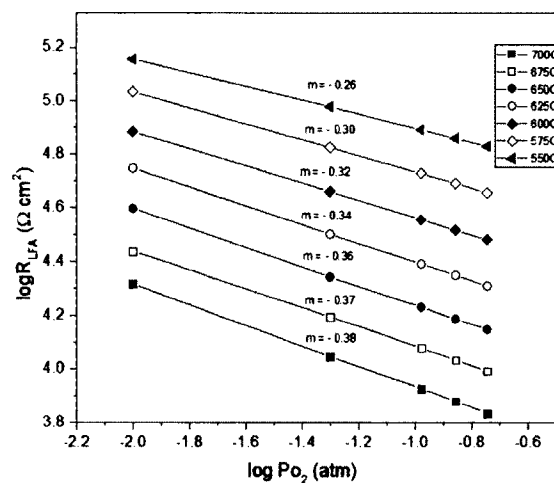
Figure 4-13: Oxygen partial pressure plot in different temperatures for the NO_x
sensor along with the slops.

4.2.2.5   Temperature Dependence. The calculated activation energies from

Figure 4-14 were approximately 1.020 ± 0.034 eV and 1.034 ± 0.022 eV for dry and

humidified conditions, respectively. The slight increase in the activation energy for

humidified gas conditions is in agreement with the slight increase in impedance observed

in **Figure 4-11b** for the humidified data. This finding indicates the addition of water may

interfere with sensor operation. Here, the water concentration in the gas stream was about

3%. The activation energies reported here are significantly lower than those typically

reported for LSM based electrochemical devices. Most likely, this difference is related to

the LSM electrode microstructure. More often, LSM electrodes are fabricated to have a

porous microstructure, which is desirable for solid oxide fuel cells.
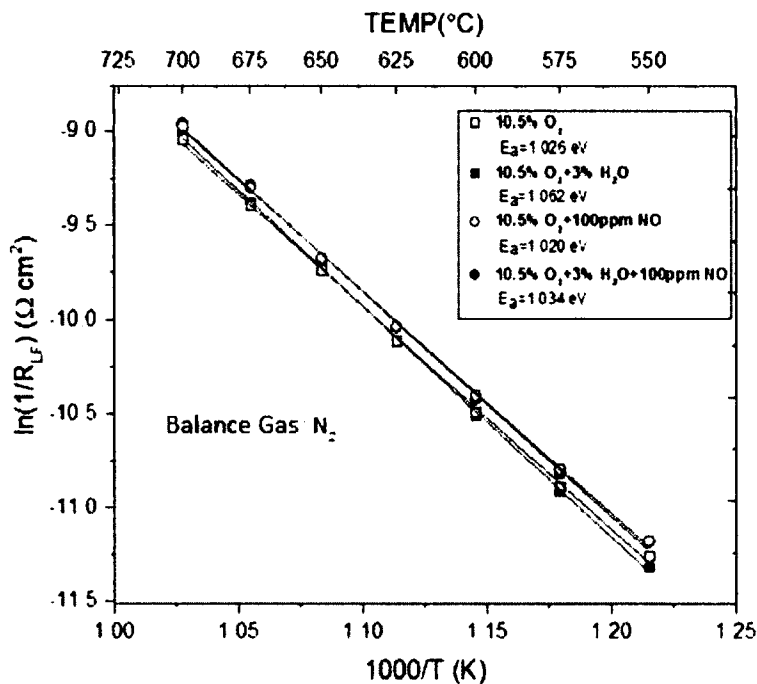
Figure 4-14: Activation energy curve for 0 and 100 ppm NO in dry and wet condition
for the NOₓ sensor.

4.2.2.6   Sensor Accuracy. In an application on-board a vehicle, the operating

temperature of the NO_x sensor may fluctuate as absolute control of the heater within in

sensor is not possible. Such temperature fluctuations can lead to errors in sensor

sensitivity measurements. The relationship between the phase angle response of the LSM

based NO_x sensors and operating temperature was studied in order to determine sensor

accuracy with respect to temperature fluctuations. The data plotted in **Figures 4-15a-c**

show the sensor operating temperature profiles with the corresponding phase angle

response for sensors operating at frequencies of 10, 20, and 40 Hz for baseline and 75

ppm NO conditions. The same approach was seen in another study [88].

Figures 4-15d-f show the $\Delta\theta$ values associated with different NO concentrations

for LSM based NO_x sensors operating at 575°C. If there is 75 ppm NO with 10.5% O_2 in

the exhaust stream and a +5 °C fluctuation occurs, according to the sensitivity

measurements in **Figure 4-15** for an operating frequency of 10 Hz, the $\Delta\theta$ measurement

would be 1.82°, indicating an erroneous concentration of 100 ppm NO. Similarly, if the

operating temperature changes to 570°C due to a -5°C fluctuation, then $\Delta\theta = 0.61°$,

indicating 41 ppm NO when it is actually 75 ppm. (These calculations were based on the

assumption that the oxygen concentration was accurately measured.) Ideally, if 75 ppm

NO is present, the NO_x sensor should detect this concentration even if the operating

temperature fluctuates by ± 5°C. **Table 4-2** illustrates the NO measurement errors that

could result from such temperature fluctuations. At 40 Hz, the sensors have a more rapid

response rate due to the higher operating frequency. However, the resulting NO

sensitivity error is over 10%. The smallest errors (~ 5 - 6%) occurred when the sensors

were operated at 20 Hz. In addition, the temperature profile in **Figure 4-15b** indicates a

minimum in the temperature profile slope at temperatures between 575 - 600°C for

sensor operation at 20 Hz, suggesting that this temperature range is more suitable for

achieving greater sensing accuracy for the LSM based NO_x sensors.
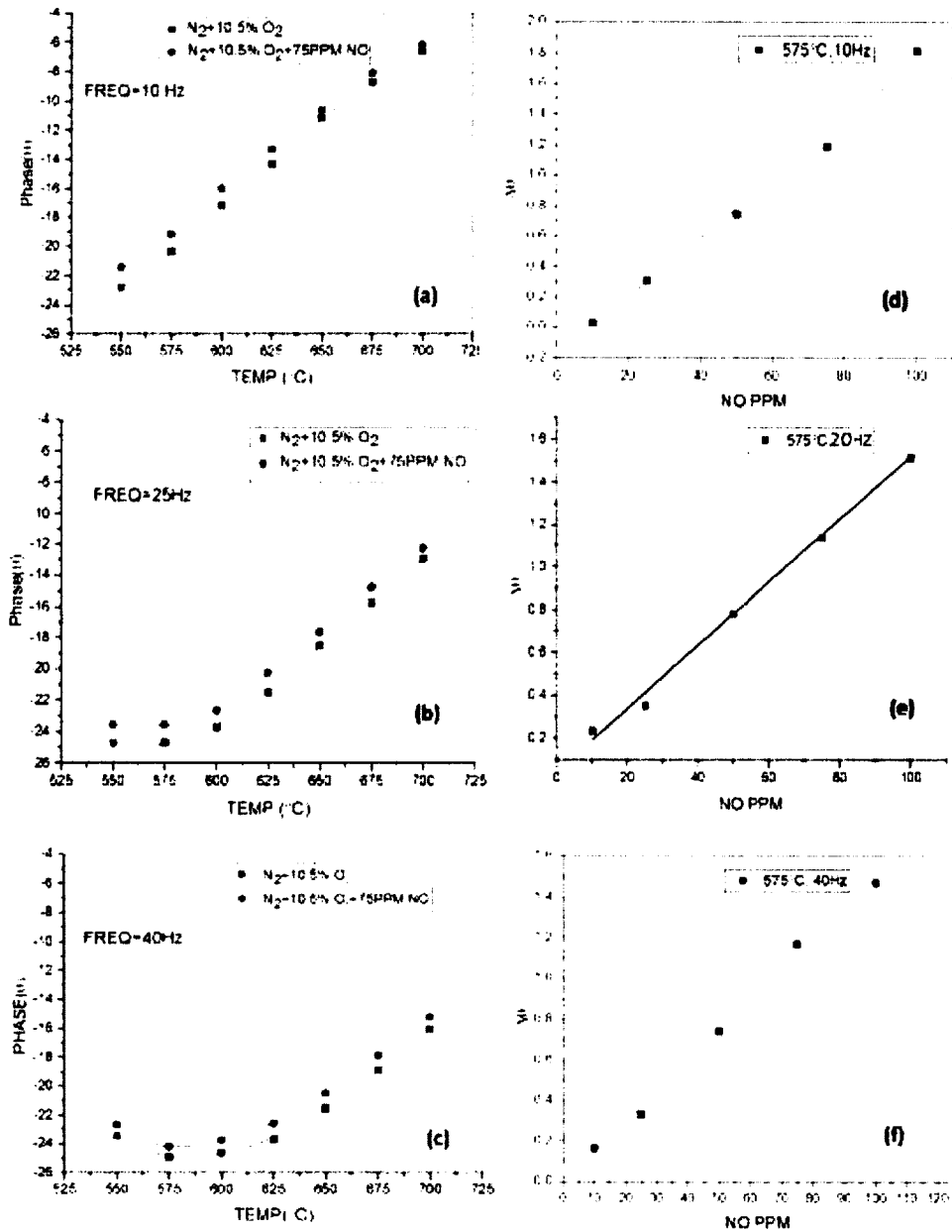
Figure 4-15: (a), (b), (c) dθ/dt plots and (d), (e), (f) Δθ vs No ppm plots for 10 Hz, 25 Hz and 45 Hz frequencies.

Table 4-2: Change in sensor phase response with corresponding NO measurement

FREQ (Hz)	TEMP (°C)	$\Delta\theta = \theta_{baseline}-\theta_{NO}$ (°)	NO Measurement (PPM)
10	575	1.25	75
	+5° PERTURBATION T= 580	1.82	100
	-5° PERTURBATION T= 570	0.61	41
20	575	1.14	75
	+5° PERTURBATION T= 580	1.24	80
	-5° PERTURBATION T= 570	1.1	71
40	575	1.12	75
	+5° PERTURBATION T= 580	1.03	68
	-5° PERTURBATION T= 570	1.25	85

4.2.3   Conclusions

NO_x sensors based on dense (La, Sr)MnO_3 perovskite supports as working

electrodes with a porous YSZ electrolyte were evaluated to understand the influence of

LSM on NO_x sensing. Sensor fabrication resulted in a chemically and mechanically

stable interface between the LSM electrode and YSZ electrolyte. The impedance of the

sensors slightly increased when 3% - 10% water was added to the gas stream possibly

due to interference of water molecules with oxygen reactions, and interference of

hydroxyls at the LSM/YSZ interface. NO sensitivity was higher for sensors operating at a

temperatures 575°C as oxygen kinetic reactions were limited, thereby, allowing NO_x

reactions to proceed more readily. The sensors were reasonably sensitive to NO_x

concentrations as low as 5 ppm, and the sensitivity to NO_x increased slightly for

humidified gas conditions. Charge transfer and oxygen adsorption were determined to be

the potential rate limiting mechanisms that were dependent on the operating temperature.

Sensor accuracy studies found operation at 20 Hz to be most suitable for minimizing errors in sensitivity measurements due to temperature fluctuations. Sensors with Au counter electrode showed reduced NO sensitivity compared to that of porous LSM counter electrode most probably due to the presence of micro cracks on the electrolyte surface above the embedded Au wires [38]. Overall, the sensing properties of the LSM electrode were influenced by the operating conditions, as well as the counter electrode.

CHAPTER 5

ENHANCED NO$_X$ SENSOR OPERATION USING DENSE COMPOSITE ELECTRODES

In this chapter, dense composite electrodes for NO$_x$ sensing will be discussed.

Three composite materials have been studied during this project. They are (1) LSM-Au,

(2) LSM-YSZ, and (3) LSM-LSCF. In Section 5.1, perovskite based composite

electrodes with porous YSZ electrolyte is discussed. Section 5.2 presents the description

of the NO$_x$ sensors composed of LSM-Au composite electrodes and YSZ based porous

composite electrolyte.

5.1   Dense Composite Electrode Study with Porous YSZ Electrolyte

As discussed in Section 2.5.3, many composite electrodes have shown improved

results for NO$_x$ sensing than single phase electrodes. The LSM based composites were

made according to their nature of conductivity. An electronic conductor Au, an ionic

conductor YSZ and a mixed conductor LSCF (strontium-doped lanthanum cobalt ferrite)

were chosen to be mixed with electronic conductor LSM. For all the composite electrode

based NO$_x$ sensors, YSZ electrolyte was used.

Ceramic electrode material LSCF is a ceramic oxide with perovskite crystal

structure. This material is a mixed ionic electronic conductor with comparatively

62

high electronic conductivity (200 + S/cm) and good ionic conductivity (0.2 S/cm) [89]. It is mainly studied for intermediate temperature solid oxide fuel cell.

5.1.1   Experimental

Powders of $La_{0.8}Sr_{0.2}MnO_3$ (LSM, Inframat Advanced Materials), Au (Alfa Aesar), 8 mol% Y_2O_3-doped ZrO_2 (YSZ, Tosoh Corporation) and $La_{0.6}Sr_{0.4}Co_{0.8}Fe_{0.2}$ (LSCF, Fuel Cell Materials) were used to fabricate 4 types of NO_x sensors based on the following dense electrode supports: LSM, LSM-Au, LSM-YSZ and LSM-LSCF. The LSM based sensors were intended for comparison purposes. The LSM-Au, LSM-YSZ and LSM-LSCF composite electrodes contained 10 wt% Au, 30 wt% YSZ, and 30 wt% LSCF, respectively. The powders for each electrode were ball-milled with 3 wt% polyvinyl buteral (PVB-76, Butvar) binder and ethanol for 10 - 16 hours. The resulting slurry was dried and uni-axially pressed at 200 MPa into pellets. The LSM and LSM-Au pellets were fired at 1400°C for 5 hours. The LSM-YSZ pellets were fired at 1325°C for 6 hours. The lower temperature was used to avoid reactions between the LSM and YSZ powders. It was found that the preferred firing temperature for the LSM-LSCF pellets was 1400°C as lower firing temperatures resulted in density less than 90%. The electrode pellets were partially coated with YSZ electrolyte slurry. The YSZ slurry contained 8 mol% Y_2O_3-doped ZrO_2 powder along with the following additives: 2 wt% B-76 Butvar binder, 2 ml phosphate ester dispersant along with ethanol and was ball milled for 12 hours. The YSZ coated pellets were fired at 1000°C for 1 hour using a ramp rate of 2°C/min. The sensors were completed by applying a counter electrode made from a slurry containing LSM, LSM-Au, LSM-YSZ or LSM-LSCF. The counter electrode slurries consisted of the desired electrode powder along with 2 wt% B-76 Butvar binder, 2 ml

corn oil dispersant with methyl ethyl ketone solvent and ball milled for 22 hours. A final

firing step at 1000°C for 1 hour at a ramp rate of 2°C/min completed sensor fabrication.

The resulting sensors were supported by a dense electrode pellet with a porous electrolyte

and porous counter electrode. The diameter of the pellet was 11 mm with a thickness of

about 1.1 mm after firing. Scanning electron microscopy (SEM), energy dispersive x-ray

(EDX) and x-ray diffraction (XRD) were used to analyze the morphology and

microstructure of the sensor components. The final schematic of the sensor was the same

as shown in **Figure 4-1**.

5.1.2   Characterization of the NO$_x$ Sensor

Microstructural characterization was mainly done using SEM. For the LSM-Au

electrodes backscattered SEM was used. Typical SEM images of the electrode pellets and

electrolyte for the sensors are shown in **Figure 5-1**.
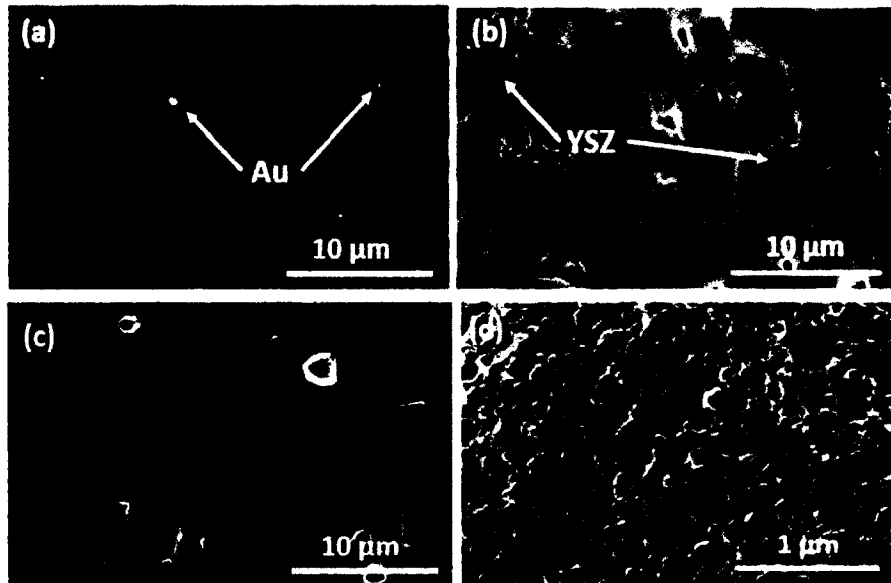
Figure 5-1. (a) Backscattered SEM image of the LSM-Au electrodes and SEM
images of dense (b) LSM-YSZ electrodes (c) LSM-LSCF electrodes (d) porous
YSZ electrolyte.

Clear observable grains and grain boundaries were seen over the surface of the

LSM-Au dense pellets in **Figure 5-1a**. The grain sizes within LSM-Au electrode pellets

ranged from about 5 μm to almost 20 μm. The backscattered SEM image of the LSM-Au

pellet indicated the Au particles were well dispersed. The density of the sensing electrode

pellets without the YSZ coating was determined by the Archimedes' method to be about

95% ± 2%. Comparable results measured by mercury intrusion porosimetry indicated the

pellets were 93% ± 3% dense.

The SEM image of the LSM-YSZ electrode pellets is shown in **Figure 5-1b**.

From the mapping images **(Figure 5-2)**, it was clear that those darker spots seen on the

SEM image **Figure 5-2b** was YSZ dispersed on LSM. **Figure 5-1c** is showing the SEM

images of LSM-LSCF sensor surface. Clear grains and grain boundaries were visible here

too like LSM-Au and LSM electrodes. The density of the pellet was determined both by

the Archimedes' method and MIP. It was almost 95% dense.
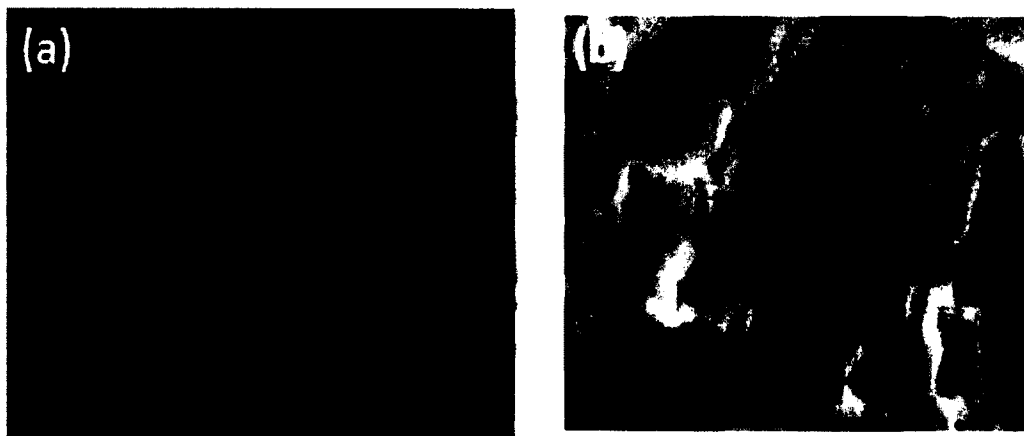
Figure 5-2. EDS mapping of the (a) YSZ on LSM-YSZ electrodes and (b) SEM
image of the same portion of the pellet.

Under the elevated temperature (>1300°C) LSM and YSZ react with each other

and form lanthanum zirconate ($La_2Zr_2O_7$) and strontium zirconate ($SrZrO_3$) phases at the

LSM-YSZ interface. The conductivity of $La_2Zr_2O_7$ and $SrZrO_3$ phases are in the order of

10^{-4}-10^{-5} S/cm, which is much lower than those of LSM and YSZ. Thus, the resistance of

the cell becomes very high [90].The composite with resistive phases in it cannot be used

as NO_x sensing electrodes because of their low conductivity. So, checking the formation

of the resistive phases was very important for the sensors when the electrodes were

sintered in 1325 °C. **Figure 5-3** is showing the XRD plot for the LSM-YSZ composite

electrode which does not develop any resistive phase after sintering in 1325°C for 6

hours.
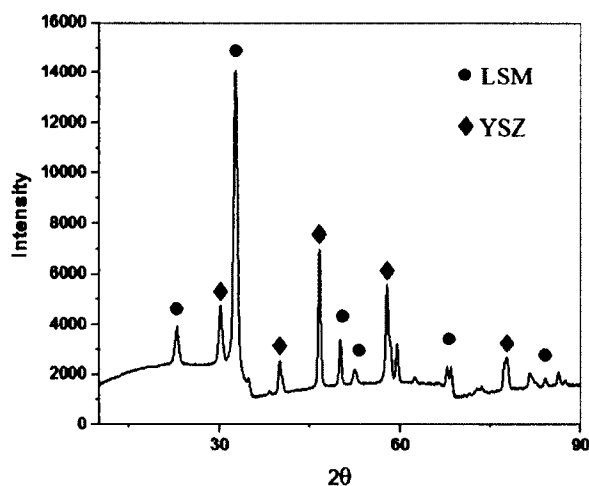
Figure 5-3. XRD plot for LSM-YSZ composite electrodes.

Figure 5-1c is showing the SEM images of LSM-LSCF sensor surface. Clear

grains and grain boundaries were visible here too like LSM-Au and LSM electrodes. The

density of the pellet was determined both by the Archimedes' method and MIP. It was

almost 95% dense.

66

SEM surface images of the YSZ coating (**Figure 5-1c**) indicated a contiguous network of particles and dispersed pores. The electrolyte porosity was estimated to be approximately 48% based on computational analysis of similarly prepared YSZ electrolyte coatings [36]. The YSZ coating was of thickness ~0.2 mm for all the sensors.

5.1.3   Result and Discussion

5.1.3.1   Impedance Behavior. **Figure 5-4a** shows the typical impedance response of LSM-Au sensing electrode based sensors with and without NO at an operating temperature of 575°C. The impedance of the LFA of the Nyquist plots of all three sensors decreased when the sensors were exposed to 100 ppm NO or NO_2, in comparison to the baseline conditions with only 10.5% O_2 (with base gas N_2) present. The same trend was observed in **Figure 5-4b** and **c** for LSM-YSZ and LSM-LSCF electrodes.

LSM-LSCF based sensors were tested after LSM-Au and LSM-YSZ based sensors. LSM-LSCF based sensors showed NO sensitivity capability less than LSM and LSM-Au based sensors (discussed in Section 5.1.3.4). Hence, water and oxygen cross-sensitivity study along with PO_2 analysis were not done with LSM-LSCF based sensors.

Figures 5-5a and **b** show the impedance response of the LSM-Au and LSM-YSZ based sensors with and without 10% water in the testing environment. The measured impedance was lesser for humidified gas conditions, in comparison to dry gas conditions for each of the sensors evaluated most probably because water facilitates charge transfer process in the TPB. The same trend was observed in case of LSM electrodes in Section 4.1.3.1.

67

Figure 5-4: Change in impedance response of the NO_x sensors with the change in NO concentration for (a) LSM-Au, (b) LSM-YSZ, and (c) LSM-LSCF.
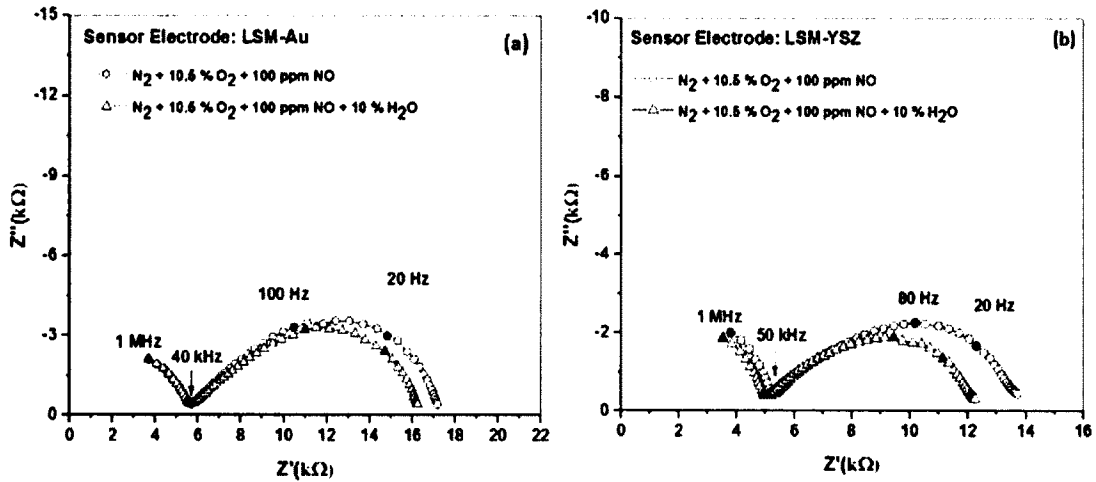
Figure 5-5: Impedance response for dry and 10 % humidified condition at 575°C of (a) LSM-Au and (b) LSM-YSZ electrodes.

From the impedance plot obtained from different operating temperatures (575°C - 675°C) in **Figure 5-6a and b,** it was found that the value of the impedance decreased with increase in the temperature. The same tendency has been reported for LSM based sensors in Section 4.1.4.1. Therefore, the probable cause behind this kind of phenomenon has already been discussed in that section.
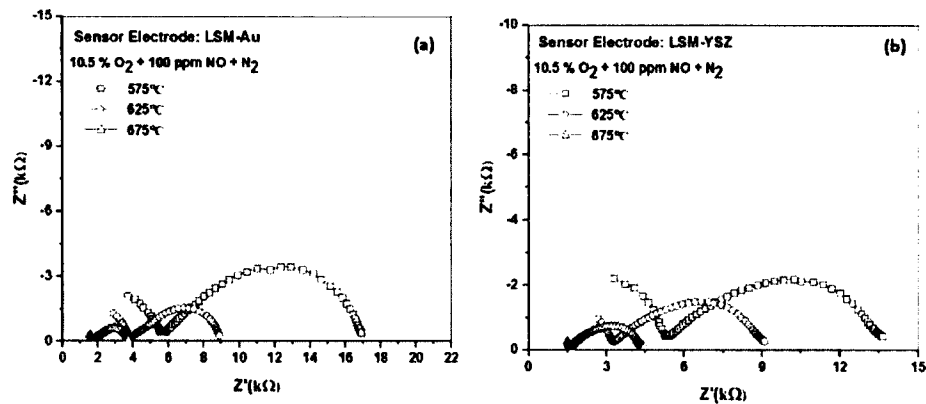
Figure 5-6: Impedance response for different operating temperature of (a) LSM-Au and (b) LSM-YSZ electrodes.

69

5.1.3.2   Equivalent Circuit. Equivalent circuit modeling was used to further

understand the electrical response of all the LSM composite based NO_x sensors. As

shown in **Figure 5-7**, two parallel circuits were found to model the impedance response

of each sensor for various operating conditions where the data at high and low

frequencies were described by $R_{HF}CPE$ and $R_{LFA}(CW)$ circuits, respectively. The errors

associated with the equivalent circuit model were between 1 – 2%. The resistance, R_{HFA},

was related with high frequency reactions which took place within the porous YSZ

electrolyte, and the constant phase element, CPE, related to non-ideal capacitance

behavior. The Warburg element defined the impedance resulting from the diffusion of

ionic species at the electrode/electrolyte interface [32].
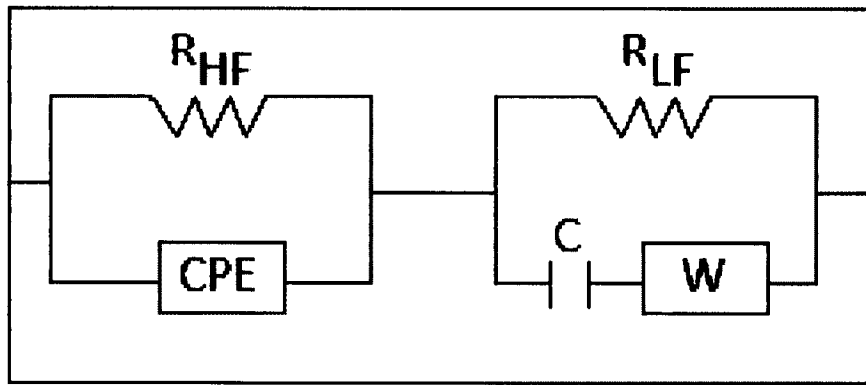
Figure 5-7: Equivalent electrical circuit for the composite electrode based NO_x
sensor.

5.1.3.3   Angular Phase Response. NO_x sensor studies report that the angular phase

response indicates changes in gas concentration with greater sensitivity and accuracy in

comparison to measuring the magnitude, |Z|, or other components of the impedance [1].

The angular phase response, θ, is defined according **Eq. [1].**

$$\theta = tan^{-1}\frac{Z''(\omega)}{Z'(\omega)}.$$

70

Figure 5-8 shows the phase angle response versus the operating frequency for

sensors operating with and without 100 ppm NO for LSM-Au, LSM-YSZ and LSM-

LSCF electrode based sensors. Peak sensitivity was achieved at 20 Hz for all the sensors.

Sensors with the LSM-Au sensing electrode attained the highest phase angle peak

response of -19.6° with 10.5% O_2 and N_2 where the lowest phase angle peak was -13.3°

by LSM-YSZ based sensor. Peak phase for LSM-LSCF was -14.36°. The addition of 100

ppm NO caused the peak phase angle to reduce for all sensors. This reduction was more

significant in sensors with the LSM-Au sensing electrode. This data suggested that the

LSM-Au sensing electrode can facilitate a larger signal and stronger response to NO, in

comparison to LSM-LSCF and LSM-YSZ sensing electrodes.

The θ versus frequency curves for 100 ppm NO with O_2 and N_2 merged with the

baseline gas data at about and 250, 158, and 125 Hz for the sensors made of LSM-Au,

LSM-YSZ, and LSM-LSCF electrodes, respectively. Hence, the LSM-Au based sensors

can potentially facilitate impedancemetric NO_x sensing over a wider range of frequencies,

which can be advantageous for optimizing sensor performance.

As in humidified condition data was not collected for LSM-LSCF based sensor, in

Figure 5-9, the angular phase response plot is shown in dry and 10% humidified
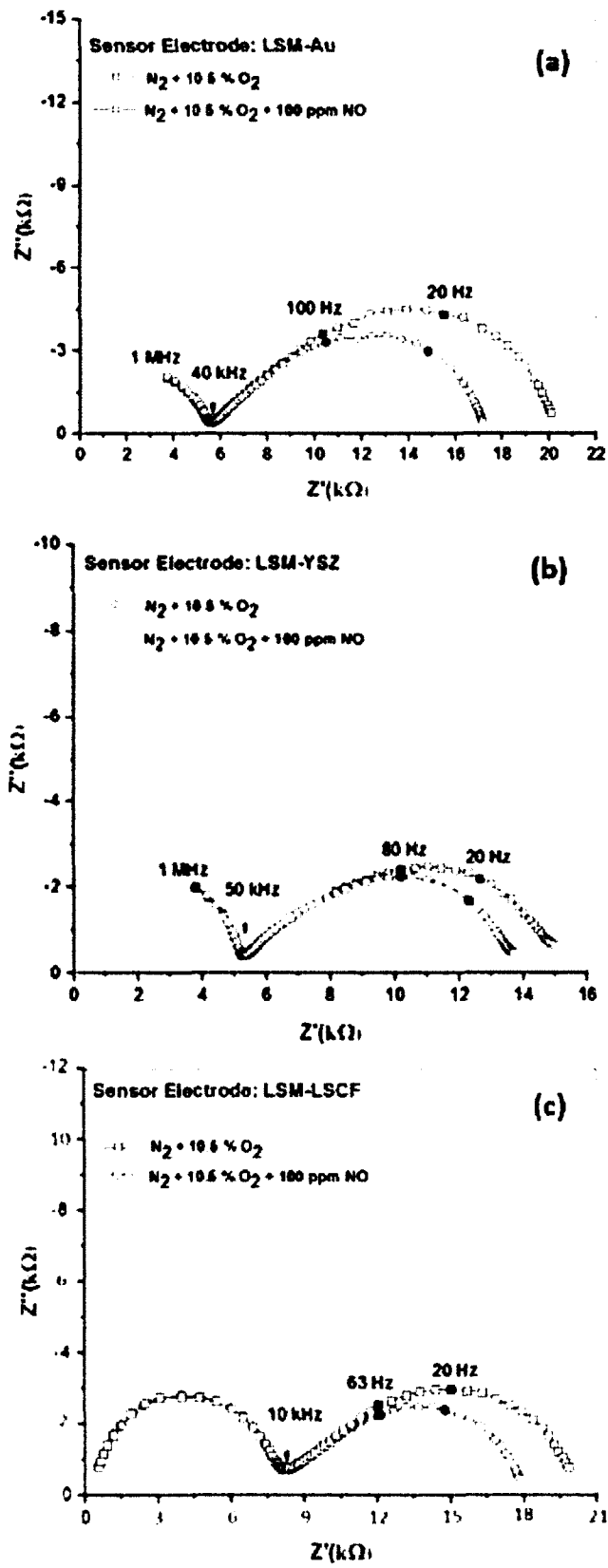
conditions for LSM-Au and LSM-YSZ based sensors.
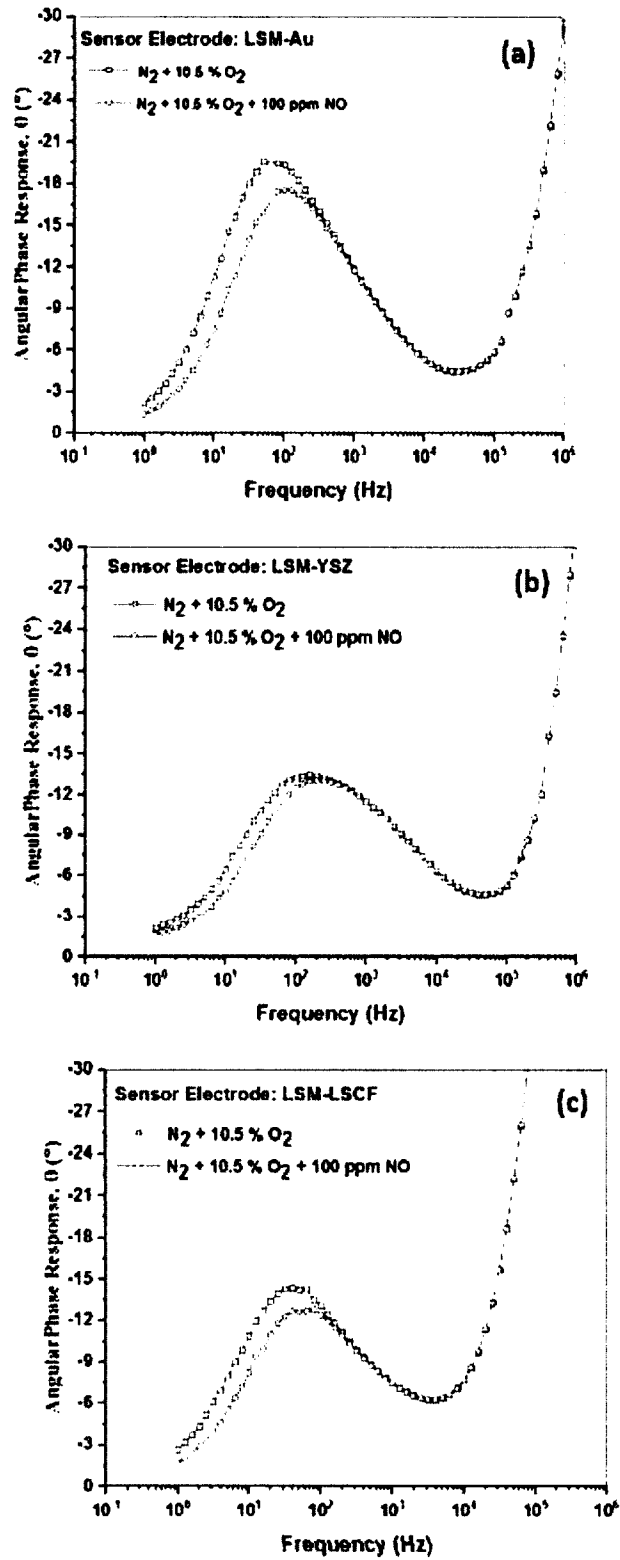
Figure 5-8: Angular phase response of the NO_x sensors with the change in NO concentration for (a) LSM-Au, (b) LSM-YSZ, and (c) LSM-LSCF.

Adding 10% H_2O to the gas stream caused a further decrease in the θ versus frequency response for the sensors. There is an overlap between dry and humidified data for LSM-Au with 100 ppm NO as seen in **Figure 5-9a**. This indicates lower water influence for LSM-Au based sensors compared to that of LSM-YSZ. In Chapter 4 while discussing LSM based NOx sensors, it was reported that those sensors were also affected by the presence of water in the testing environment. It seems adding Au with LSM reduced water dependence of NO_x sensors.
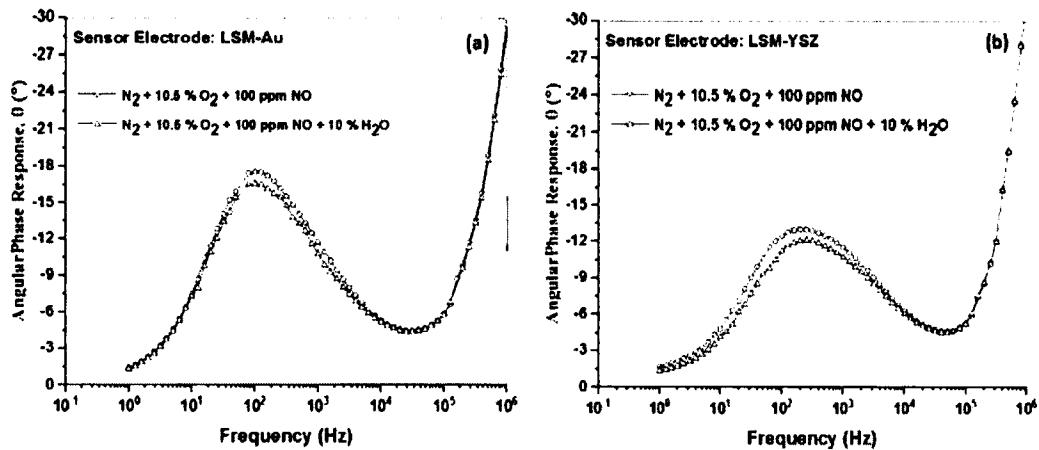
Figure 5-9: Angular phase response for dry and 10% humidified condition at 575°C of (a) LSM-Au and (b) LSM-YSZ electrodes.

5.1.3.4   NO Sensitivity. The sensitivity to NO for the LSM and LSM composite electrode sensors was based on the change in the angular phase response, Δθ, for various NO concentrations according to the following:

$$NO\ Sensitivity\ (m) = \Delta\theta/\Delta[NO]$$ **Eq. [10]**

73

Here, **Figure 5-10** shows NO sensitivity for all the LSM composite based NOx

sensors. LSM based sensors are shown here for comparison purpose. While studying NO

sensitivity, a pattern was observed as the sensitivity was increased with increasing

electronic conductivity of the electrode. Confirming this trend LSM-Au showed

maximum sensitivity. Here, as LSM based electrodes, there are two zones of sensitivity

depending on the NO ppms has been reported. From 0 - 50 ppm NO LSM-Au showed ~

40% - 50% more sensitivity than LSM-YSZ and LSM-LSCF based sensors and ~ 25%

more sensitivity than that of LSM based sensors at 575°C.

NO Sensitivity, $\Delta\theta/[\Delta NO]$ (deg/ppm), Dry Condition		
	NO Concentration	
Sensor Electrode	0-50 ppm	50-100 ppm
LSM-YSZ	0.027	0.018
LSM-LSCF	0.032	0.020
LSM	0.041	0.028
LSM-Au	0.051	0.032
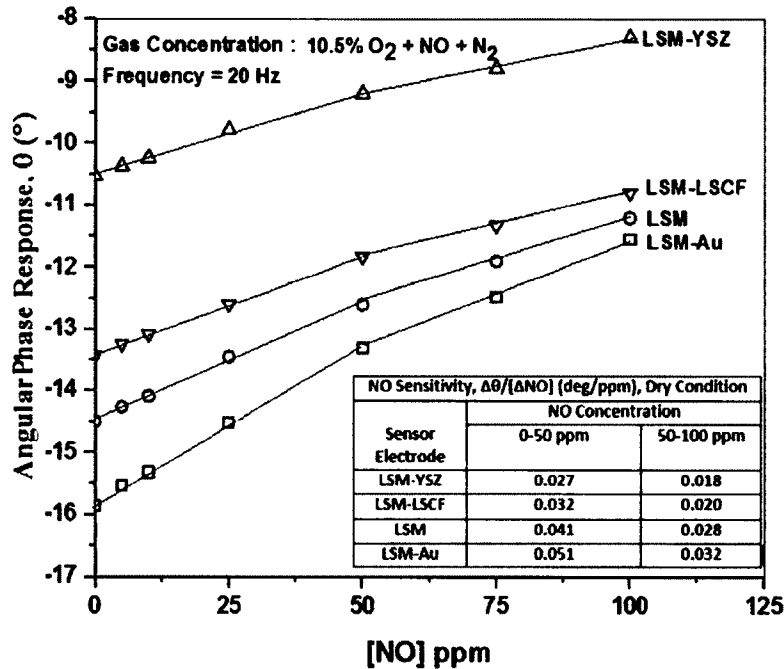
Figure 5-10: NO sensitivity plot of LSM composite electrode based sensors for dry
condition at 575°C.

For 10% humidified condition the NO sensitivity data from LSM, LSM-Au and

LSM-YSZ based sensors have been compared in **Table 5-1**.The LSM-Au based NO_x

sensors showed almost a 7% greater sensitivity to NO for 10% humidified gas conditions,

whereas LSM and LSM-YSZ based NO_x sensors showed almost 25 - 33% greater

sensitivity to NO for 10% humidified gas conditions. These results suggest the humidity

of the gas stream may interfere with oxygen catalytic reactions, but it is much less in the

presence of Au.

Table 5-1: Comparative study on humidified condition NO sensitivity

NO Sensitivity, Δθ/[ΔNO] (deg/ppm), 10% Humidified Condition		
Sensor Electrode	**NO Concentration**	
	0-50 ppm	**50-100 ppm**
LSM	0.050	0.030
LSM-Au	0.055	0.034
LSM-YSZ	0.036	0.026

Figure 5-11 shows the water cross-sensitivity plots for LSM, LSM-Au and LSM-

YSZ sensor for different concentrations (3 - 10%) of water in the testing environment.

NO sensitivity for all three types of the sensors was almost unchanged with the increase

in water concentration. From this result, it can be concluded that the NO sensitivity of

LSM and LSM composite based sensors increased by the presence of water in the

operating environment, but this change in sensitivity is independent of the concentration

of water present.
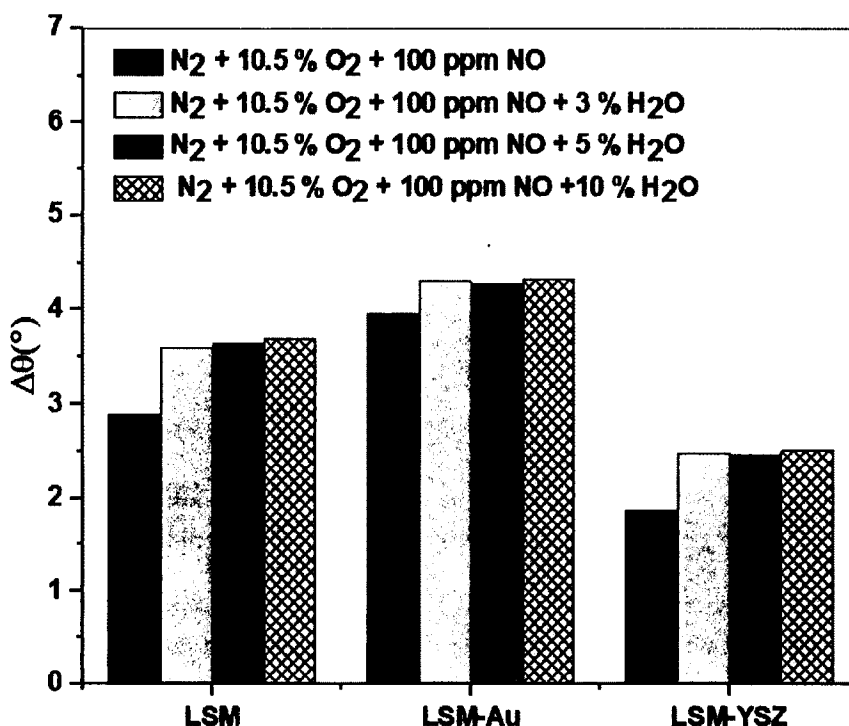
Figure 5-11: NO sensitivity comparison for dry and different humidified conditions at 575°C for 20 Hz.

5.1.3.5   Oxygen Cross-sensitivity. In this study the data was collected for different

concentration of O_2 (5% - 18%). **Figures 5-12a** and **b** show the O_2 sensitivity of the

LSM-Au and LSM-YSZ based NO_x sensor at 575°C for 20 Hz and 1000 Hz without NO.

Figures 5-12c and d are showing the NO sensitivity of the LSM-Au and LSM-YSZ

based NO_x sensor with 10.5% O_2 at 575 °C for 20 Hz and 1000 Hz. The data showed the

same tendency as LSM electrode based sensors **(Figure 4-7)**. Therefore, it can be said

from the data that at 1000 Hz frequency, this sensor acts as an oxygen sensor. It can be

further inferred that as NO sensitivity, oxygen sensitivity is also dependent on frequency

of the input signal for LSM and all the LSM based composite sensors.
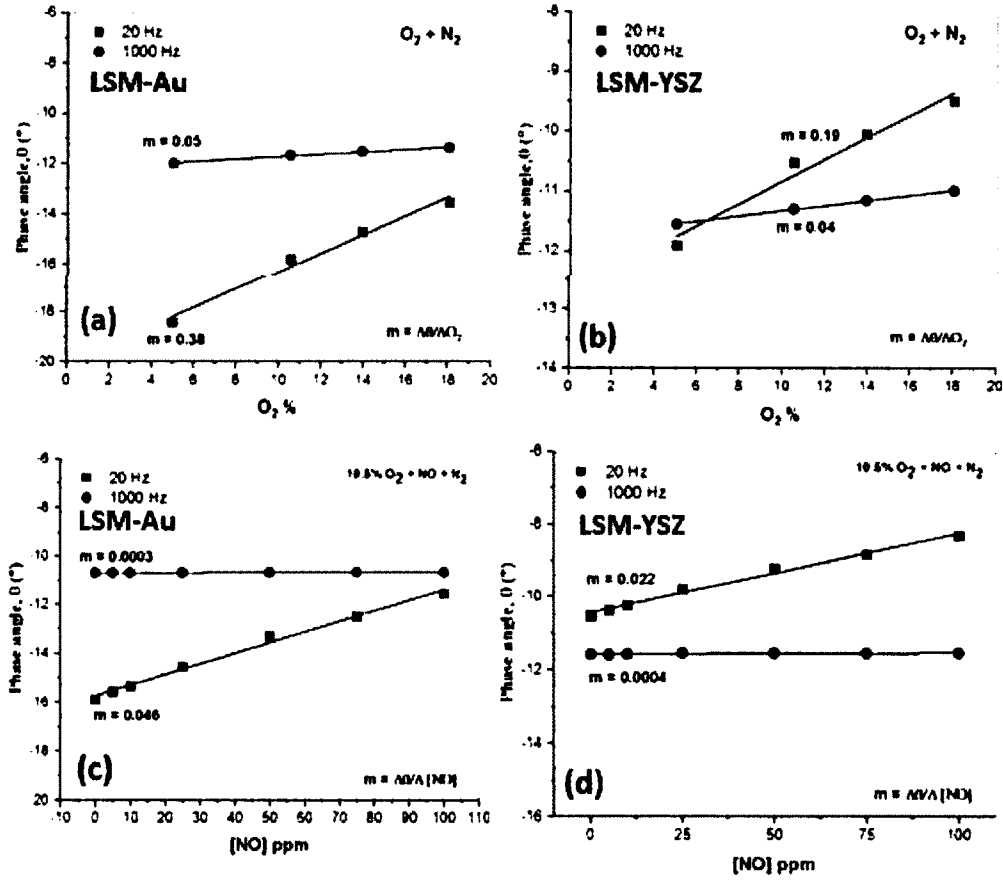
Figure 5-12: Comparison of O_2 sensitivity of (a) LSM-Au and (b) LSM-YSZ and NO sensitivity of (c) LSM-Au and (d) LSM-YSZ based NO_x sensor at 575°C for 20 Hz and 1000 Hz.

Table 5-2 shows LSM-Au and LSM-YSZ based NO_x sensors' oxygen partial

pressure dependence for operating temperature 575°C with and without NO and 10%

water vapor where the oxygen concentration varied from 5 - 18% with N_2 as the

background gas. As discussed in Section 4.1.4.4 the value of *m* is associated with a

particular rate limiting mechanisms describing oxygen related processes at the electrode and electrode/electrolyte interface.

Here, m was found to range from approximately -0.2 to -0.26 for LSM-Au based sensors as the operating condition changes. The data suggested the sensing response of the LSM-Au electrodes seemed to be primarily limited by the rate of oxygen reduction at the TPB as m was close to -0.25 for the various gas conditions evaluated.

The LSM-YSZ based sensors had a weak P_{O2} dependence under dry operating conditions. Adding NO caused a slight reduction in the P_{O2} dependence, whereas adding H_2O generated a stronger dependence. Similar behavior was observed for the LSM-Au based sensors, although the overall P_{O2} dependence was greater. Other studies have reported that a $(P_{O2})^{-0.25}$ dependence describes the transport of partially reduced atomic oxygen to the TPB [83], [87]. In addition, the complete reduction on oxygen at the TPB is represented by a $(P_{O2})^m$ relationship where $m = 0$.

Table 5-2: PO$_2$ dependence for LSM-Au and LSM-YSZ based NO$_x$ sensors

	Value of *m* in 575°C			
Electrode Material	10.5% O₂+ N₂	10.5% O₂ + 75ppm NO + N₂	10.5% O₂ + 10 % H₂O +N₂	10.5% O₂ +10 % H₂O +75 ppm NO+ N₂
LSM-Au	-0.24	-0.20	-0.26	-0.23
LSM-YSZ	-0.14	-0.12	-0.21	-0.20

Thus, it is possible that under dry conditions the response of the LSM-YSZ sensing electrodes was limited by a combination of atomic oxygen transport and oxygen reduction. Adding H_2O to the gas stream appeared to improve atomic oxygen transport as

78

the value of m approached -0.25. **Table 5-2** shows the PO_2 dependence of LSM-YSZ

electrode based NO_x sensors in different operating conditions.

5.1.3.6   Temperature Dependence. As discussed in Section 4.1.4.5, the temperature

dependence of the sensors is described by the Arrhenius plot shown in using R_{LF} values

from the equivalent circuit modeling results. The temperature dependence data for

different operating conditions for LSM-Au and LSM-YSZ based sensors is shown in

Table 5-3. The values are very near to those of LSM electrode based NO_x sensors and the

same trend is observed. From drastic difference in the values of **A** (pre-exponential factor

of Arrhenius eq.) it is clear that the reaction mechanism changes with presence of NO in

the environment and NO sensitivity is least in LSM-YSZ based sensors.

Table 5-3: Temperature dependence for LSM-Au and LSM-YSZ based NO_x sensors

Electrode Material	Value of A (S⁻¹)			Activation Energy (eV)		
	N_2 + 10.5% O_2	N_2 + 10.5% O_2 + 100ppm NO	N_2 + 10.5% O_2 +100 ppm NO + 10 % H_2O	N_2 + 10.5% O_2	N_2 + 10.5% O_2 + 100ppm NO	N_2 + 10.5% O_2 +100 ppm NO + 10 % H_2O
LSM-Au	1245.46	426.23	234.85	1.09 ± 0.04	1.05 ± 0.04	1.00 ± 0.01
LSM-YSZ	226.65	170.97	61.29	1.07 ± 0.03	1.04± 0.04	1.00± 0.02

5.1.3.7   NO Response Rate. The response time of the LSM, LSM-Au and LSM-YSZ

based sensors was assessed by measuring the change in the angular phase angle over

time. **Figure 5-13** shows time based study of the sensors for base-line conditions with

10.5% O_2 and N_2 along with 5, 10, and 25 ppm NO for an operating frequency of 20 Hz

at 575 °C. The LSM and LSM-YSZ based sensors had an average response time, τ_{90}, of

15 and 17 seconds, respectively, whereas, LSM-Au based sensors were sluggish as τ_{90}

was 20 seconds based on data collected at 5 ppm NO. In other sensor studies it was found

that the sensitivity to CO was dependent upon the size of the Au particles composing the

$ZnCr_2O_4$-Au sensing electrode [52]. Thus, it may be possible to improve the LSM-Au

sensor response time by altering the size of the Au particles. The recovery time for LSM-

Au and LSM based sensors to return to baseline conditions was ~35 seconds, and, the

LSM-YSZ based sensors had a slightly faster recovery of about 30 seconds. The recovery

time of the sensors was possibly related to the adsorption of NO at the electrode [67].
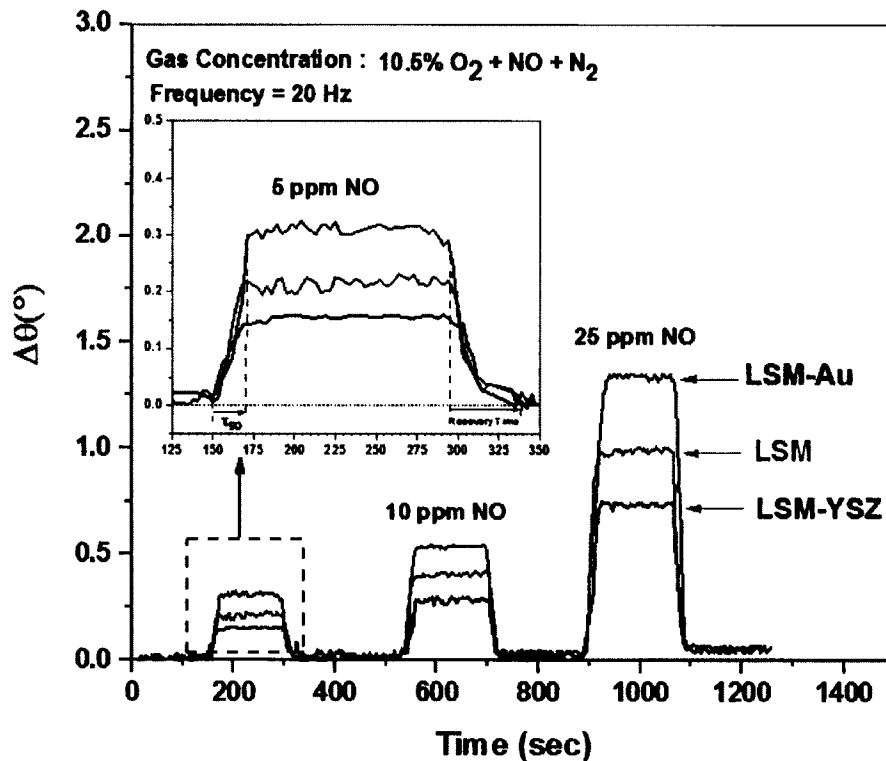
Figure 5-13: Comparison of the speed of NO_x sensing of LSM, LSM-Au and LSM-YSZ electrode based sensors at 575°C.

It is apparent from the NO sensitivity study and water cross-sensitivity study that

LSM-Au based NOx sensors showed a much improved response compared to LSM and

other LSM composite based sensors. Hence, to get deeper understanding on LSM-Au

based sensors some additional investigations like CH_4 cross-sensitivity analysis, stability study, accuracy study, etc. were done on only these type of sensors.

5.1.3.8 CH4 Cross-Sensitivity of LSM-Au Based Sensors. LSM-Au based NO_x sensors showed much improved CH_4 cross-sensitivity than LSM based sensors (Figure 5-14). Though the cross-sensitivity was increasing with increase in temperature. Still at 575°C, the $\Delta\theta$ value for NO was considerably higher than CH_4 and this trend continued in 600°C also. The presence of Au most probably was the reason behind the improvement in CH_4 cross-sensitivity.
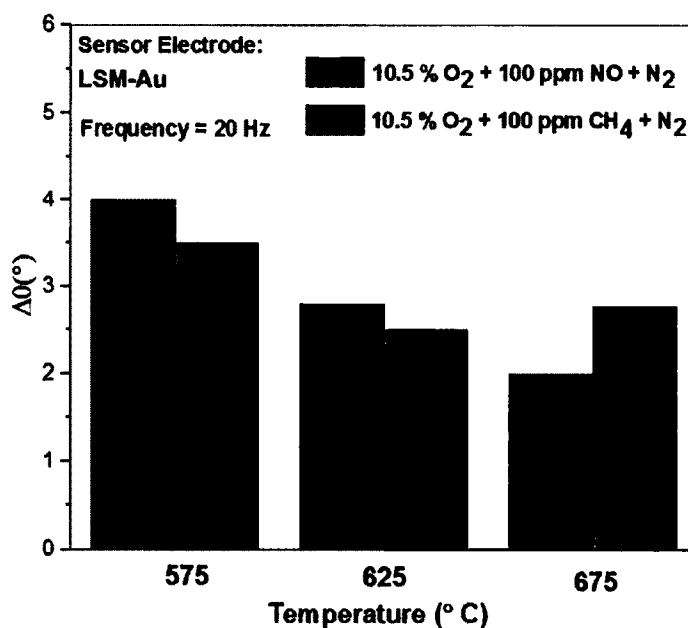
Figure 5-14: Cross-sensitivity study for CH_4 in dry condition at different operating temperature.

Probably the CH_4 cross-sensitivity of LSM-Au based sensors can be further decreased by changing the particle size of Au [52].

5.1.3.9   Stability Analysis of the LSM-Au Based NOx Sensor. The LSM-Au based

sensors were studied for 360 hours under dry and 10% humidified condition to

understand the durability profile of these sensors. Backscattered SEM images were also

taken before and after 360 hours of testing to see the changes of the sensor surface

(**Figure 5-15**). From **Figure 5-16,** it can be concluded that the LSM-Au based sensors

showed stable sensing performance under both dry and humidified conditions. The

performance of the sensor was not adversely affected by 10% humidified environment
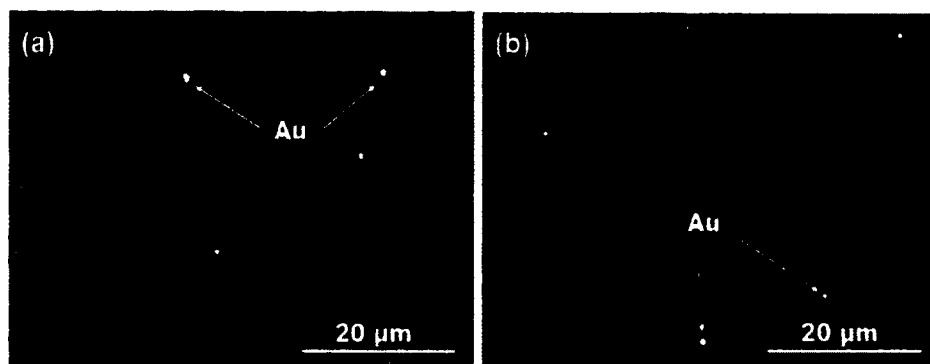
Figure 5-15: SEM images of LSM-Au pellets (a) before and (b) after 360 hours of testing as a NOx sensor under dry condition.
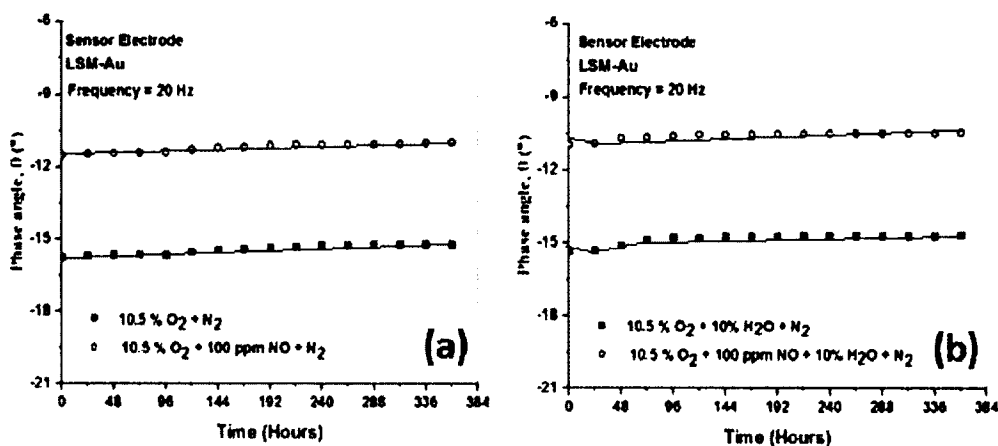
Figure 5-16: Durability test of LSM-Au based NOx sensors at 575°C for (a) dry and (b) humidified condition.

which also validated the observation of lower water influence on LSM-Au based NO_x sensors.

5.1.3.10   Sensor Accuracy Study. The relationship between the phase angle response of the LSM-Au based NO_x sensors and operating temperature was studied in order to determine sensor accuracy with respect to temperature fluctuations. The data plotted in **Figure 5-10a** shows the sensor operating temperature profiles with the corresponding phase angle response for sensors operating at frequency of 20 Hz for baseline and 50 ppm NO conditions. **Figure 5-17b** shows the $\Delta\theta$ values associated with different NO concentrations for LSM-Au based NO_x sensors operating at 625°C. If there is 50 ppm NO with 10.5% O_2 in the exhaust stream and a +5°C fluctuation occurs, according to the sensitivity measurements in **Figure 5-17b** for an operating frequency of 20 Hz, the $\Delta\theta$ measurement would be 0.74°, indicating an erroneous concentration of 47 ppm NO. Similarly, if the operating temperature changes to 595°C due to a -5°C fluctuation, then $\Delta\theta$ = 0.85°, indicating 54 ppm NO when it is actually 50 ppm. (These calculations were based on the assumption that the oxygen concentration was accurately measured.)
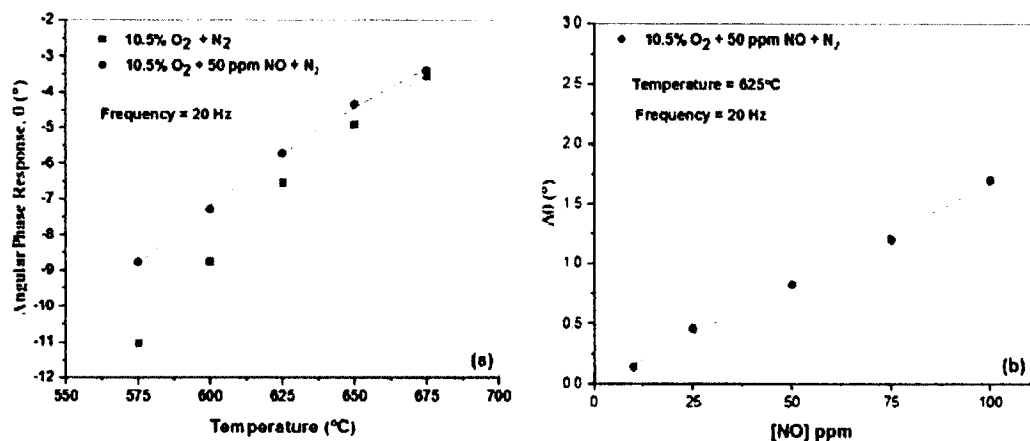
Figure 5-17: (a) θ vs. temperature plot and (b) NO sensitivity plot for LSM-Au based sensor for accuracy calculation.

83

Ideally, if 50 ppm NO is present, the NO_x sensor should detect this concentration even if the operating temperature fluctuates by ± 5°C. **Table 5-4** illustrates the NO measurement errors that could result from such temperature fluctuations. The accuracy was ± 4 ppm for ± 5°C temperature fluctuation at 625°C.

Table 5-4: Accuracy calculation for LSM-Au based NO_x sensors

FREQ (Hz)	TEMP (°C)	$\Delta\theta = \theta_{baseline} - \theta_{NO}$ (°)	NO Measurement (PPM)
	625	0.80	50
20	+5° PERTURBATION T = 630	0.74	47
	-5° PERTURBATION T = 620	0.85	54

5.1.4   Conclusions

The impedancemetric NO_x sensing behavior of dense LSM-Au, LSM-YSZ and LSM-LSCF electrodes were evaluated under dry and humidified (except LSM-LSCF) gas conditions for a range of operating frequencies. The LSM-Au composite electrodes demonstrated the highest response to NO with limited cross-sensitivity to H_2O, in comparison to the LSM and LSM-YSZ electrodes. The angular phase versus the frequency behavior of the sensors indicated the maximum sensing response to NO was achieved at 20 Hz with an operating temperature of 575°C. Managing oxygen cross-sensitivity could potentially be carried out by monitoring the sensor response at frequencies over 5 kHz. The response and recovery times for the LSM-Au sensing electrodes were not as rapid as those for LSM and LSM-YSZ, however, altering the Au

particle size may improve the performance rate of LSM-Au based sensors. Oxygen reduction appeared to be the dominant rate limiting mechanism for the sensors during operation with humidified gas conditions. For dry gas conditions, transport of atomic oxygen became an additional rate limiting mechanism for the LSM and LSM-YSZ based sensors. Overall, the Au addition to LSM appeared to enhance sensor sensitivity and selectivity to NO by enabling NO_x reactions to proceed more readily than oxygen reactions.

5.2 Dense LSM-Au Based NO_x Sensor with Porous Composite Electrolyte

In Chapter 4 and the first part of Chapter 5 we have discussed different single-phase and composite electrodes and their applications as NO_x sensors inside any diesel vehicle exhaust system. From that discussion it was evident that LSM-Au based NO_x sensors showed most promising results in terms of NO sensitivity, water cross-sensitivity and sensor accuracy. From another study on composite electrolytes by Khawlah Kharashi, it was found that NO_x sensors based on 50 wt% YSZ-50 wt% PSZ composite electrolyte and Au wire electrodes showed very good NO_x sensing capability and lower water cross-sensitivity [91]. To study the combined effect of LSM-Au electrode and YSZ-PSZ (50-50) composite electrolyte on NO_x sensing, a novel composite NO_x sensor was made; 2 wt% Alumina was added to the electrolyte because another study showed this amount of alumina can enhance NO_x sensitivity further [92]. In this chapter, the fabrication method, NO sensitivity, water cross-sensitivity and PO_2 dependence of this novel composite NO_x sensor will be discussed.

5.2.1   Experimental

The electrode powder was made by mixing LSM with 10 wt% Au. This mixture was ball-milled with 3 wt% polyvinyl buteral (PVB-76, Butvar) binder and ethanol for approximately 16 hours. The resulting slurry was dried and uni-axially pressed at 200 MPa into pellets. The electrolyte slurry was made by ball-milling 50wt % YSZ, 50 wt% PSZ, 2wt% Al_2O_3 and 20 ml corn oil for 16 hours. The rest of the process was the same as Sections 3.1.1 and 3.1.2. Figure 5-18 shows the schematic diagram of the novel composite NO_x sensor.
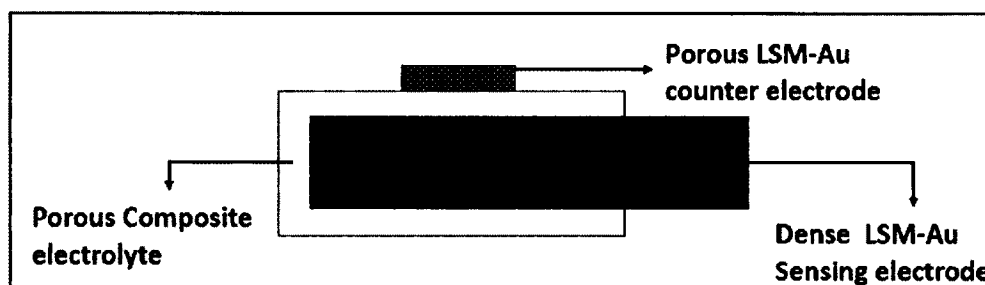
Figure 5-18: Schematic diagram of the novel composite NO_x sensor.

5.2.2   Characterization of the NO_x Sensor

Typical SEM images of the electrode pellets and electrolyte for the sensors are shown in **Figure 5-19**. Clear observable grains and grain boundaries were seen over the surface of the LSM-Au dense pellets. The grain sizes within LSM-Au electrode pellets ranged from about 5 μm to almost 20 μm. The backscattered SEM image of the LSM-Au pellet indicated the Au particles were well dispersed. The density of the sensing electrode pellets without the YSZ coating was determined by the Archimedes' method to be about

95% ± 2%. Comparable results measured by mercury intrusion porosimetry indicated the pellets were 93% ± 3% dense.
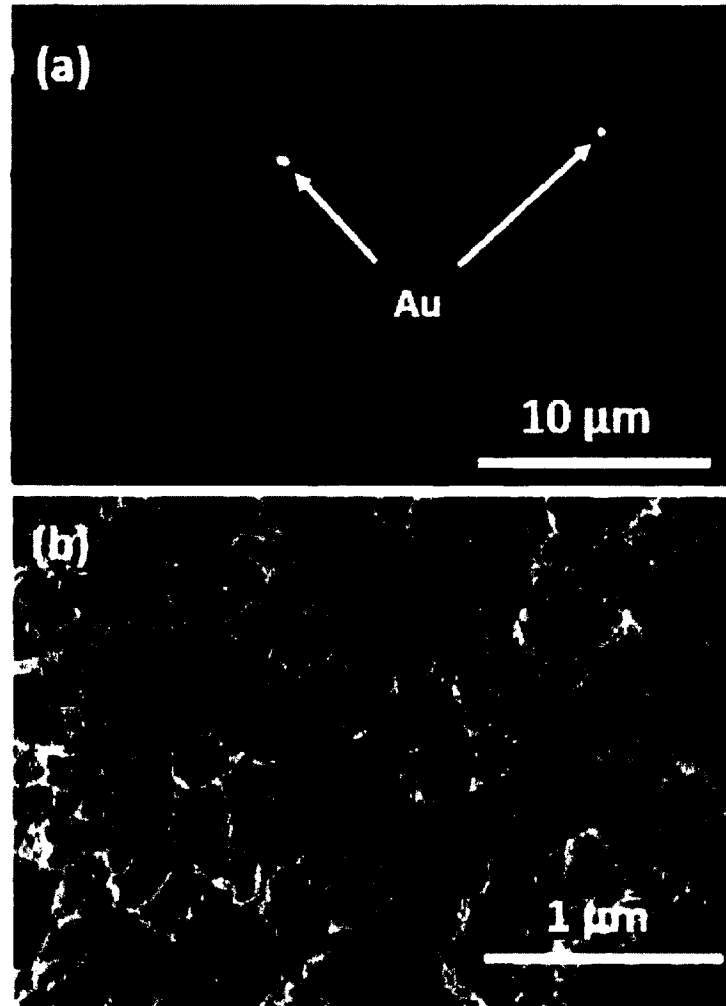
Figure 5-19. (a) Backscattered SEM image of the LSM-Au electrodes and (b) SEM image of YSZ electrolyte.

SEM surface images of the YSZ coating indicated a contiguous network of particles and dispersed pores. The electrolyte porosity was estimated to be approximately 48% based on computational analysis of similarly prepared YSZ electrolyte coatings [91]. The YSZ coating was determined to have a thickness of ~ 0.2 mm.

5.2.3 Result and Discussion

5.2.3.1 Impedance Behavior.

Figure 5-20a shows the typical impedance response of LSM-Au sensing electrode based novel composite sensors with and without NO at an operating temperature of 575°C. **Figure 5-20b** shows the impedance response of the sensor with and without 10% water in the testing environment. The impedance of the LFA arc of the Nyquist plots of all three sensors decreased when the sensors were exposed to 100 ppm NO or NO_2 in comparison to baseline conditions with only 10.5% O_2 (with base gas N_2) present.
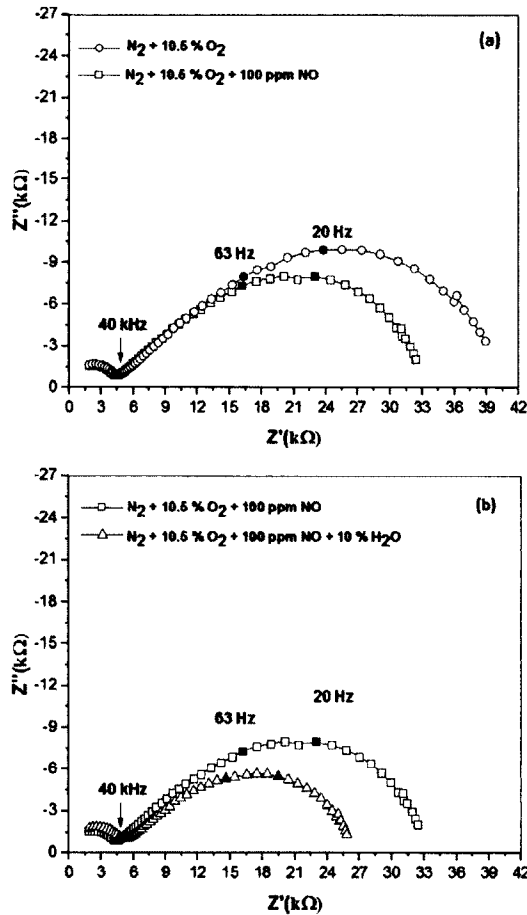
Figure 5-20: Change in impedance response of the NO_x sensors with the change in (a) NO concentration and (b) dry and 10% water.

5.2.3.2   Equivalent Circuit Modeling. It's exactly the same as the circuit model

discussed in section 4.1.4.2 for LSM electrode.

5.2.3.3   NO Sensitivity. The NO sensitivity of the novel composite NO_x sensor was

also divided into two zones like LSM or LSM-YSZ based sensors (**Figure 5-21**). The

high sensitivity zone was for < 25 ppm NO and the low sensitivity zone was for > 25

ppm NO. For the lower ppms of NO, this sensor showed ~ 28% more sensitivity, and for

higher NO ppms, this sensor was ~ 24% more sensitive than LSM-Au based sensor

which was discussed in Section 5.1. As the electrode for both sensors was the same, this

increase in NO sensitivity most probably attributed by the composite electrolyte. The

water cross-sensitivity for novel composite sensor increased compared to the LSM-Au

based sensor discussed in Section 5.1. The sensitivity almost decreased 33% in 10%

humidified condition than that of dry condition.
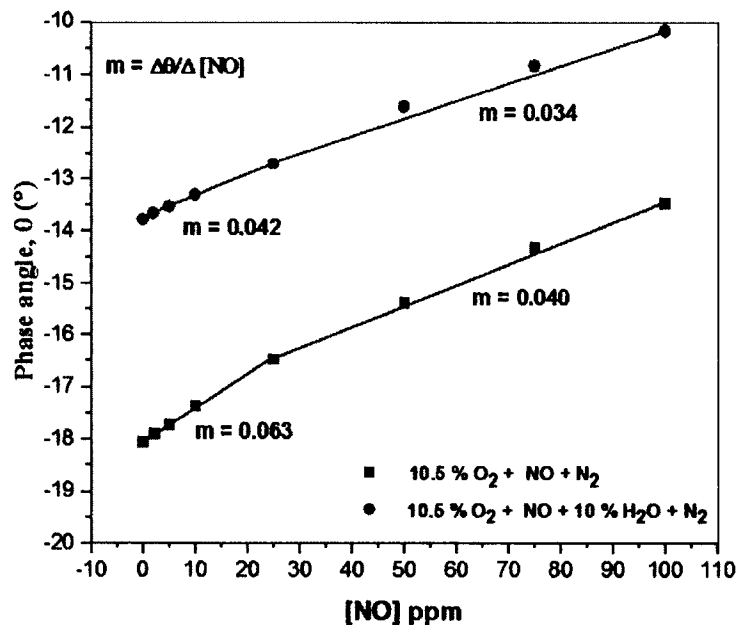
Figure 5-21: NO sensitivity plot of novel composite sensor for dry and 10%
humidified condition at 575°C.

89

From the time based study (**Figure 5-22**) of the novel composite sensor, the value

of τ_{90} was calculated and the value of τ_{90} for 2 ppm NO was ~33 seconds. The τ_{90} value

for all the NO ppms was in the range of 33-36 seconds. The recovery time was also

calculated which was very close to τ_{90} value and was in a range of 34-36 seconds. The

recovery time for both the novel composite and LSM-Au based sensor was comparable

but τ_{90} was lower in the LSM-Au based sensor. This novel composite NO_x sensor was

slower but showed better NO sensitivity than LSM-Au based NO_x sensors discussed in

Section 5.1.
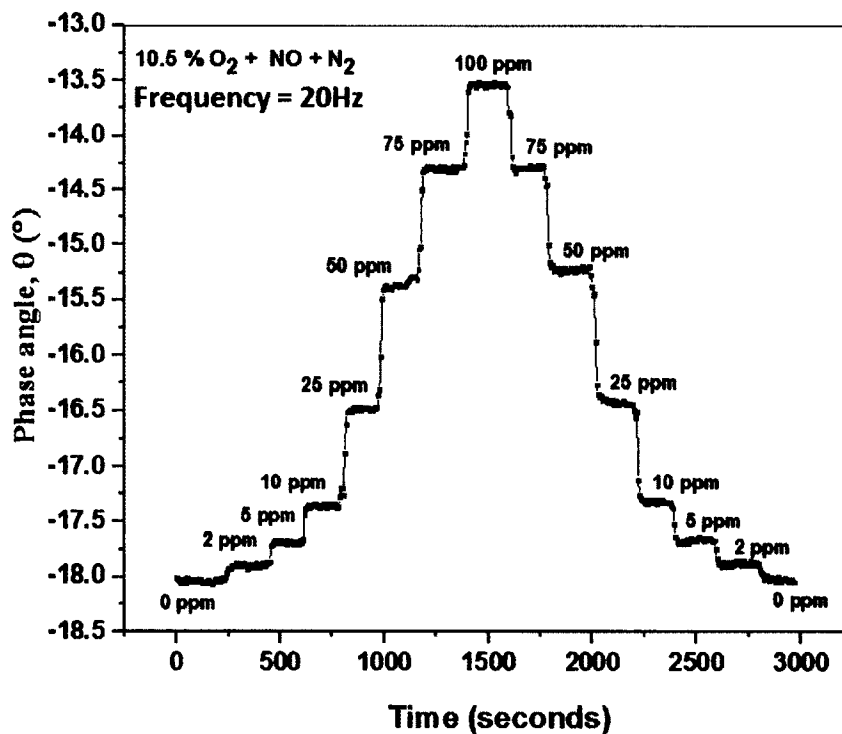
Figure 5-22: NO sensitivity time based study of novel composite sensor for dry
condition at 575°C.

5.2.3.4   Oxygen Sensitivity. In this study, the data was collected for different

concentration of O_2 (5%-18%). **Figure 5-23a** shows the O_2 sensitivity of the novel

composite NO_x sensor at 575°C for 20 Hz and 1000 Hz without NO. **Figure 5-23b** shows

the NO sensitivity of the novel composite NO_x sensor with 10.5% O_2 at 575°C for 20 Hz

and 1000 Hz. The data showed the same tendency as LSM electrode based sensors

(**Figure 4-7**). Therefore, it can be said from the data that at 1000 Hz frequency this sensor

acts as oxygen sensor and oxygen sensitivity is dependent on frequency of the input

signal.
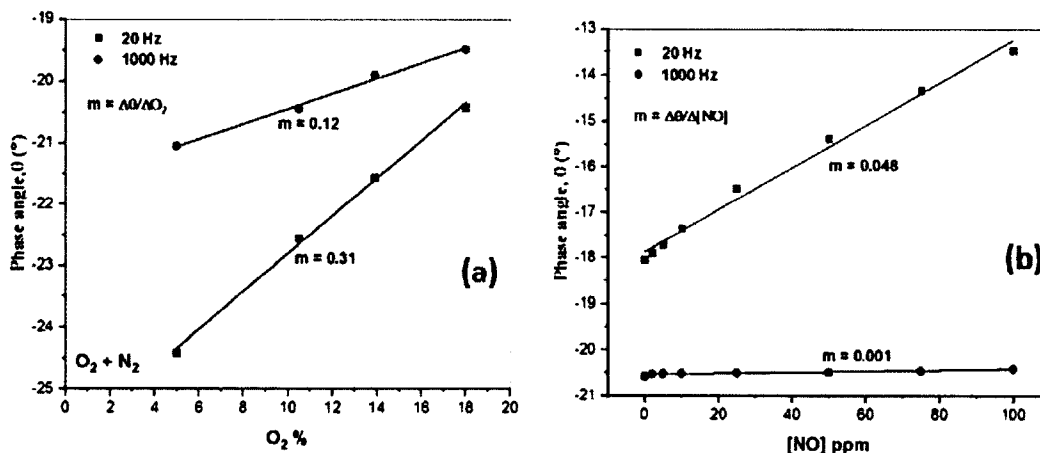
Figure 5-23: Comparison of (a) O_2 and (b) NO sensitivity of the novel composite NO_x sensor at 575°C for 20 Hz and 1000 Hz.

Figure 5-24 shows the NO_x sensor oxygen partial pressure dependence for an

operating temperature of 575°C with and without NO and 10% water vapor where the

oxygen concentration varied from 5 - 18% with N_2 as the background gas. As discussed

in Section 4.1.4.4, the value of m is related to a particular rate limiting mechanisms

describing oxygen related processes at the electrode and electrode/electrolyte interface.

Here, m was found to range from approximately -0.23 to -0.32 as the operating condition changes.

The data in **Figure 5-24** corresponding to the sensor operation at 575°C suggested the sensing response of the novel composite sensor seemed to be primarily limited by the rate of oxygen reduction at the TPB as m was close to -0.25 for the dry gas conditions. However, for humidified gas conditions, the oxygen partial pressure dependence was increasing. In presence of 10% water, most probably atomic oxygen adsorption was the rate limiting factor [83].
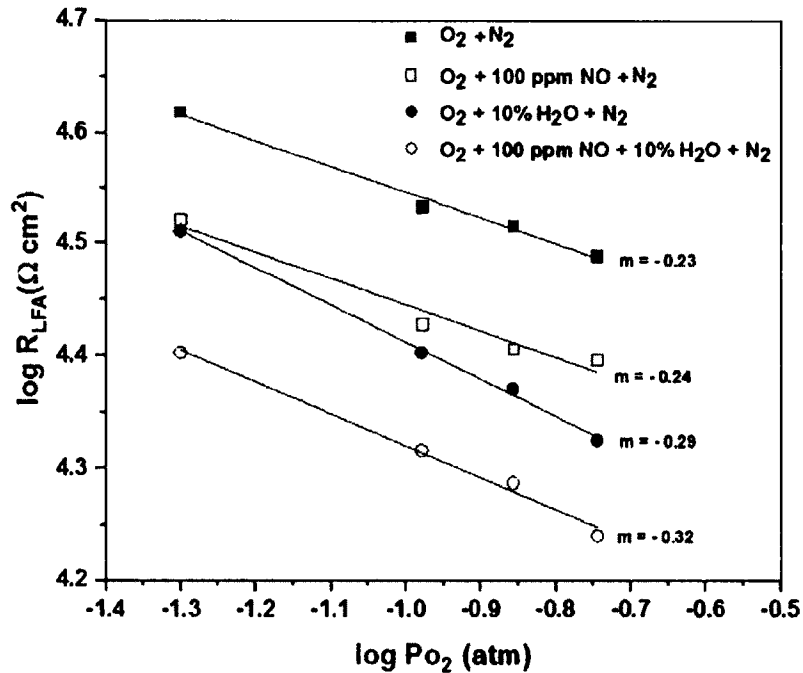
Figure 5-24: PO_2 dependence of novel composite NO_x sensor at 575°C for dry and humidified condition with and without NO.

5.2.4 Conclusions

The novel composite sensor was made of composite electrode and composite electrolyte. Both the electrode and the electrolyte separately showed improved NO_x sensitivity and low water cross-sensitivity. Therefore, the novel composite sensor was very promising in NO sensing, but the water cross-sensitivity was reported to be higher. In dry conditions, the sensor was sluggish compared to LSM-Au based NO_x sensors. This sensor also showed the same type of oxygen dependence as LSM, LSM-Au and LSM-YSZ based sensors. The oxygen dependence changed with the operating frequency, and at 1000 Hz, the sensor was only sensitive to oxygen. So, frequency dependent oxygen compensation can be done for this sensor. The rate limiting factor for the dry condition was the amount of oxygen reduction, but in the humidified condition this factor changed to atomic oxygen adsorption.

In the future, the cross-sensitivity study with other exhaust gases would be interesting for this novel composite sensor. To manage the water cross-sensitivity, the ratio of YSZ and PSZ in the electrolyte composition can be changed. Overall, this novel composite sensor showed much improved NO sensitivity with moderate speed of response.

CHAPTER 6

GOLD AND PLATINUM DENSE ELECTRODE STUDY

This chapter will cover the study on dense Au and Pt electrodes for NO_x sensing. Section 6.1 discusses the study with Au and Pt sensing electrodes using 2-point and 3-point measurement technique. Section 6.2 presents the description of Au/Pt twine electrode. Au/Pt sensing electrodes were considered as a means to capitalize on the NO_x sensing behavior of Au electrodes while incorporating Pt to extend the processing temperature tolerance of the electrode.

6.1   Au and Pt Sensing Electrode Study

Here, the electrochemical response of NO_x sensors composed of Pt, Au, and Au/Pt twine electrodes were evaluated. The sensors were based on a porous zirconia-alumina electrolyte. The alumina addition to the electrolyte was expected to enhance sensor durability and ionic conductivity. Presented here are preliminary results for Pt/ YSZ-Al_2O_3/Au NO_x sensors.

6.1.1   Experimental

The fabrication process has been discussed in Section 3.1.2.

Electrochemical data were collected by placing a sensor into a quartz tube on a

ceramic holder that was placed into a tube furnace, which exposed the electrolyte and

electrodes to the same environment. Temperatures of 600-700°C, NO concentrations of

0-100 ppm, and 10.5% O_2 concentration with N_2 as the balance gas were the conditions

utilized to test the sensors. A gas handling system was used to control the concentrations

of NO and O_2. A Gamry Reference 600 was used to measure the electrical response of

the sensors and the signal amplitude was 100 mV. Scanning electron microscopy (SEM),

element mapping, and Archimedes method were used to evaluate the microstructure of

the sensor components; 3-point measurements were taken using Pt and Au as the working

electrode to study the individual contribution of Platinum and gold in NO_x sensing

(**Figure 6-1**). 2 point measurements were also taken to determine the overall response of

the sensor. The Nyquist plots of 3-point and 2-point measurements have been shown in

the 'result and discussion' section.
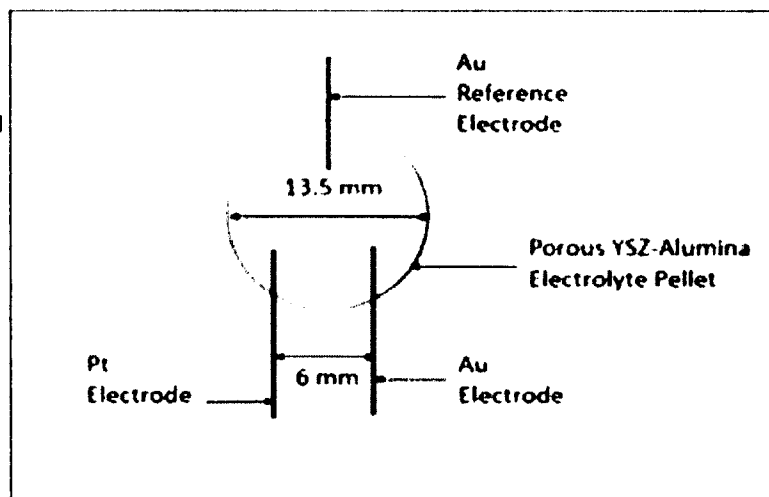
Figure 6-1: Schematic diagram of the $YSZ-Al_2O_3$ NO_x sensor.

6.1.2   Characterization of the NO$_x$ Sensor

Presented here are the SEM and preliminary results for the electrical response of the Pt/YSZ-2%Al$_2$O$_3$/Au NO$_x$ sensors based on impedance spectroscopy. **Figure 6-2a** is a SEM image of the surface of the YSZ-2%Al$_2$O$_3$ electrolyte. The microstructure was composed of a network of porous YSZ and Al$_2$O$_3$ particles, and the surface appeared to be free of cracks. The lighter regions resulted from surface charging during SEM imaging. Higher magnification images have indicated the particle size range between 60 to 80 nm. The Al$_2$O$_3$ particles tended to be more irregular in shape in comparison to the YSZ particles. Elemental mapping was used to determine the distribution of the Al$_2$O$_3$ particles. **Figure 6-2b** shows the mapping results collected from the area shown in **Figure 6-2a**. The bright green regions indicated the location of Al$_2$O$_3$ particles. It appeared that the Al$_2$O$_3$ particles were well distributed. These results were typical of the YSZ-2%Al$_2$O$_3$ electrolytes.

a   b
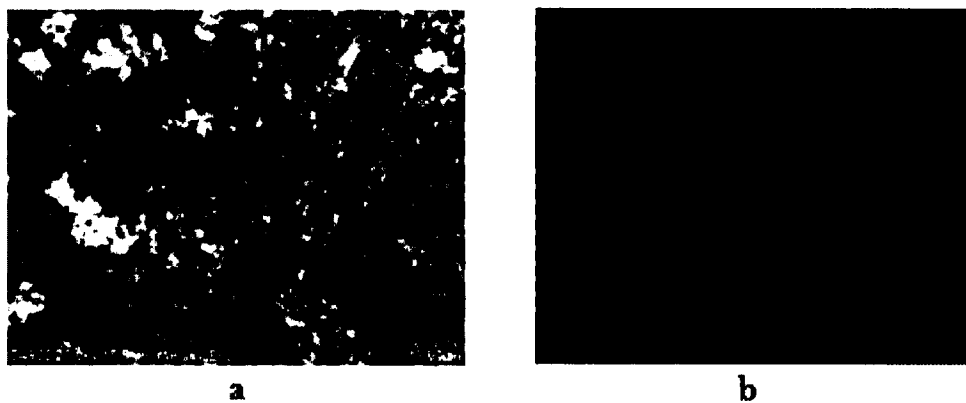
Figure 6-2: a) SEM images of an YSZ-Al$_2$O$_3$ pellet, and b) corresponding mapping results illustrating the distribution of Al$_2$O$_3$ particles.

Based on the Archimedes' method, the porosity of the YSZ-2%Al_2O_3 pellets was approximately 53%. The porous microstructure allows the NO, O_2 and N_2 gases to readily diffuse to the electrode/electrolyte interface where electrochemical reactions take place. The porosity also influences the triple-phase-boundary density, which is based on contact between the electrode, electrolyte and gas phase.

6.1.3   Result and Discussion

6.1.3.1   Impedance Behavior. The impedance data is frequency dependent, and the NO concentration, O_2 concentration, and the operating temperature influence the reactions occurring at the sensor electrodes. **Figure 6-3** shows a Nyquist plot for the sensors collected at operating temperatures of 600°C, 650°C, and 700°C in the presence of 10.5% O_2 + N_2. For each temperature, a high and low frequency arc resulted. The high frequency arc was substantially larger than the low frequency arc. The high frequency arc corresponded to the electrochemical behavior of the YSZ-2% Al_2O_3 electrolyte. Al_2O_3 has been reported to enhance grain boundary conductivity through YSZ. However, it can also cause an increase in the YSZ bulk resistivity [93]. As the temperature increased, the high and low frequency arc decreased.
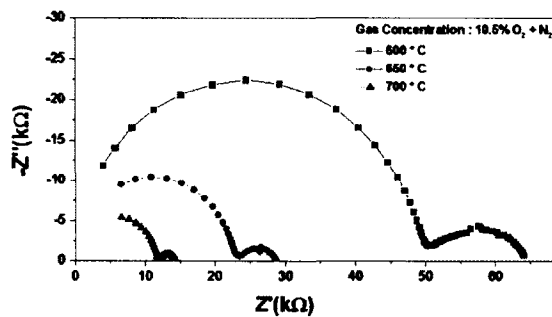
Figure 6-3: The impedance data collected at temperatures of 600°C, 650°C, and 700°C.

The impedance at high frequency was likely impacted by the YSZ bulk resistivity.

The smaller arc occurred at lower frequencies. This arc was also slightly suppressed

below the real axis in comparison to the high frequency arc. The low frequency arc is

understood to describe interfacial and electrode reactions. **Figure 6-3** depicts data

collected using a 2-point electrode impedance measurement technique that yields the

combined electrical response of reactions occurring at the Pt and Au electrodes. **Figures**

6-4a and **4b** show the 3-point measurement Nyquist plots with Au and Pt as working

electrodes respectively at 625°C. From **6-4b** it can be seen that Pt does not significantly

contribute to NO sensing, but from **6-4a** we can see that Au is sufficiently sensitive to

NO.
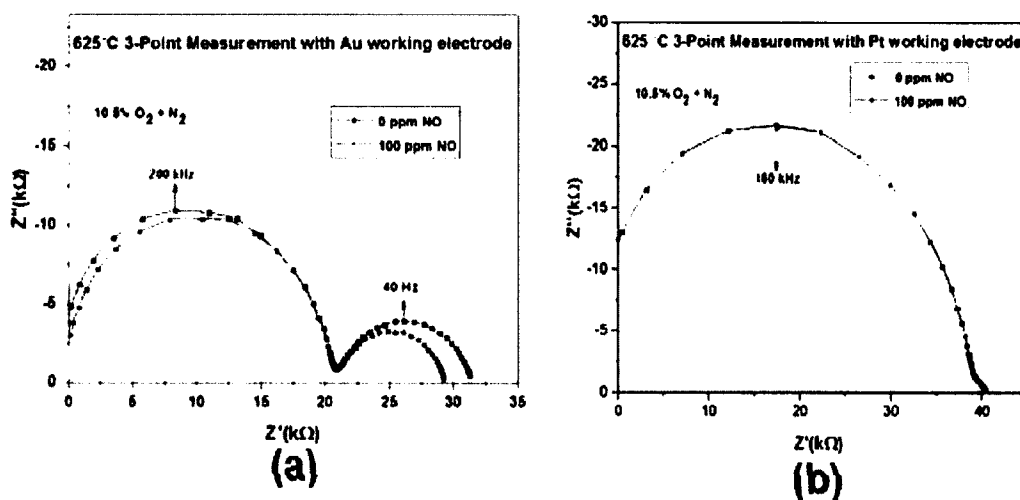
Figure 6-4: a) Nyquist Plot for the 3-point measurement Au as working electrode and b) Nyquist Plot for the 3-point measurement Pt as working electrode.

Figure 6-5 shows the Nyquist plot for the 2-point measurement data, which is the

overall response of the sensor. From the information of **Figure 6-4** and **Figure 6-5**, we

can conclude that the sensitivity of this sensor is mostly coming from Au electrodes.
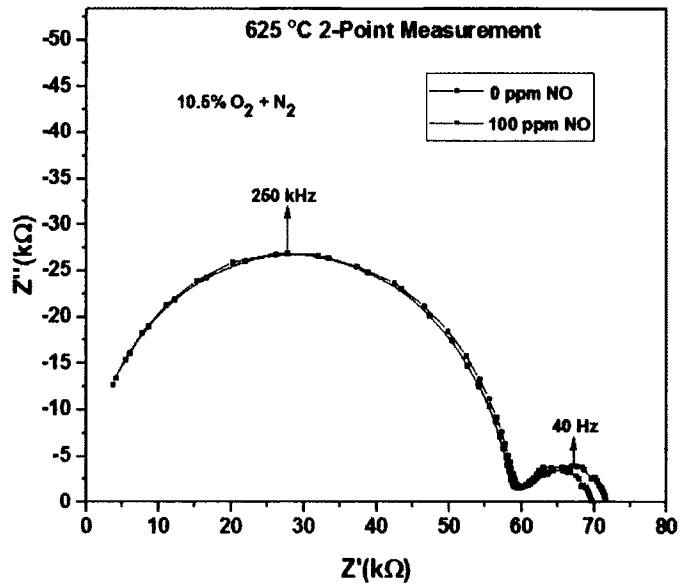
Figure 6-5: Nyquist Plot for the 2-point measurement of the NO$_x$ Sensor.

6.1.3.2   NO Sensitivity.

From the sensitivity plot in **Figure 6-6,** it can be seen that the sensor is more

sensitive in lower temperatures. Sensitivity decreases with an increase in temperature.
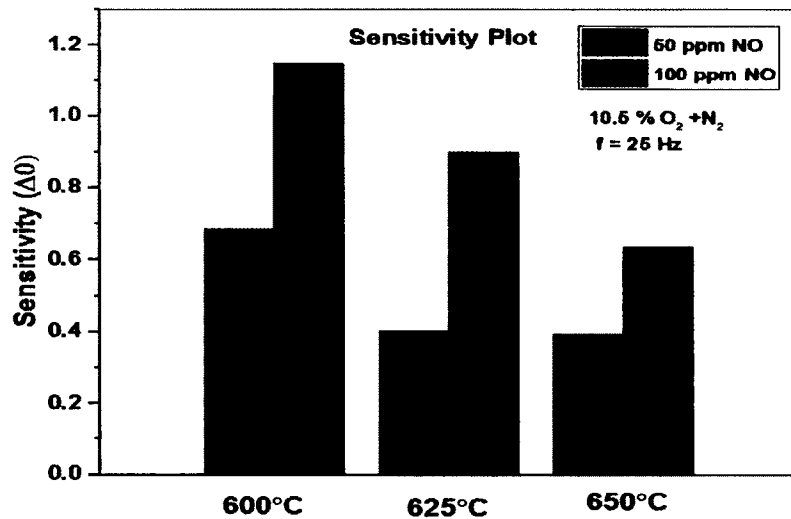
Figure 6-6: Sensitivity plot for the NO$_x$ sensor.

99

Here, $\Delta\theta = \theta_{O2} - \theta_{NOx}$. Here, θ_{O2} corresponded to the phase angle response with only 10.5% O_2 and N_2 present; θ_{NOx} corresponded to the phase angle response with the addition of NO in the gas stream.

6.1.3.3   PO$_2$ Dependence. The slope associated with the oxygen partial pressure dependence is generally correlated with specific reaction mechanisms describing oxygen related processes at the TPB. For Au sensing electrode (**Figure 6-7**), in the absence of NO, the rate limiting mechanism is the dissociative adsorption of oxygen, suggested by the value of m. As NO is introduced in the environment, the charge transfer becomes the rate limiting factor.
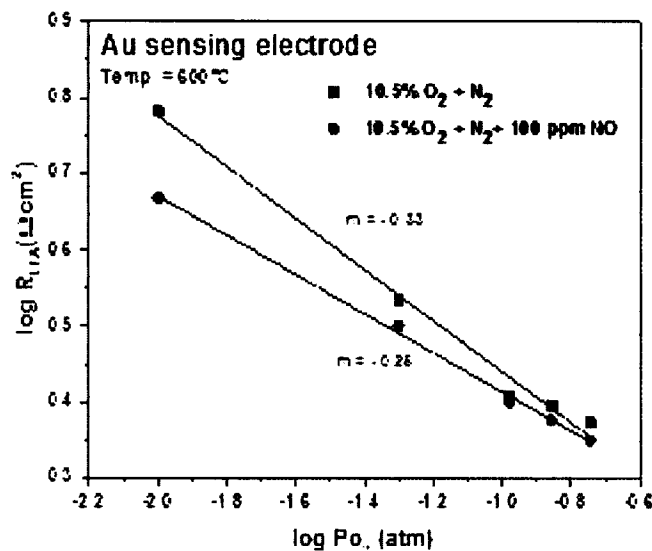
Figure 6-7: Oxygen partial pressure plot with and without NO for the NO$_x$ sensor along with the slops.

6.1.4   Conclusions

Au/YSZ-Al$_2$O$_3$/Pt NO$_x$ sensors were studied in order to understand the electrical behavior of Pt and Au electrodes with a YSZ-Al$_2$O$_3$ electrolyte. Understanding the individual contribution of each electrode is expected to aid in the interpretation of the

100

NO_x sensing behavior of Au/Pt twine electrodes using the same electrolyte. The preliminary results presented indicated sensor fabrication methods resulted in a suitable porous YSZ-2%Al_2O_3 composite electrolyte microstructure that was free of surface cracks. The elemental mapping results indicated are reasonable distribution of Al_2O_3 particles throughout the electrolyte. The impedance data collected at different temperatures indicated the impedance decrease with increasing temperature. Overall, the high frequency arc for the sensors dominated the impedance response. Since this result was independent of temperature, it was likely due to the presence of 2 wt% Al_2O_3 within the electrolyte. The impedance data collected using the 2-point method illustrated the combined electrical response of the Pt and Au electrodes within the NO_x sensor. This information will be used to analyze data collected using a 3-point impedance measurement technique, which will allow the individual contributions of the Pt and Au electrodes to be distinguished. An understanding of the electrical behavior of the Pt and Au electrodes is expected to be useful for interpreting the electrical behavior of Au/Pt twine electrodes at YSZ-Al_2O_3 based NO_x sensors.

6.2   Au/Pt Twine Electrode Study with Pt Counter Electrode

Dense Au/Pt electrodes made from wires that are twined together are expected to extend the processing temperature tolerance of the electrode, but may also limit the reaction sites along the triple phase boundary (TBP) and compromise NO_x sensitivity. The aim of this study was to explore the feasibility of dense Au/Pt twine electrodes for NO_x sensing.

6.2.1   Experimental

The process has already been discussed in the Section 3.1.1.2. **Figure 6-8** shows the schematic of the sensor Au/Pt electrode.
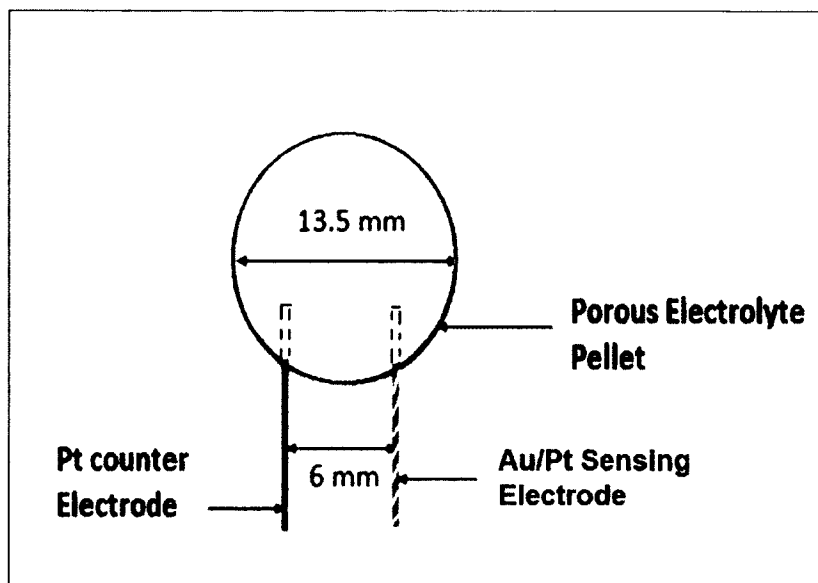
Figure 6-8: Schematic diagram of the NO_x Sensors with Au/Pt twined sensing electrode.

Electrochemical data were collected by placing a sensor into a quartz tube on a ceramic holder that was placed into a tube furnace, which exposed the electrolyte and electrodes to the same environment. Temperatures of 600-700°C, NO concentrations of 0-100 ppm, and 10.5% O_2 concentration with N_2 as the balance gas were the conditions utilized to test the sensors. Here, the electrolyte was 8 mol% YSZ mixed with 2 wt % Al_2O_3.

6.2.2   Result and Discussion

6.2.2.1   Impedance Behavior.

Figure 6-9 depicts data collected using a 2-point electrode impedance measurement technique. **Figures 6-9 a** and **6-9 b** display the 2-point measurement Nyquist plots with Au/Pt and Au as the working electrodes at 625°C. From these plots it can be concluded that there is a decrease in RLF in the presence of NO in the environment.
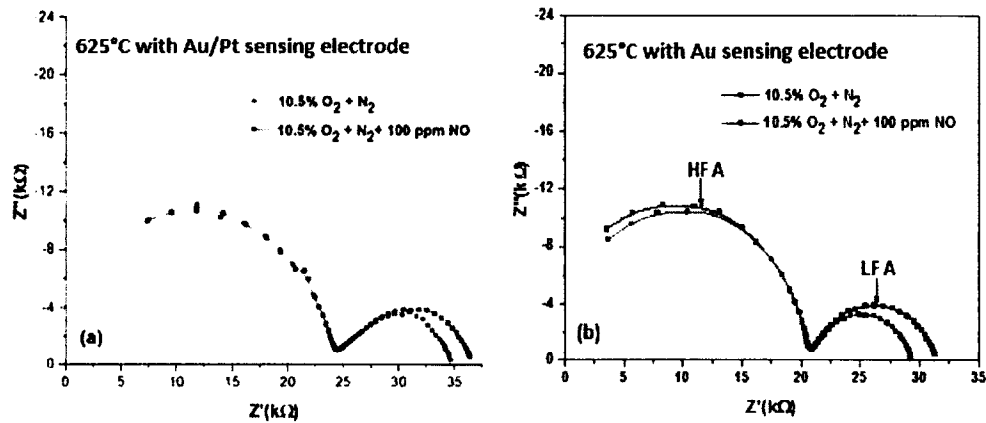
Figure 6-9: Nyquist plot of the NOx Sensors with (a) Au/Pt (b) Au sensing electrode.

6.2.2.2   NO Sensitivity.

Figure 6-10 shows the NO sensitivity plots using Au/Pt twine and Pt sensing electrodes. NOx sensors based on the Au/Pt twine sensing electrode demonstrated similar sensitivity to that observed for Au sensing electrodes. Thus, Pt had a negligible effect on the sensing behavior. From **Figure 6-11**, it can be said that the temperature dependence of the Au/Pt sensing electrodes was also very similar to that of Au as the sensitivity decreased with the operating temperature. Overall, the data indicated the Au/Pt sensing electrode is a promising alternative to Au sensing electrodes.
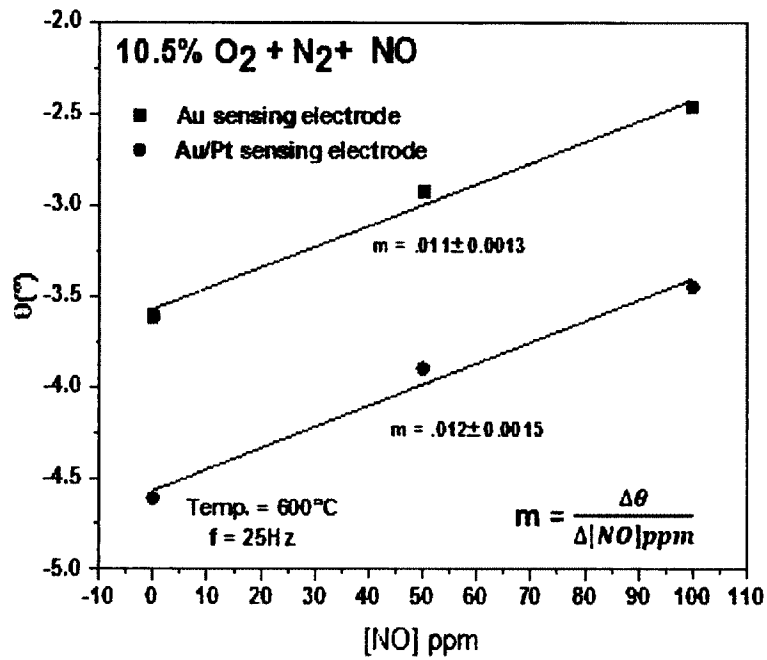
Figure 6-10: NO sensitivity plot of the NO$_x$ Sensors with Au/Pt and Au sensing electrode at 600°C.
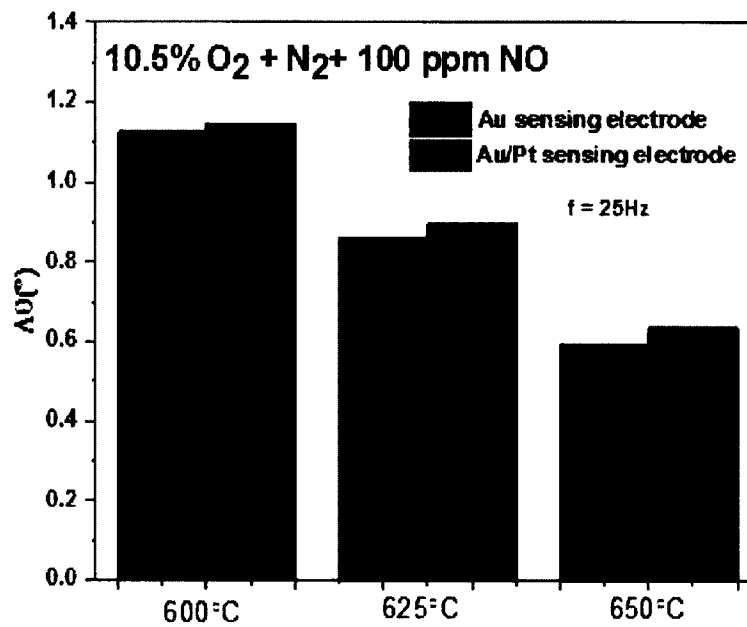
Figure 6-11: NO sensitivity plot of the NO$_x$ Sensors with Au/Pt and Au sensing electrode in different operating temperatures.

6.2.3 Conclusions

By comparison of the NO_x sensors containing Au/Pt twine sensing electrodes and Au sensing electrodes, it was seen that Pt wire wrapped with Au wire was not affecting the NO sensitivity, but can enable the sensing electrode to be more robust from a fabrication point of view.

CHAPTER 7

CONCLUSIONS AND FUTURE WORK

7.1   Conclusions

The work presented here has discussed the application of different dense single-phase and composite electrodes in NO_x gas sensing for any diesel vehicle exhaust system. From the entire study, these following conclusions can be drawn:

- The dense LSM electrode study was done using both porous LSM and dense Au counter electrodes and a difference in the NO sensitivity resulting was reported. The sensor with porous LSM counter electrode showed much improved sensing activity than that of the Au counter electrode at 575°C. The reason behind it most probably is the thermal coefficient mismatch between the electrolyte (YSZ) and the Au wire. This study showed how the micro-cracks on the electrolyte surface can deteriorate the sensing performance of the sensor. Though the sensor with porous LSM counter electrode showed good NO sensitivity, there was also a considerable amount of water and CH_4 cross-sensitivity.

- For the perovskite based composite electrode study, LSM was mixed with one electronic conductor, Au, and an ionic conductor, YSZ, and a mixed conductor, LSCF. In comparing the results for LSM-Au, LSM-YSZ and LSM-LSCF based sensors, it was established that the LSM-Au composite showed ~ 25% higher sensitivity than

106

LSM based sensors ~ 50% higher sensitivity than LSM-YSZ based sensors and ~ 35% higher sensitivity than LSM-LSCF based sensors at 575°C. From the angular frequency analysis, it was found that 20 Hz was the frequency that yielded the highest NO sensitivity for all of the perovskite based sensors. Water cross-sensitivity for the LSM-Au based sensors was much lower (~ 7%) than that of LSM and LSM-YSZ based sensors (~ 20 - 30%). The addition of Au probably increased the NO sensitivity and reduced the water cross-sensitivity. CH_4 cross-sensitivity was also improved after adding Au with LSM. Mixing YSZ with LSM most probably reduced the length of the TPB, in turn reducing the NO sensing capability.

- The sensor accuracy study for both LSM and LSM-Au based sensors showed LSM-Au based sensors had better accuracy than that of LSM when temperature perturbations were considered. The LSM-Au based sensors also showed a stable performance after 360 hours of testing under dry and 10% humidified conditions.

- The novel composite NO_x sensor composed of LSM-Au based composite electrode and YSZ-PSZ (50:50) based composite electrolyte was studied. This sensor showed ~ 23% greater NO sensitivity compared to LSM-Au based sensor with YSZ electrolyte. However, the water cross-sensitivity of this novel composite sensor was higher than that of the sensor with only YSZ electrolyte and LSM-Au composite electrode. Overall, achieving such a high NO sensitivity with the novel composite sensor was a promising outcome of the project. The response rate of this sensor was also comparable to other composite electrode (LSM-Au and LSM-YSZ) based sensors tested during this project.

- Au/Pt twine electrodes were also a part of this study. Those electrodes were studied to explore the possibilities of making Au/Pt composite electrodes to facilitate NO_x sensing. Au/Pt twine electrodes were tested for NO sensing and compared to the results with pure Au wire electrodes for NO sensing. The result showed no significant compromise in NO sensing due to the presence of Pt wire in the twine electrode. This result was promising as the preceding step of making Au/Pt composite.

7.2   Future Work

These are some areas of this thesis work where there is potential for future studies:

- During the study with LSM-Au electrodes, it was found that the rate of response of the sensor was not that fast as the sensor made of pure LSM electrodes. According to another study, the sensor response rate can be improved by changing the Au particle size [52]. So, there can be an interesting study on how the size of an Au particle in LSM-Au composite influences the NO_x sensitivity of the sensor.

- While studying the novel composite sensor, high water cross-sensitivity was reported when the composite YSZ-PSZ electrolyte was used. Changing the ratio of YSZ and PSZ in the composite electrolyte may improve the water cross-sensitivity as other studies have shown that water behaviour of the sensors alter with the change in quantity of YSZ and PSZ in the composite electrolyte [91]. In addition, there may be a more suitable operating frequency to apply as other works with such an electrolyte were conducted at a higher operating frequency (40 Hz) compared to the 20 Hz used in the present work.

- The cross-sensitivity of the novel composite sensor can also be tested for other exhaust gases like NH_3, hydrocarbons, CO, and CO_2.

APPENDIX A

TEST OF LSM AND LSM-Au BASED NO$_x$ SENSORS UNDER DIFFERENT AC SIGNAL AMPITUDE

NO$_x$ sensor testing under different AC signal amplitude was done to further

understand the sensing mechanism. This test was done on LSM-Au based sensors as

these showed the best performance among all the sensors tested. LSM based sensors were

tested for comparison purpose.

A.1   Experimental

LSM and LSM-Au base sensors were tested at 575°C in the presence of 10.5% O$_2$

and N$_2$ as a balance gas with and without 100 ppm NO. The AC amplitude was changed

from 50-150 mV by using Gamry Reference 600 and the corresponding electrical

responses were collected.

A.2   Result and Discussion
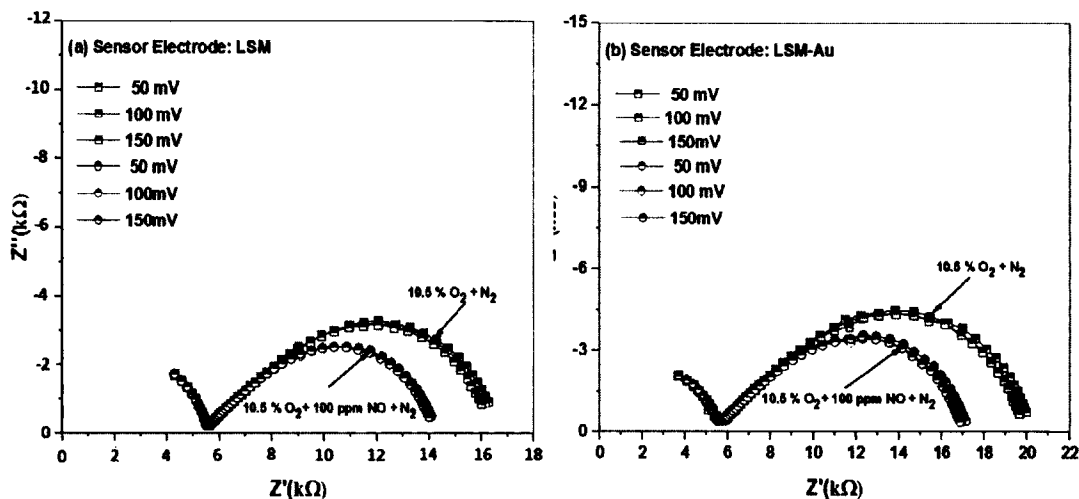
Figure A-1: Nyquist plot under different AC amplitude test for (a) LSM and (b) LSM-Au based NO$_x$ sensors.

There was no substantial change reported for the test under different AC

magnitude of the input signal from **Figure A-1**. Hence, it can be concluded that AC

magnitude of the input signal within that specific range does not have a significant effect

on the sensor response.

REFERENCES

[1] L. P. Martin, L. Y. Woo, and R. S. Glass, "Impedancemetric NO_x Sensing Using YSZ Electrolyte and YSZ/Cr_2O_3 Composite Electrodes," J. Electrochem. Soc., vol. 154, no. 3, p. J97, 2007.

[2] B. B. J. Cooper, "Challenges in emission control catalysis for the next decade," Appl. Catal. B Environ., vol. 3, no. 4, pp. N26–N28, 1994.

[3] R. Burch, J. P. Breen, and F. C. Meunier, "A review of the selective reduction of NOx with hydrocarbons under lean-burn conditions with non-zeolitic oxide and platinum group metal catalysts," Appl. Catal. B Environ., vol. 39, no. 4, pp. 283–303, 2002.

[4] G. I. Barenblatt and R. A. Sunyaev, Eds., "25. The Oxidation of Nitrogen in Combustion and Explosions," in Selected Works of Yakov Borisovich Zeldovich, Volume I, Princeton: Princeton University Press, 1992, pp. 364–403.

[5] G. L. Borman and K. W. Ragland, Combustion engineering. McGraw-Hill, 1998.

[6] Robert Bosch GmbH., Diesel-engine management., 4th ed. John Wiley & Sons, 2007.

[7] R. R. Rajaram and S. Poulston, "NO_x-trap," US7287370 B2, Patent, 2007.

[8] W. Harrington, "The Design of Effective Regulations of Transport," OECD Publishing, 2008.

[9] R. Brezny, "Vehicle Emission Standards and Emission Control Experience MECA Technology Portfolio Covers Criteria and GHG Emission Control Technologies," 2017.

[10] Jonathan Michael Rheaume, "Electronic Thesis and Dissertations Solid State Electrochemical Sensors for Nitrogen Oxide Detection in Lean Exhaust Gases," U. C. Berkeley, Dissertation 2010.

[11] N. Docquier and S. Candel, "Combustion control and sensors: a review," Prog. Energy Combust. Sci., vol. 28, no. 2, p. 135, 2002.

[12] L. Y. Woo, R. S. Glass, R. F. Novak, and J. H. Visser, "Effect of Electrode Material and Design on Sensitivity and Selectivity for High Temperature Impedancemetric NO_x Sensors," J. Electrochem. Soc., vol. 157, no. 3, p. J81, 2010.

[13] J. Zou, Y. Zheng, J. Li, Z. Zhan, and J. Jian, "Potentiometric NO_2 Sensors Based on Thin Stabilized Zirconia Electrolytes and Asymmetric (La0.8Sr0.2)0.95MnO3 Electrodes," Sensors, vol. 15, no. 7, pp. 17558–17571, 2015.

[14] N. Miura, T. Sato, S. A. Anggraini, H. Ikeda, and S. Zhuiykov, "A review of mixed-potential type zirconia-based gas sensors," Ionics , vol. 20, no. 7, pp. 901–925, 2014.

[15] J. M. Rheaume and A. P. Pisano, "A review of recent progress in sensing of gas concentration by impedance change," Ionics, vol. 17, no. 2, pp. 99–108, 2011.

[16] L. Y. Woo, L. P. Martin, R. S. Glass, W. Wang, S. Jung, R. J. Gorte, E. P. Murray, R. F. Novak, and J. H. Visser, "Effect of Electrode Composition and Microstructure on Impedancemetric Nitric Oxide Sensors Based on YSZ Electrolyte," October, vol. 155, no. May 2011, pp. 32–40, 2007.

[17] Y. X. Liu, J. Parisi, X. C. Sun, and Y. Lei, "Solid-state gas sensors for high temperature applications - a review," J. Mater. Chem. A, vol. 2, no. 26, pp. 9919–9943, 2014.

[18] M. Noda, N. Kato, and H. Kurachi, "Electrochemical NO_x sensor," US4770760 A, Patent, 1988.

[19] E. M. Logothetis and R. E. Soltis, "Method for determining relative amount of oxygen containing gas in a gas mixture," US5288375 A, Patent, 1994.

[20] T. Ueda, T. Nagano, H. Okawa, and S. Takahashi, "Zirconia-based amperometric sensor using La-Sr-based perovskite-type oxide sensing electrode for detection of NO_2," Electrochem. commun., vol. 11, no. 8, pp. 1654–1656, 2009.

[21] J. Yoo, S. Chatterjee, and E. D. Wachsman, "Sensing properties and selectivities of a WO_3/YSZ/Pt potentiometric NO_x sensor," Sensors Actuators B Chem., vol. 122, no. 2, pp. 644–652, 2007.

[22] S. Zhuiykov and N. Miura, "Development of zirconia-based potentiometric NOx sensors for automotive and energy industries in the early 21st century: What are the prospects for sensors?," Sensors Actuators B Chem., vol. 121, no. 2, pp. 639–651, 2007.

[23] M. E. Orazem and B. Tribollet, Electrochemical Impedance Spectroscopy. Hoboken, NJ, USA: John Wiley & Sons, Inc., 2008.

[24] E. Magori, G. Reinhardt, M. Fleischer, R. Mayer, and H. Meixner, "Thick film device for the detection of NO and oxygen in exhaust gases," Sensors Actuators B Chem., vol. 95, no. 1, pp. 162–169, 2003.

[25] J. E. Bauerle, "Study of solid electrolyte polarization by a complex admittance method," J. Phys. Chem. Solids, vol. 30, no. 12, pp. 2657–2670, Dec. 1969.

[26] S. Killa, L. Cui, E. P. Murray, and D. S. Mainardi, "Kinetics of nitric oxide and oxygen gases on porous Y-stabilized ZrO_2-based sensors," Molecules, vol. 18, no. 8, pp. 9901–9918, 2013.

[27] R. Barfod, A. Hagen, S. Ramousse, P. V. Hendriksen, and M. Mogensen, "Break Down of Losses in Thin Electrolyte SOFCs," Fuel Cells, vol. 6, no. 2, pp. 141–145, Apr. 2006.

[28] Autolab, "Basic overview of the working principle of a potentiostat/galvanostat (PGSTAT) – Electrochemical cell setup." [Online]. Available: http://www.metrohmautolab.com/download/Applicationnotes/Autolab_Applicatio n_Note_EC08.pdf. [Accessed: 27-May-2017].

[29] T. Striker, V. Ramaswamy, E. N. Armstrong, P. D. Willson, E. D. Wachsman, and J. a. Ruud, "Effect of nanocomposite Au–YSZ electrodes on potentiometric sensor response to NO_x and CO," Sensors Actuators B Chem., vol. 181, pp. 312–318, 2013.

[30] P. K. Sekhar, E. L. Brosha, R. Mukundan, M. A. Nelson, D. Toracco, and F. H. Garzon, "Effect of yttria-stabilized zirconia sintering temperature on mixed potential sensor performance," Solid State Ionics, vol. 181, no. 19–20, pp. 947–953, Jul. 2010.

[31] E. Di Bartolomeo and M. L. Grilli, "YSZ-based electrochemical sensors: From materials preparation to testing in the exhausts of an engine bench test," J. Eur. Ceram. Soc., vol. 25, no. 12, pp. 2959–2964, 2005.

[32] E. Di Bartolomeo, "Planar electrochemical sensors based on tape-cast YSZ layers and oxide electrodes," Solid State Ionics, vol. 171, no. 3–4, pp. 173–181, Jul. 2004.

[33] A. Dutta, N. Kaabbuathong, M. L. Grilli, E. Di Bartolomeo, and E. Traversa, "Study of YSZ-Based Electrochemical Sensors with WO_3 Electrodes in NO_2 and CO Environments," J. Electrochem. Soc., vol. 150, no. 2, p. H33, 2003.

[34] J. Meija, "Atomic weights of the elements 2013 (IUPAC Technical Report)," 2015.

115

[35] L. Y. Woo, R. S. Glass, R. F. Novak, and J. H. Visser, "Diesel engine dynamometer testing of impedancemetric NO_x sensors," Sensors Actuators B Chem., vol. 157, no. 1, pp. 115–121, 2011.

[36] L. Cui, F. Han, W. Dai, and E. P. Murray, "Influence of Microstructure on the Sensing Behavior of NO_x Exhaust Gas Sensors," J. Electrochem. Soc., vol. 161, no. 3, pp. B34–B38, 2013.

[37] J. M. Rheaume and A. P. Pisano, "Investigation of an impedancemetric NO_x sensor with gold wire working electrodes," J. Solid State Electrochem., vol. 16, no. 11, pp. 3603–3610, Nov. 2012.

[38] W. L. D. Frane, L. Y. Woo, R. S. Glass, R. F. Novak, and J. H. Visser, "Substrate Effects on an Electrochemical NOx Sensor Based on Porous Y_2O_3-Stabilized ZrO_2 (YSZ) and Sr-doped $LaMnO_3$ (LSM)," ECS Trans., vol. 45, no. 14, pp. 3–11, 2013.

[39] L. Woo and R. Glass, "NO_x sensor development," Report, 2010.

[40] D. L. West, F. C. Montgomery, and T. R. Armstrong, "'Total NO_x' Sensing Elements with Compositionally Identical Oxide Electrodes," J. Electrochem. Soc., vol. 153, no. 2, p. H23, 2006.

[41] S.W. Song, L. P. Martin, R. S. Glass, E. P. Murray, J. H. Visser, R. E. Soltis, R. F. Novak, and D. J. Kubinski, "Aging Studies of Sr-Doped $LaCrO_3$/YSZ/Pt Cells for an Electrochemical NO_x Sensor," J. Electrochem. Soc., vol. 153, no. 9, p. H171, 2006.

[42] J. Fergus, "Materials for high temperature electrochemical NO_x gas sensors," Sensors Actuators B Chem., vol. 121, no. 2, pp. 652–663, 2007.

[43] T. Ueda, T. Nagano, H. Okawa, and S. Takahashi, "Zirconia-based amperometric sensor using La–Sr-based perovskite-type oxide sensing electrode for detection of NO_2," Electrochem. commun., vol. 11, no. 8, pp. 1654–1656, Aug. 2009.

[44] J. Zou, X. Liu, H. Jin, Z. Zhan, and J. Jian, "NO_2 sensing properties of electrode-supported sensor by tape casting and co-firing method," Ionics , vol. 21, no. 9, pp. 2655–2662, 2015.

[45] T. Ueda, M. Umeda, H. Okawa, and S. Takahashi, "Effects of Sr Addition to La-Based Perovskite Sensing-Electrode on YSZ-Based Amperometric-Type NO_x Sensor," IOP Conf. Ser. Mater. Sci. Eng., vol. 18, no. 21, p. 212012, 2011.

[46] T. J. Armstrong and A. V. Virkar, "Performance of Solid Oxide Fuel Cells with LSGM-LSM Composite Cathodes," J. Electrochem. Soc., vol. 149, no. 12, p. A1565, 2002.

116

[47] A. Urushibara, Y. Moritomo, T. Arima, A. Asamitsu, G. Kido, and Y. Tokura, "Insulator-metal transition and giant magnetoresistance in $La_{1-x}Sr_xMnO_3$," Phys. Rev. B, vol. 51, no. 20, pp. 14103–14109, May 1995.

[48] P. Elumalai, V. V. Plashnitsa, Y. Fujio, and N. Miura, "Highly sensitive and selective stabilized zirconia-based mixed-potential-type propene sensor using NiO/Au composite sensing-electrode," Sensors Actuators, B Chem., vol. 144, no. 1, pp. 215–219, 2010.

[49] U. Guth and J. Zosel, "Electrochemical solid electrolyte gas sensors — hydrocarbon and NO_x analysis in exhaust gases," Ionics , vol. 10, no. 5–6, pp. 366–377, Sep. 2004.

[50] V. V. Plashnitsa, P. Elumalai, Y. Fujio, T. Kawaguchi, N. Miura, and U. Guth, "Spontaneous gradual accumulation of hexagonally-aligned nano-silica on gold nanoparticles embedded in stabilized zirconia: a pathway from catalytic to NH3-sensing performance," Nanoscale, vol. 3, no. 5, p. 2286, 2011.

[51] F. Sun, X. Li, L. Liu, and J. Wang, "Novel Zn–M–O (M=Sn, Co) sensing electrodes for selective mixed potential CO/C_3H_8 sensors," Sensors Actuators B Chem., vol. 184, pp. 220–227, 2013.

[52] Y. Fujio, S. A. Anggraini, H. Ikeda, N. Terasaki, and N. Miura, "Improvement in Response/Recovery Characteristics of Mixed-Potential-Type Zirconia-Based CO Sensor Using $ZnCr_2O_4$ Added with Au Particles-Sensing Electrode," Trans. ECS Soc. Electrochem., vol. 75, no. 16, pp. 59–64, 2016.

[53] R.-J. Wu, C.-H. Hu, C.-T. Yeh, and P.-G. Su, "Nanogold on powdered cobalt oxide for carbon monoxide sensor," Sensors Actuators B Chem., vol. 96, no. 3, pp. 596–601, 2003.

[54] D. Schönauer-Kamin, M. Fleischer, and R. Moos, "Half-cell potential analysis of an ammonia sensor with the electrochemical cell AU | YSZ | Au, V_2O_5-WO_3-TiO_2," Sensors (Switzerland), vol. 13, no. 4, pp. 4760–4780, 2013.

[55] D. Schönauer, K. Wiesner, M. Fleischer, and R. Moos, "Selective mixed potential ammonia exhaust gas sensor," Sensors Actuators B Chem., vol. 140, no. 2, pp. 585–590, 2009.

[56] E. L. Brosha, R. Mukundan, D. R. Brown, and F. H. Garzon, "Mixed potential sensors using lanthanum manganate and terbium yttrium zirconium oxide electrodes," Sensors Actuators, B Chem., vol. 87, no. 1, pp. 47–57, 2002.

117

[57]   T. Schwebel, M. Fleischer, H. Meixner, and C.-D. Kohl, "CO-Sensor for domestic use based on high temperature stable Ga_2O_3 thin films," Sensors Actuators B Chem., vol. 49, no. 1, pp. 46–51, 1998.

[58]   Y. Suetsugu, T. Sato, M. Breedon, and N. Miura, "C_3H_6 sensing characteristics of rod-type yttria-stabilized zirconia-based sensor for ppb level environmental monitoring applications," Electrochim. Acta, vol. 73, pp. 118–122, 2012.

[59]   A. Hashimoto, T. Hibino, K. Mori, and M. Sano, "High-temperature hydrocarbon sensors based on a stabilized zirconia electrolyte and proton conductor-containing platinum electrode," Sensors Actuators B Chem., vol. 81, no. 1, pp. 55–63, 2001.

[60]   T. Hibino, S. Kakimoto, and M. Sano, "Non-Nernstian Behavior at Modified Au Electrodes for Hydrocarbon Gas Sensing," J. Electrochem. Soc., vol. 146, no. 9, p. 3361, 1999.

[61]   J. Wang, P. Elumalai, D. Terada, M. Hasei, and N. Miura, "Mixed-potential-type zirconia-based NO_x sensor using Rh-loaded NiO sensing electrode operating at high temperatures," Solid State Ionics, vol. 177, no. 26, pp. 2305–2311, 2006.

[62]   S. Zhuiykov, T. Ono, N. Yamazoe, and N. Miura, "High-temperature NO_x sensors using zirconia solid electrolyte and zinc-family oxide sensing electrode," Solid State Ionics, vol. 152, pp. 801–807, 2002.

[63]   P. Elumalai, V. V. Plashnitsa, T. Ueda, and N. Miura, "Sensing characteristics of mixed-potential-type zirconia-based sensor using laminated-oxide sensing electrode," 2008.

[64]   V. V. Plashnitsa, T. Ueda, and N. Miura, "Improvement of NO_2 a Sensing Performances by an Additional Second Component to the Nano-Structured NiO Sensing Electrode of a YSZ-Based Mixed-Potential-Type Sensor," Int. J. Appl. Ceram. Technol., vol. 3, no. 2, pp. 127–133, Mar. 2006.

[65]   W. Xiong and G. M. Kale, "Novel high-selectivity NO_2 sensor incorporating mixed-oxide electrode," Sensors Actuators B Chem., vol. 114, no. 1, pp. 101–108, 2006.

[66]   C. Yin, Y. Guan, Z. Zhu, X. Liang, B. Wang, Q. Diao, H. Zhang, J. Ma, F. Liu, Y. Sun, J. Zheng, and G. Lu, "Highly sensitive mixed-potential-type NO_2 sensor using porous double-layer YSZ substrate," Sensors Actuators, B Chem., vol. 183, no. 2, pp. 474–477, 2013.

[67]   I. Romanytsia, J.-P. Viricelle, P. Vernoux, and C. Pijolat, "Application of advanced morphology Au–X (X=YSZ, ZrO_2) composites as sensing electrode for solid state mixed-potential exhaust NOx sensor," Sensors Actuators B Chem., vol. 207, no. 2, pp. 391–397, 2015.

[68] S. Barison, M. Battagliarin, S. Daolio, M. Fabrizio, E. Miorin, P. L. Antonucci, S. Candamano, V. Modafferi, E. M. Bauer, C. Bellitto, and G. Righini, "Novel $Au/La_{1-x}Sr_xMnO_3$ and $Au/La_{1-x}Sr_xCrO_3$ composites: Catalytic activity for propane partial oxidation and reforming," Solid State Ionics, vol. 177, no. 39–40, pp. 3473–3484, 2007.

[69] P. Schmidt-Zhang, "Studies on the development of amperometric high temperature-NO-gas sensors on the basis of zirconium dioxide," Technical University of Berlin, Berlin, Germany, 2008.

[70] R. M. L. Werchmeister, K. K. Hansen, and M. Mogensen, "Characterization of $(La_{1-x}Sr_x)_{(s)}MnO_3$ and Doped Ceria Composite Electrodes in NO_x-Containing Atmosphere with Impedance Spectroscopy," J. Electrochem. Soc., vol. 157, no. 5, pp. P35–P42, 2010.

[71] D. Vladikova, G. Raikova, Z. Stoynov, J. A. Kilner, and S. J. Skinner, "Electrical Properties in Yttria Stabilized Zirconia Investigated by Impedance Spectroscopy," Recent Progress and Future Perspectives in Infrared Microscopy and Spectroscopy with Advanced Light Sources, 2004, pp. 1–3.

[72] Eric D. and S. C. Singhal, "Solid Oxide Fuel Cell Commercialization, Research, and Challenges," The Electrochemical Society Interface, vol. 18, no. 3, pp.38-43, 2009.

[73] L. Y. Woo, L. P. Martin, R. S. Glass, and R. J. Gorte, "Impedance Characterization of a Model Au/Yttria-Stabilized Zirconia/Au Electrochemical Cell in Varying Oxygen and NO_x Concentrations," J. Electrochem. Soc., vol. 154, no. 4, p. J129, 2007.

[74] E. Navickas, T. M. Huber, Y. Chen, W. Hetaba, G. Holzlechner, G. Rupp, M. Stöger-Pollach, G. Friedbacher, H. Hutter, B. Yildiz, and J. Fleig, "Fast oxygen exchange and diffusion kinetics of grain boundaries in Sr-doped LaMnO 3 thin films," Phys. Chem. Chem. Phys., vol. 17, no. 12, pp. 7659–7669, 2015.

[75] K. A. Stoerzinger, W. T. Hong, G. Azimi, L. Giordano, Y.-L. Lee, E. J. Crumlin, M. D. Biegalski, H. Bluhm, K. K. Varanasi, and Y. Shao-Horn, "Reactivity of Perovskites with Water: Role of Hydroxylation in Wetting and Implications for Oxygen Electrocatalysis," J. Phys. Chem. C, no. 1, p. 150715102419000, 2015.

[76] D. T. Chaopradith, D. O. Scanlon, and C. R. A. Catlow, "Adsorption of Water on Yttria-Stabilized Zirconia," J. Phys. Chem. C, vol. 119, no. 39, pp. 22526–22533, 2015.

[77] N. Sakai, K. Yamaji, T. Horita, Y. P. Xiong, H. Kishimoto, M. E. Brito, and H. Yokokawa, "Effect of water on electrochemical oxygen reduction at the interface between fluorite-type oxide-ion conductors and various types of electrodes," Solid State Ionics, vol. 174, no. 1–4, pp. 103–109, 2004.

[78] J. Macdonald, "Impedance spectroscopy: Models, data fitting, and analysis," Solid State Ionics, vol. 176, no. 25–28, pp. 1961–1969, 2005.

[79] B. Van Hassel, B. Boukamp, and A. Burggraaf, "Electrode polarization at the Au, $O_2(g)$/yttria stabilized zirconia interface. Part II: electrochemical measurements and analysis," Solid State Ionics, vol. 48, pp. 155–171, 1991.

[80] M. Stranzenbach and B. Saruhan, "Planar , Impedancemetric NO_x Sensor with Spinel- type SE" Sensors Actuators B Chem., vol. 127, no. 1, pp. 224–230, 2007.

[81] E. Koep, D. S. Mebane, R. Das, C. Compson, and M. L. Liu, "Characteristic thickness for a dense $La_{0.8}Sr_{0.2}MnO_3$ electrode," Electrochem. Solid State Lett., vol. 8, no. 11, pp. A592–A595, 2005.

[82] G. J. la O', B. Yildiz, S. McEuen, and Y. Shao-Horn, "Probing Oxygen Reduction Reaction Kinetics of Sr-Doped LaMnO[sub 3] Supported on Y_2O_3-Stabilized ZrO_2," J. Electrochem. Soc., vol. 154, no. 4, p. B427, 2007.

[83] Y. Takeda, "Cathodic Polarization Phenomena of Perovskite Oxide Electrodes with Stabilized Zirconia," J. Electrochem. Soc., vol. 134, no. 11, p. 2656, 1987.

[84] B. Morel, R. Roberge, S. Savoie, T. W. Nappom, and M. Meunier, "Catalytic activity and performance of LSM cathode materials in single chamber SOFC," Appl. Catal. A Gen., vol. 323, pp. 181–187, 2007.

[85] N. Sakai, "Significant effect of water on surface reaction and related electrochemical properties of mixed conducting oxides," Solid State Ionics, vol. 175, no. 1–4, pp. 387–391, Nov. 2004.

[86] G. J. la O' and Y. Shao-Horn, "Oxygen Surface Exchange Kinetics on Sr-Substituted Lanthanum Manganite and Ferrite Thin-Film Microelectrodes," J. Electrochem. Soc., vol. 156, no. 7, p. B816, 2009.

[87] L. Navarrete, C. Solís, and J. M. Serra, "Boosting the oxygen reduction reaction mechanisms in IT-SOFC cathodes by catalytic functionalization," J. Mater. Chem. A, vol. 3, no. 32, pp. 16440–16444, 2015.

[88] E. P. Murray, R. Novak, D. Kubinski, R. Soltis, J. Visser, L. Woo, L. Martin, and R. Glass, "Investigating the Stability and Accuracy of the Phase Response for NO_x Sensing 5% Mg-modified $LaCrO_3$," ECS Trans., no. x, pp. 43–62, 2008.

[89]   S. P. S. Badwal, S. Giddey, C. Munnings, and A. Kulkarni, "ChemInform Abstract: Review of Progress in High Temperature Solid Oxide Fuel Cells," ChemInform, vol. 46, no. 31, pp. 2-11, Aug. 2015.

[90]   N. P. Bansal, P. Singh, S. Widjaja, and D. Singh, Eds., "Advances in solid oxide fuel cells VII," in 35th International Conference on Advanced Ceramics and Composites, 2011, p. 89.

[91]   E. P. Murray, K. Kharashi, and K. Adedeji, "Managing H_2O Cross-Sensitivity Using Composite Electrolyte NO_x Sensors," Electrochemical Sensor Technology, 2017.

[92]   K. Kharashi and E. P. Murray, "Effect of Al_2O_3 in Porous Zirconia Electrolytes for NO Sensing," J. Electrochem. Soc., vol. 163, no. 13, pp. B633–B637, Sep. 2016.

[93]   A. J. Feighery and J. T. S. Irvine, "Effect of alumina additions upon electrical properties of 8 mol.% yttria-stabilised zirconia," Solid State Ionics, vol. 121, no. 1, pp. 209–216, 1999.

121